DISCRETE FORMULATION FOR MULTI-OBJECTIVE OPTIMAL DESIGN OF PRODUCED WATER TREATMENT

Maryam Falahi

A dissertation submitted in partial fulfillment

of the requirements for the degree of

Doctor of Philosophy

of

University College London.

Chemical Engineering Department

University College London

July 30, 2024

I, Maryam Falahi, confirm that the work presented in this thesis is my own. Where information has been derived from other sources, I confirm that this has been indicated in the work.

Abstract

Produced water is the largest waste stream generated during oil and gas production. In offshore platforms, the majority of the produced water is discharged into the ocean. This results in an increase in the amount of toxic organic and inorganic compounds in the receiving environment and hence may threaten marine life. Therefore, many environmental agencies have enforced limits on the concentrations of toxic contaminants in the discharged water. To meet these regulations and to secure another potential source of fresh water, especially in water-stressed countries, the treatment of produced water becomes an attractive alternative to discharging the water. However, most of the research to date has focused on the economics of water treatment without consideration of other aspects, such as environmental and social impacts. These other aspects may have a significant impact on design decisions.

This paper presents a multi-objective optimization model for the identification and design of alternative configurations for the treatment of produced water. The design problem is formulated as a mixed integer dynamic optimization model. In this approach, different technologies are assigned and linked in a given sequence resulting in a process flowsheet. The mixed integer dynamic optimization problem is solved using a nature-inspired meta-heuristic optimization procedure based on plant propagation. The design of the individual processing steps in the flowsheet is based on population balance modeling. The models take into account the evolution of the oil droplet and solid particle distribution due to breakage and coalescence phenomena. The distribution is represented by a discrete formulation based on a logarithmic discretization of the space (droplet/particle volume). Multiple case studies are presented which consider two criteria for design: economics and en-

vironmental impact. The pool of considered technologies in this study includes a variety of processing steps such as gravity separation, hydrocyclone, and membrane technologies aiming to meet the requirements of different destinations. The result is a set of designs that trade-off the two criteria, providing some of the necessary information for a decision maker to choose a particular design for implementation.

Impact Statement

The proposed research addresses the critical issue of produced water management, a significant challenge in the fossil fuel extraction industry due to the large volumes of contaminated water generated. This naturally occurring water, trapped with hydrocarbons, is brought to the surface as an undesired byproduct during extraction processes, leading to substantial environmental and economic concerns. Managing produced water involves complex processes to remove contaminants and meet strict environmental regulations, making it a costly and technically demanding task. The current practices of disposal, re-injection, and reuse each come with their own set of challenges, from high costs and environmental risks to technical limitations in treatment efficiency.

To mitigate these issues, this research develops a flexible multi-objective optimization model aimed at identifying the optimal combination and sequence of treatment technologies. This approach minimizes both the total costs and environmental impact of produced water treatment processes, accommodating the variability in water volumes and compositions. Such a model addresses the inefficiencies and high costs currently associated with existing produced water treatment methods, offering a more sustainable and economically feasible solution.

In addition to improving the efficiency of produced water management, the research emphasizes the potential for treated produced water to be utilized for beneficial uses, such as crop irrigation and industrial applications. This focus on the reuse of treated produced water not only helps conserve freshwater resources but also aligns with global sustainability goals. By ensuring that the treated water meets the necessary quality standards for various applications, the framework supports the

shift from viewing produced water as waste to recognizing it as a valuable resource. This shift can significantly reduce the environmental footprint of the oil and gas industry and contribute to water resource sustainability.

Moreover, the decision-making tool proposed in this research has broader implications for the industry. By integrating various treatment technologies and considering multiple criteria, the model provides a tool for industry stakeholders to evaluate various design alternatives for produced water treatment processes. This approach enhances the ability to handle additional contaminants and adapt to dynamic changes in droplet and particle size distributions.

Acknowledgements

I am deeply grateful for the opportunity to begin my PhD journey, which started with a casual conversation with my colleague, Mais, and evolved into a life-changing experience that transformed how I see life and, most importantly, how I see myself. During the pandemic, I often thought I would never reach the end of this journey. However, the support, friendship, guidance, and insights from many individuals made it possible for me to reach this point. I would like to take this opportunity to recognize and thank all those who made this journey possible.

First and foremost, I would like to thank my supervisors, Professor Eric Fraga and Professor Vivek Dua. I appreciate their patience, support, and invaluable guidance throughout my time at UCL, particularly during the challenging times of the Covid-19 pandemic.

A special thank goes to my colleagues in the UCL Chemical Engineering department. I am grateful to my group members, Andres, Oliver, and Raymond, for their help and support. I also thank the Chemical Engineering Researchers' Society (CheERS) committee for their efforts in making my time in the department more enjoyable and for giving me the opportunity to be part of their team. To all my colleagues at UCL Chemical Engineering, thank you for being part of this inspiring journey.

I am extremely grateful to my friends, Deema and Amjad, for their companionship, laughter, and support during our time together in London. Their shared experiences and wisdom have made the PhD journey more manageable and enjoyable. I also thank my friends Mai and Latifa for their endless support and encouragement, and Aisha and Nikos for the lovely weekends we spent cooking together. To Farah,

Sara, Basma, Odai, Alaa, Ali, and Hamad, thank you for believing in me even more than I believed in myself.

I am indebted to my family. To my parents, Ahmad and Aisha, for their unconditional love, sacrifice, and unwavering support. I am grateful for everything they have done to help me become who I am today. To my siblings, Hassan, Fatema, and Salman, their encouragement and belief in me have been the driving force behind my achievements. I would also like to thank my nephews and niece, Fahad, Sultan, and Haya, for bringing joy and inspiration into my life. Their love has been a constant source of motivation throughout my PhD journey.

Contents

List of Figures

List of Tables

Chapter 1

Introduction

1.1 Background

1.1.1 Energy Demand

Global energy demand is expected to grow by 50% in the next few decades to meet the needs of the substantially growing population. While transportation energy consumption increases by about 40% [Nalley and LaRose, 2021], electricity will be the major energy consumer in 2050 as it will account for 25% of the total global demand compared to 18% currently. Emerging economies in Asia, China, and India, account for 71% of the new capacity [Nyquist, 2016]. Urbanization and rising income will increase energy consumption in the buildings section globally by 65% [Nalley and LaRose, 2021].

The growth of the global energy demand is coupled with a change in the energy mix consumption. Renewable energy is the fastest growing energy consumption with 3.1% annually compared with 0.6% of oil. This reduction in oil consumption is due to the increase in vehicle efficiency and the number of electric cars. Similar to oil, coal growth will be limited to 0.4% annually to contribute to 16% only of the global energy consumption. Natural gas consumption will increase by 40% as it will be used in electricity generation and the industrial sector [Nalley and LaRose, 2021].

Regardless of the diversification and the growth of the renewable energy share and consumption, fossil fuel will dominate energy use through 2050 although it will

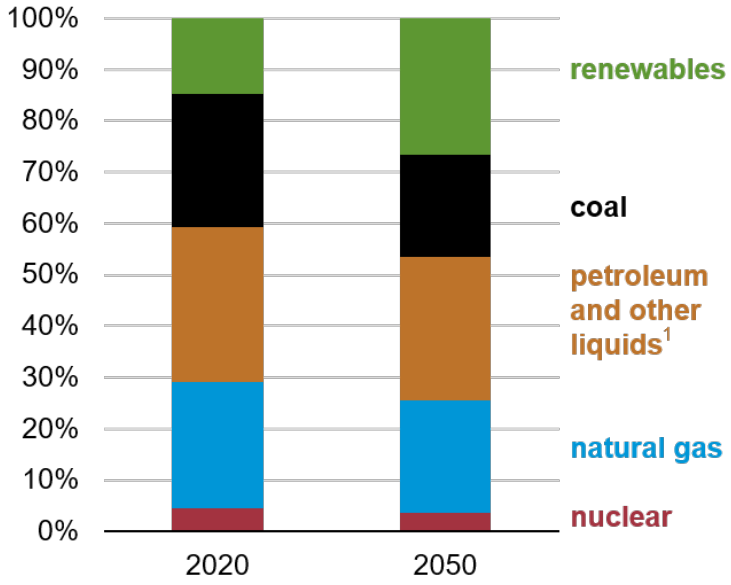

Figure 1.1: Share of primary energy consumption by source, world. Source: U.S. Energy Information Administration [Nalley and LaRose, 2021] .

drop from 66% currently to %38 in 2050 [Nyquist, 2016]. Figure (1.1) illustrates the global share of primary energy consumption by source, showing that energy from hydrocarbons will dominate global consumption through 2050 [Nalley and LaRose, 2021].

1.1.2 Produced Water

The extraction of fossil fuels is associated with a large volume of waste generated during the extraction processes. A naturally occurring water that is trapped with the hydrocarbon is brought to the surface as an undesired byproduct which is known as Produced Water. Whether it is extracted onshore or offshore, from conventional or unconventional sources, produced water has almost the same properties with different compositions [Igunnu and Chen, 2012].

1.1.2.1 Produced Water Volume

The age of the well is a significant factor that affects the volume of produced water. As the well ages and is near depletion, the volume of produced water could reach 98% for 2% hydrocarbon as illustrated in Figure (1.2) [McCabe, 2020] which shows the volume of produced water generated compared with the oil production in m^3. However, the average ratio of water to hydrocarbon at a global level is 3:1

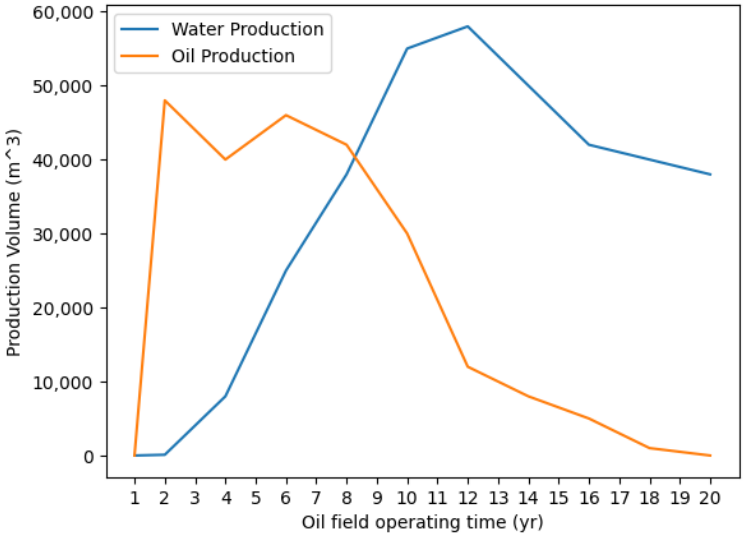

Figure 1.2: Production of produced water and oil for a typical oil field showing the increase in the ratio between water and oil production over the lifetime of the filed [McCabe, 2020]

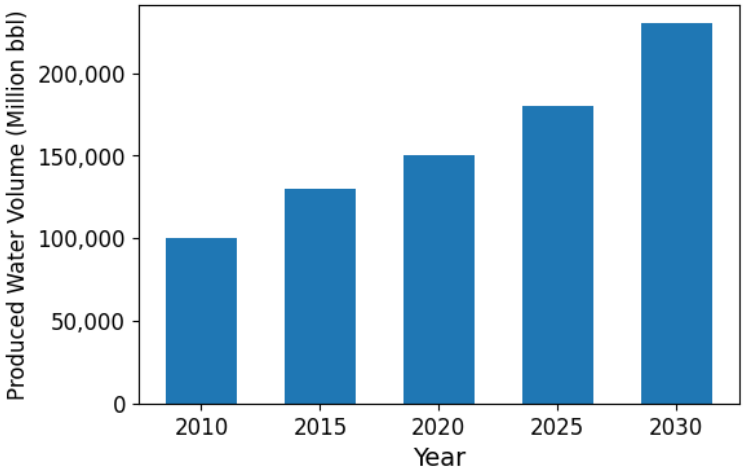

Figure 1.3: Global produced water volume forecast [Produced Water Society, 2024, Amakiri et al., 2023]

barrel which makes it the largest waste stream in the oil and gas industry. Figure (1.3) shows an increase of 65% in produced water volume from 2020 to 2030 which corresponds to 243,000 million barrels per day in 2030 [Produced Water Society, 2024]. The major contributors to produced water production globally are Asia followed by North America and then Europe as displayed in Table (1.1) [Gangwar et al., 2024] which shows the continent's contribution to produced water generation globally.

Table 1.1: Produced water generation per continent in 2022. The volume of produced water is estimated based on the average water-oil-ratio of 1.9 and total petroleum and other liquids in 2022 [Gangwar et al., 2024].

Continent	Contribution
Africa	7%
Asia	42%
Australia	1%
Europe	15%
North America	28%
South America	7%

1.1.2.2 Produced Water Composition

Produced water is not a single product but a mixture of different compounds. The composition of the produced water varies with the field's geological location, reservoir life span, and hydrocarbon chemical composition. One of the major contaminants of concern in the produced water is salinity which is also known as total dissolved solids which exceeds that of seawater [Al-Ghouti et al., 2019]. Others are oil and grease, suspended solids, and chemicals added to improve the drilling and operations such as corrosion and scale inhibitors, emulsion breakers, coagulants, and solvents. These additives increase the overall toxicity of produced water as they become part of its composition. A complete list of main constituents available in the produced water with their typical concentrations can be found in [Ghafoori et al., 2022].

1.1.2.3 Produced Water Destinations

Currently, the produced water is managed through disposal, re-injection, and reuse [Ghafoori et al., 2022]. In offshore facilities, discharging is the most adopted practice. This option can result in polluting surface water in addition to the health hazard for both animals and plants. To mitigate the risk of the discharge process, many countries imposed very rigorous standards for produced water disposal and in some cases abandoned some disposal practices [Zheng et al., 2016]. Therefore, the disposal by such method in remote areas is shrinking and increasingly costly as meeting these regulations requires a very efficient treatment process.

Re-injecting produced water for enhancing oil recovery is another option that

is adopted widely onshore. Produced water can be transformed from waste into a valuable resource. The benefits of this option are that it reduces the amount of produced water disposal to the ocean and the amount of freshwater needed to maintain the pressure in the reservoir that drops with the oil and gas extraction. However, this option has its drawbacks. To avoid reaching irrigation and drinking water aquifers, produced water should be injected very deep which requires high pressure and consequently high cost [Nesic and Streletskaya, 2018]. Moreover, the re-injection results in formation damages due to fracturing of the aquifer's internal wall which makes it unsustainable for the long run [Obe et al., 2017]. Other challenges are related to the requirements of injected water. The water has to be treated to avoid plugging reservoir rock pores with total suspended solids. Likewise, bacteria and dissolved solids have to be removed before injection as they result in the corrosion of the well pipes [Ghafoori et al., 2022].

The third practice of produced water management is beneficial reuse. Treated produced water can be used for crop irrigation and livestock watering. Irrigation consumes about 21% of the total withdrawn water in Europe and around 59% in the United States. Re-utilizing the produced water can contribute to the sustainability of water resources. Yet, irrigation requires a large volume of water with a high purity level. The salinity of the produced water can affect the yield of the crop in case exceeds specific limits. Sodium can be another threat to the soil as it affects plant growth and soil quality and changes its physical and chemical characteristics [Veil and Clark, 2011]. Therefore, the Food and Agriculture Organization has imposed limits on the constituents of the produced water to be used for irrigation [Ayers and Westcot, 1985]. Using produced water for potable consumption is another option that is challenged by high treatment cost, potential toxicity, and public acceptance [Mendhe et al., 2017]. Table (1.2) displays the limit of selected contaminants for various destinations.

1.1.2.4 Treatment Challenges

The previous highlights the challenges associated with the disposal and re-injection of produced water, given the constraints imposed by environmental regulations and

Table 1.2: The limits of selected produced water contaminants for various destinations.

Destination	Contaminant	Limit	Unit	Reference
Discharge	Oil and grease	40	mg/L	[Ghafoori et al., 2022]
Re-injection	Total suspended solids	10	mg/L	[Bader, 2007]
	Oil and grease	42	mg/L	[Bader, 2007]
Reuse				
Desalination	Sulfate	10	mg/L	[Alzahrani and Mohammad, 2014]
	Ammonia	50	mg/L	[Alzahrani and Mohammad, 2014]
	Total dissolved solids	200	mg/L	[Alzahrani and Mohammad, 2014]
Cooling Towers	Total suspended solids	150	mg/L	[Alzahrani and Mohammad, 2014]
	Chloride	1,500	mg/L	[Alzahrani and Mohammad, 2014]
	Alkalinity	3,000	mg/L	[Alzahrani and Mohammad, 2014]
	Conductivity	6,000	$\mu S/cm$	[Alzahrani and Mohammad, 2014]
Livestock	Oil and grease	-	mg/L	[Fakhru'l-Razi et al., 2010]
	Total suspended solids	-	mg/L	[Fakhru'l-Razi et al., 2010]
	Total dissolved solids	1,000	mg/L	[Fakhru'l-Razi et al., 2010]
Irrigation	pH	4.3–10.0	-	[Cooper et al., 2021]
	Total dissolved solids	500	mg/L	[Cooper et al., 2021]
	Total suspended solids	-	mg/L	[Fakhru'l-Razi et al., 2010]
	Oil and grease	0.05	mg/L	[Fakhru'l-Razi et al., 2010]
	Conductivity	3,000	$\mu S/cm$	[Echchelh et al., 2018]

technical considerations. This difficulty emphasizes the viability of reuse as an alternative. Nevertheless, opting for reuse demands a more rigorous treatment process compared to other alternatives. Despite its potential benefits, the design of an effective treatment system encounters the following challenges:

Produced water Volume: The uncertainty in the volume of produced water makes the sizing of the treatment plan difficult especially since the size of the units is significantly associated with the treatment efficiency and cost planning.

Produced Water Composition: Designing a water treatment system for produced water proves challenging due to the variability in its composition. According to [Al-Ghouti et al., 2019], no single technology exists that can fully meet the specifications of the final destination. For instance, streams with exceptionally high concentrations of oil and grease may require additional treatment stages to fulfill reuse criteria compared to scenarios involving marine discharge.

Treatment Technology: There are various treatment technologies for produced water each with its capabilities and drawbacks. Given the variable composition of produced water, the challenge with the available technologies is to choose the most suitable combination with the highest removal efficiency [Ghafoori et al., 2022].

Treatment Cost: The cost of treatment is proportional to the quality requirements of the final destination. For example, the cost associated with meeting the reuse quality requirements is higher than the cost of disposal and re-injection which makes this option less feasible to pursue [Olajire, 2020].

Droplet and Particle Size: Produced water contains contaminants in the form of dissolved solids, free droplets, and particles that undergo separation from the water. The effectiveness of the separation process is significantly influenced by the size of these droplets and particles [Jia et al., 2019]. Contaminants appear in water as varying-sized droplets or particles. The treatment process

faces additional challenges due to the changing distribution of droplet and particle sizes [Li and Huang, 2017].

Emission: Wastewater treatment plants are recognized for releasing a substantial volume of greenhouse gases (GHGs) primarily attributed to high electricity consumption, accounting for 5% to 30% of the plant's operational costs [Ghoneim et al., 2016]. Given the global commitment to mitigate climate change and the rising energy prices, these facilities face a significant challenge in minimizing greenhouse gas emissions associated with their operations [Yang et al., 2023].

1.2 Thesis Aim

This thesis proposes a flexible, multi-objective optimization model designed to address the complexities of produced water treatment processes. The model's flexibility stems from its ability to identify the optimal combination and sequence of technologies to minimize system costs and environmental impact, regardless of water volume or composition. Also, it ensures that the treatment meets the requirements of various destinations by accommodating the dynamic evolution of droplet and particle size distributions throughout the process. Additionally, the model's versatility allows for the integration of various treatment technologies to handle additional contaminants, making it adaptable to a wide range of scenarios. This work proposes a comprehensive decision-making framework, aiding in the identification and evaluation of diverse design alternatives for produced water treatment processes, considering multiple criteria.

1.3 Thesis Structure

The subsequent sections of this thesis are structured as follows: Chapter (2) presents a comprehensive review of relevant literature regarding produced water treatment design. In Chapter (3), the research methodology is detailed, including the modeling approach and solution method. The mathematical formulation of the proposed multi-objective optimization model is presented in Chapter (4 and 5). Chapter (6)

outlines the outcomes obtained from implementing the model across various case studies. Finally, Chapter (7) summarizes the research findings and outlines potential future work.

Chapter 2

Produced Water Treatment

With the aim of this thesis in mind, the subsequent sections will outline the relevant concepts, review existing research done so far, and highlight potential contributions yet to be accomplished.

2.1 Introduction

Water treatment plays a crucial role in today's economy, significantly contributing to public health, industry sustainability, and environmental protection. The primary purpose of the treatment process is to purify water by removing impurities to make it suitable for human usage. One of the main areas of water treatment is seawater desalination which aims at removing salt and securing a source of fresh water. Unlike seawater, wastewater generated by the industry contains a diverse range of contamination and impurities that vary from one industry to another [Mao et al., 2021, Noor et al., 2023]. This chapter provides an overview of the water treatment process with more emphasis on the treatment of the wastewater generated by the oil and gas industry.

2.2 Water Treatment Process Overview

The water treatment process generally consists of multiple stages, depending on the number of contamination and the required purity level [Freeman et al., 2020]. For instance, seawater goes through two main stages; the pre-treatment stage which removes the suspended solids and organic matter followed by the desalination stage

[Abdul Ghani et al., 2021]. The first stage is achieved by conventional methods such as coagulation-flocculation [Shaheen and Cséfalvay, 2022], sedimentation [Badruzzaman et al., 2019], dissolved air flotation [Altmann et al., 2023], and non-conventional pre-treatment such as micro-filtration [Shaheen and Cséfalvay, 2022] and ultra-filtration [Brover et al., 2022]. The existing water desalination technologies are also classified into conventional (thermal) and non-conventional (membrane). Thermal technologies, which are mostly used in large-scale plants, are multi-effect distillation [Lin et al., 2021], mechanical vapor compression [Shamet and Antar, 2023], and multi-stage flash [Ali et al., 2024]. The membrane technologies on the other hand are forward osmosis [Abounahia et al., 2023], reverse osmosis [Kim et al., 2024], and electrodialysis [Lin et al., 2021].

Similarly, municipal and industrial wastewater passes through multiple stages with different types of processes [Christian et al., 2023]. For example, physical processes such as sedimentation, filtration, and flotation purify water by removing the solid content. On the other hand, the turbidity and heavy metals are removed through chemical processes such as coagulation-flocculation. Biological treatment, which can remove organic matter, includes activated sludge [Waqas et al., 2023] and anaerobic digestion [Hashmi et al., 2023]. Other processes are membrane-bioreactor, adsorption, sonication, and advanced oxidation processes [Noor et al., 2023, Oztekin and Sponza, 2013, Ahmed et al., 2021].

2.3 Produced Water Treatment Process Overview

Produced water treatment presents a challenge for the conventional treatment processes. The main factor that differentiates this stream from other sources of water is the existence of valuable hydrocarbons, which need to be recovered, along with industry-related contamination. The complex nature of produced water composition requires the usage of a combination of processes to remove these contaminants [Al-Ghouti et al., 2019].

In addition to the produced water-specific separation technologies that aim at removing hydrocarbons such as horizontal separators [Amakiri et al., 2022] and

corrugated plate interceptors [Boraey, 2018], existing technologies are tailored to suit the complex nature of this stream such as hydrocyclones [Amakiri et al., 2022] and centrifuges [White et al., 2020, Lekomtsev et al., 2021]. Additionally, flotation techniques, including induced gas flotation and dissolved gas flotation, have proven invaluable in reducing the oil and solid content of produced water [Amakiri et al., 2022]. The integration of an emulsification agent further enhances the separating of oil by de-stabilizing the oil in water emulsion as in the case of chemical treatment processes [Nasiri and Jafari, 2017]. Coagulants and flocculants are other types of chemical agents that promote the aggregations of droplets and solids to enhance their separation by other means such as sedimentation and coalescence [Amakiri et al., 2022].

In terms of organic and dissolved matter, more advanced technologies with distinct advantages in separation efficiency have been adopted. Biological treatment degrades the organic contamination using microorganisms [Camarillo and Stringfellow, 2018, Amakiri et al., 2022]. Membrane technologies are applied in different stages of produced water treatment based on their pore sizes [Rajbongshi and Gogoi, 2023, Amakiri et al., 2022]. For example, ultra-filtration with pore sizes of 10 μm can remove large particles and organic matter while reverse osmosis became one of the most efficient technologies for removing dissolved compounds and salts [Asad et al., 2020]. Desalination processes, which are the most mature among all, are widely applied to reduce the salinity of the produced water. These processes include multi-effect distillation [Onishi et al., 2017a], mechanical vapor compression [Shaffer et al., 2013], and freeze-thaw/evaporation [Amakiri et al., 2022].

The separation of various contaminants cannot take place within one stage as different processes are needed for each purpose. Consequently, produced water is treated in multiple stages with each stage having a unique purpose and hence employing different technologies [Al-Ghouti et al., 2019]. The following section outlines the multiple stages of produced water treatment along with the working principles of selected produced water treatment technologies utilized at each stage.

Pre-treatment Stage: The purpose of this stage is to remove the free and dispersed

oil droplets and solid particles [Al-Ghouti et al., 2019, Szep and Kohlheb, 2010] which is achieved using mechanical devices such as Gravity Separators, also known as American Petroleum Institute separators [Amakiri et al., 2022], or Corrugated Plate Interceptor separators [Boraey, 2018]. These devices work by using gravity to separate large oil droplets and suspended solids. The process relies on the difference in specific gravity between the continuous and dispersed phases [Backi and Skogestad, 2017]. For effective separation, the specific gravity difference between oil and produced water should be smaller than that between suspended solids and water. This ensures that the suspended solid particles settle at the bottom of the separator while the oil droplets rise to the top. After this step, oil and the suspended solids are removed by other means [Schultz, 2005].

American Petroleum Institution Separator: The separation of the oil droplets in this device is based on the rise rate or vertical velocity of the oil droplets to the separator surface due to the difference in density between phases according to Stockes' Law. Any oil droplets with a rise rate greater than the surface loading rate, which is the flow rate divided by the separator surface area, will reach the surface of the separator within the processing residence time and will be removed. American Petroleum Institution Separator is a rectangular tank with two baffles to provide quiescent flow [American Petruelem Institute, 1990, Odiete and Agunwamba, 2019].

Corrugated Plat Interceptors: It is an improvement of the American Petroleum Institution separator with a smaller volume and higher efficiency and a set of plates added to the separation tank. The plates aim to increase the coalescence between the oil droplets which increases their rise rate and hence the separation efficiency [Boraey, 2018].

Secondary Treatment Stage: The purpose of this stage is to further reduce the concentration of the contaminants by removing the smaller droplets and par-

ticles that could not be removed by the pre-treatment stage [Al-Ghouti et al., 2019]. More advanced treatment processes are employed which include the following:

Induced Gas Flotation: Similar to American Petroleum Institution separator and Corrugated Plat Interceptors, Induced Gas Flotation separation is based on the difference in density between phases. In this process, the difference is increased by inducing gas bubbles in the unit. The bubbles attach to the oil droplets and solids. The new agglomerate has a lower density than oil and hence rises faster to the surface where they are skimmed off [Amakiri et al., 2022, Saththasivam et al., 2016].

Hydrocyclone: It is a separation device that utilizes inertia to remove droplets and particles from liquids. The rotating body of the hydrocyclone creates a spiral vortex. The droplets and particles gain inertia. The larger and denser droplets/particles' inertia is higher therefore, they can not follow the high-speed spiral motion of the water. Consequently, they hit the internal wall of the hydrocyclone body and move down to the collection point where they leave the stream. The smaller droplets/particles, on the other hand, follow the vortex due to their smaller inertia and move upward in the same direction as the clean feed that leaves the device [Amakiri et al., 2022].

Centrifuges: Centrifuges function based on a similar principle as hydrocyclones, albeit with a slight distinction. Unlike hydrocyclones, in centrifugal separation, the entire chamber undergoes rotation, not just the wastewater. This rotation generates a greater force, leading to more effective solid separation [White et al., 2020].

Nutshell filtration: This device can separate hydrocarbon liquids from wastewater down to very low concentrations. In this process, the produced water enters the nutshell vessel and passes through Nut Shell Media which absorbs the oil and fine solids and prevents them from passing with the clean water [Sobolciak et al., 2020].

Membrane Technology: The membrane separation principle is based on size exclusion. When feed water passes through the membrane, only liquid and small particles smaller than the membrane's pores can flow through. The membrane can be classified according to the pore size into Microfiltration, Ultrafiltration, Nanofiltration, and Reverse Osmosis. The quality of treated water and applied pressures increase as the pore size decreases. Therefore, the order of the membrane in terms of highest water quality is Reverse Osmosis followed by Nanofiltration, Ultrafiltration, and finally Microfiltration [Rajbongshi and Gogoi, 2023, Amakiri et al., 2022, Munirasu et al., 2016].

Tertiary Treatment Stage: The tertiary stage aims to remove or reduce the concentration of the salt and dissolved matter from the treated produced water coming from the secondary stage [Al-Ghouti et al., 2019]. The separation of these fine particles can be achieved through a distillation process that includes heating, evaporation, and condensation [Shaffer et al., 2013, Onishi et al., 2017a]. The following are examples of desalination technologies:

Multi-Effect Distillation: Water undergoes evaporation and condensation in multiple stages. The process initiates by simultaneously supplying water to all effects, achieved through methods like spraying or distributing water onto hot tube surfaces. The water is preheated to its boiling point in this stage. Steam, produced by heating the tubes with steam from a boiler, condenses within the tubes and is returned to the boiler for reuse. The evaporated water on the tubes transforms into steam, which is utilized to heat the tubes in the subsequent stage. Here, it condenses back into fresh water within the tube, releasing heat to evaporate water in that stage. Un-vaporized water from each stage is then gravity-fed through pipes to the next stage, with a brine pump removing it at the final stage [Onishi et al., 2017a].

Mechanical Vapour Compression: The mechanical vapor compression

system comprises an evaporator, condenser, mechanical vapor compressor, and a heat exchanger for pre-heating the feed stream by cooling the distillate and brine streams. The process begins by introducing seawater into the heat exchanger for heating. It then enters the evaporator, where a portion transforms into vapor, while the brine remains on the evaporator surface and exits the system through the heat exchanger. The resulting vapor moves into the compressor, undergoes compression, and is directed to the condenser for condensation. Finally, the condensed product returns to the heat exchanger for cooling and exits the system as distilled water [Shaffer et al., 2013].

As demonstrated above, the effectiveness of separation is closely associated with the size of droplets/particles, a factor that presents challenges due to its variable nature. The next section in this chapter explains the phenomena influencing Droplet and Particle Size Distribution, detailing their effects on the separation process.

2.4 Droplet/Particle Size Distribution

Oil and solids exist in water in the form of droplets and particles that range from 0.5 to greater than 200 microns in diameter. The droplet and particle size distributions have a significant influence on the performance of the separation unit especially when the separation is based on stock law where the rise rate of the droplet is a function of its diameter [Doran, 2013a]. The droplet and particle size distributions do not remain constant during the treatment process due to breakage and coalescence phenomena. The following paragraphs outline the mechanism of these phenomena and the existing models that describe them in the literature.

2.4.1 Droplet Breakage

Breakage poses a negative impact on the separation process, with smaller droplets proving more challenging to separate, requiring the use of advanced processes which results in a higher cost. In a multi-phase flow, the breakage of a droplet is a result of two opposing forces applied to the droplet—one internal and one external. The external is the pressure applied to the droplet by the surrounding liquid

to break it and the internal force is the one that restores the form of the droplet. The internal force is the sum of the droplets' surface stress and the liquid's viscosity inside it.

The breakage of droplets arises from various mechanisms associated with different types of flow. For instance, in turbulent flow, turbulent fluctuation on the droplet surface or collision with eddies generates pressure, leading to surface instability, deformation, and subsequent breakage. Breakage occurs when the turbulent kinetic energy of the droplets or impacting eddies surpass critical thresholds. In laminar flow, the shear force exerted by the continuous phase creates a velocity gradient at the interface, causing droplet deformation and breakup. Here, the droplet is influenced by both the viscous stress of the continuous phase and its surface tension [Liao and Lucas, 2009a].

Breakage can also occur due to various mechanisms related to droplet size, such as the shearing-off process. In this process, the shear force resulting from velocity gradients at the interface causes larger droplets to fragment into smaller ones. Additionally, interfacial instability arises when a droplet transitions from a light to a heavy liquid, resulting in droplet breakage, a phenomenon known as Rayleigh-Taylor instability [Liao and Lucas, 2009a].

Surface stress and surface tension are interfacial forces that influence the behavior of droplets in a continuous phase. Surface tension is a property of liquids that minimizes the surface area of a droplet due to the cohesive forces between its molecules, maintaining the droplet's spherical shape. This feature of surface tension prevents breakage by resisting deformation and enhances coalescence by facilitating the drainage of the thin film between droplets, leading to their merging.

In contrast, surface stress refers to the internal forces acting within the surface of the material in response to external forces, creating weak points and instabilities that can lead to droplet breakage. The presence of surfactants significantly affects this balance. Surfactants, which reduce surface tension by adsorbing at the oil-water interface, introduce surface stress that dominates over surface tension. This promotes droplet breakage by destabilizing the interface and prevents coalescence

by creating a barrier that keeps droplets from merging.

In systems without surfactants (pure systems), surface tension is the dominant force, leading to less breakage and more coalescence of droplets. In summary, surface tension maintains droplet stability and promotes coalescence in pure systems, while surface stress introduced by surfactants promotes breakage and prevents coalescence [Aarts et al., 2005, Soligo et al., 2019].

The breakage models include two quantities, the first is the breakage frequency which estimates the likelihood of droplet breakage. The available breakage frequency models are classified according to the mechanisms described above. The other quantity related to the droplet breakage calculation is the Daughter Size Distribution which calculates the size of the generated particles due to breakage. There exist several models that are classified into statistical and phenomenological. The former assumes that the droplet size distribution is a random variable and follows a normal, beta, or uniform distribution while the latter is formulated to relate empirical observations to each other and it includes Bell-shape, U-shape, and M-shape models. More details about the models and their mathematical formulation can be found at [Liao and Lucas, 2009a].

2.4.2 Particle Breakage

When it comes to solid particles, breakage occurs through two primary mechanisms. Firstly, fluctuating pressure differences act on opposite sides of the aggregate, leading to breakage. Secondly, breakage can occur when aggregates collide with each other, as well as with the impeller, baffles, and walls of the processing unit [Lu et al., 1998].

The breakage rate of particle aggregate is described through exponential or power law function. The mathematical formulation of the breakage rate of the aggregate along with the breakage distribution function can be found at [Jeldres et al., 2018].

2.4.3 Droplets Coalescence

Together with breakage, coalescence contributes to the evolution of particle size distribution in multi-phase flow. The coalescence depends on the contact and collision between droplets. Since not all collision results in coalescence, the concept of coalescence frequency is introduced which measures the percentage of collision that will result in coalescence between the droplets. The coalescence frequency is the product of collision frequency and coalescence efficiency.

According to [Liao and Lucas, 2010a], the existing models for calculating the coalescence frequency are classified into two categories; empirical and physical. The former depends on the experimental set-up and their geometrical parameters are tuned to fit experimental data. Contrarily, the physical models are derived from physical laws which are based on the collision mechanisms between the droplets/particles.

The collision of droplets occurs due to various factors depending on the flow conditions. In turbulent flows, droplets collide due to the fluctuating turbulent velocity of the liquid surrounding them. In uniform and laminar flows, collision can occur because of velocity gradients. Additionally, a collision may happen when droplet size is smaller than the energy-dissipating eddies in turbulent flows, where droplet velocity matches that of the surrounding flow, making viscosity the primary factor affecting collision.

Moreover, the rise rate of droplets plays a significant role in increasing collision probabilities. Droplets of different sizes have varying rise rates, causing them to collide as they ascend toward the liquid surface. This phenomenon, known as Buoyancy-induced collision, contributes to droplet interaction. Similarly, during droplet rise, the liquid behind them is displaced and accelerated, intensifying collisions as droplets enter this region or ”wake.”

As of now, no model captures the impact of all these mechanisms on the droplet collision. The selection of the model depends on the problem characteristics. Table (2.1) presents some of the models proposed based on the above-mentioned mechanisms.

Table 2.1: Models proposed by various authors to quantify the collision frequency between droplets in continuous phase

Mechanism	Reference
Turbulent collisions	[Prince and Blanch, 1990]
Shear collisions	[Friedlander, 2000]
Buoyant collisions	[Wang et al., 2005]
Wake entrainments	[Kalkach-Navarro et al., 1994]

After collision, only a fraction of the droplets coalesce to form larger ones, a phenomenon known as coalescence efficiency. Various models have been developed to estimate this quantity [Liao and Lucas, 2010a]. According to the energy model proposed by [Howarth, 1964], the likelihood of coalescence increases as the collision energy between droplets rises. Based on this concept, [Sovova, 1981] developed a model that correlates the interfacial energy of the droplet with the kinetic collision energy. This model incorporates factors such as interfacial tension between droplets, droplet surface areas, average volume, and relative colliding velocity of two drops. Contrarily, coalescence is more likely to occur if the relative velocity between two droplets is less than the critical approach velocity, as proposed by the critical approach velocity model [Doubliez, 1991].

Film drainage model [Ross, 1971], the most popular one to know, finds the coalescence efficiency using two time variables; the contact time between two droplets and the drainage time. According to this model, the coalescence will occur if the time needed for the film between two droplets to reach a critical value is higher than the contact time between the droplets.

Different models have been built based on this theory with a difference in the way the drainage and contract time are calculated. In the model proposed by [Prince and Blanch, 1990], the duration of contact between two droplets is impacted by both the size of the bubbles and the intensity of turbulence. Larger bubbles create a larger contact area, which promotes coalescence. However, higher turbulence intensity increases the likelihood of turbulent eddies separating the droplets before film drainage can occur.

On the other hand, [Kamp et al., 2001] proposed a model that highlights the

relation between surface free energy and kinetic energy in determining the contact time between droplets. If the increase in surface free energy dominates, the droplets may separate before merging. Contrarily, if the decrease in kinetic energy exceeds the increase in surface free energy, the droplets remain in contact for a longer duration, promoting coalescence. The complete list of all models can be found at [Liao and Lucas, 2010a].

2.4.4 Particles Aggregation

Similar to droplet coalescence, the aggregation rate of particles is a product of the collision frequency between the particles and the aggregation efficiency. Three main mechanisms lead to particle collision which are: random Brownian motions of particles, differential sedimentation results from the difference in settling velocities of particles, and finally the flow shear [Song et al., 2018]. According to [Van de Ven and Mason, 1977], the likelihood that two colloidal particles will adhere to form an aggregate depends on the ratio between Van Der Waals force that arises from the fluctuation of electrons around the particles and leads to attraction between them [Dzyaloshinskii et al., 1961], and flow shear force that results from the difference in velocity between the fluid adjacent layers.

2.5 Population Balance Modeling

Population Balance Equations describe the change in the number of entities in a discrete or continuous space due to the interaction with their environment. Population Balance Equations serve as a valuable tool for quantifying the influence of breakage and coalescence phenomena on separation performance [Xiao et al., 2015]. The model is characterized by dispersed and continuous phases in which the dispersed phase is made out of particles, droplets, or bubbles. The origin of the Population Balance Equations can be traced back to 1916 when [Smoluchowski, 1918] proposed a set of nonlinear differential equations to describe the coagulation process of particles [Rigopoulos, 2010]. The change due to the fragmentation of particles was added later by [Melzak, 1957]. Today, Population Balance Equations are considered in many engineering and science branches such as polymerization

[Kiparissides et al., 2004], separation [Xiao et al., 2015], and size reduction operations in mills [Datta and Rajamani, 2002].

The population of the entities evolves due to the interaction between the entities themselves or the entities and the continuous phase. Due to these interactions, entities may appear or disappear in the property space. In the context of Population Balance Equations, the breakage of a particle results in the death of that particle which is also known as the parent, and the birth of new 'daughter' or 'child' particles. Similarly, the coalescence or the agglomeration of two particles will result in their death and the birth of new particles [Solsvik and Jakobsen, 2015].

In the following section, the system of equations that describes the birth and death rates of the entities due to coalescence and breakage in the dispersed phase is presented. The terms include integrals as the birth and death processes include particles of different sizes [Solsvik and Jakobsen, 2015].

2.5.1 Governing Equations

Population Balance Equations govern the evolution of the droplet/particle Number Density Functions which describe the distribution of the property of interest, volume of mass, at any time. Given that $n(v,t)$ is the number of droplets of volume v at any point in time t, the source term S represents the rate of change of the property due to the breakage, coalescence, and aggregations.

$$S(v,t) = B_c(v,t) - D_c(v,t) + B_b(v,t) - D_b(v,t) \tag{2.1}$$

where $B_c(v,t)$ and $D_c(v,t)$ the birth and death rate of droplets of volume v at time t due to coalescence and $a(v,v^*)$ is the coalescence rate between droplets of volume v and v^*:

$$B_c(v,t) = \frac{1}{2}\int_0^v a(v-v^*,v^*)\, n(v-v^*,t)\, n(v^*,t)\, dv^* \tag{2.2}$$

$$D_c(v,t) = \int_0^\infty a(v,v^*)\, n(v,t)\, n(v^*,t)\, dv^* \tag{2.3}$$

Similarly, the birth rate $B_b(v,t)$ and the Death rate $D_b(v,t)$ of droplets of volume v at time t due to breakup are given by Eq. (2.4 and 2.5):

$$B_b(v,t) = \int_v^\infty g(v^*)\,\beta(v^*,v)\,n(v^*,t)\,dv^* \tag{2.4}$$

$$D_b(v,t) = g(v)\,n(v,t) \tag{2.5}$$

where $g(v)$ is the breakage rate of droplets of size v, $\beta(v,v^*)$ is the probability density function of droplets breaking from volume v^* to v [Solsvik and Jakobsen, 2015].

2.5.2 Solution Methods

There are several numerical methods to solve the population balance equations in the literature. The following section describes three selected categories. A more comprehensive list can be found at [Omar and Rohani, 2017].

Class/Sectional Method: In this method, the size/volume space is discretized into several classes or sections. Each represents a range of sizes or volumes. The problem then is solved as a set of ordinary differential equations to find out how the number of droplets evolves. The accuracy of the solution is highly dependent on the number of class sizes which makes it computationally very expensive for problems with a higher number of classes.

Moment Method: Similar to the previous method, the moment method is based on solving ordinary differential equations to describe the evolution of droplets over time. However, the number of particles in each class is replaced by the statistical moments of the population such as mean, variance, and skewness which makes this method computationally less expensive than the previous one.

Quadrature-Based Moment Method: The continuous size distribution space is divided into segments or nodes similar to the class method. However, the

selection of the nodes is done using different techniques such as Gauss-Legendre Quadrature and Adaptive Node Placement. The selection of the node discretization aims to improve the accuracy in representing the change in distribution behavior due to breakage and coalescence. Similar to the moment method, the moments of each segment are calculated and a system of ordinary differential equations is solved to trace the change in the moments. To further enhance the accuracy of the calculation, weights are assigned to the segments to prioritize their contribution to the representation of the distribution.

A common limitation of these methods is the computational expense when dealing with a high number of classes, higher moments, and a large number of quadratic nodes. Therefore, a balance between accuracy and computational expenses should be considered with all the methods. Additionally, the selection of the method depends on the nature of the problem. While the class/sectional method is straightforward and provides an accurate description of the distribution of each class, it does not provide statistical information like the moment method and does not have the precision and flexibility of the quadratic method. Another aspect to be considered when choosing between the class/sectional and moment method is the distribution type. The class/sectional method works better with discrete distribution while the moment method can handle a wide range of distributions as it outperforms the class/sectional method in continuous size representation.

2.5.3 Applications to Produced Water Treatment

In the context of produced water treatment, one of the main application areas of population balance equations is the separation of oil, water, and suspended solids from the water stream. The high complexity of produced water composition requires a deep understanding of the evolution of droplets and particle dynamics as a result of breakage and coalescence phenomena. The ability to predict the particle/droplet distribution and the impact of changing operational parameters on their behavior plays a significant role in improving the separation efficiency of the treatment process [Raesi and Maddahian, 2022]. This includes optimizing the design

of the separation unit such as hydro cyclones [Raesi and Maddahian, 2022, Li and Huang, 2017], flotation units, and coalescers or adjusting the operational parameters such as flowrate [Li and Huang, 2017] to achieve the optimal level of separation.

The hydrocyclone stands out as the most extensively studied unit for quantifying the effects of coalescence and breakage mechanisms using population balance equations. [Raesi and Maddahian, 2022] investigated the impact of injecting air flow in a de-oiling hydrocyclone. population balance equations enabled the quantification of the impact of injected air on the breakage and coalescence of droplets and hence optimized the air-liquid ratio and injected bubble diameter to optimize the separation efficiency. The findings reported improvement in the accuracy of the results when considering the effect of breakage and coalescence of droplets compared to previous results. Similarly [Li and Huang, 2017] tested different inlet designs of hydrocyclone and found that the design results in a higher removal efficiency compared to the standard one as reduced the droplet breakage. [Xing et al., 2022] proposed a hydraulic coalescer coupled with a hydrocyclone to promote the coalescence between oil droplets before centrifuge separation. The motive of this study was the difficulty in separating small droplets by a regular hydrocyclone therefore, a coalescer was introduced to the design to enlarge the oil droplets by coalescence.

For the flotation tank, population balance equations were employed to describe the coalescence between oil droplets and gas bubbles and its impact on the removal efficiency of the flotation unit [Huang and Long, 2020]. [Cai et al., 2017a] used population balance equations to find the optimal inlet flow rate of oily wastewater that balances the forces to turbulence forces that maximize the coalescence and prevent the impact of droplet breakage. [Cai et al., 2017b] investigated the impact of design parameters on the droplets' behavior and hence on the separation efficiency of oil from water. The study found that the increase of the inlet velocity combined with a high preliminary separation zone promoted the coalescence between droplets.

In terms of the coalescence and breakage kernels integrated into the population balance equations, [Li and Huang, 2017] adopted [Tsouris and Tavlarides, 1994] model for the breakage and [Prince and Blanch, 1990] model for coalescence. [Cai

et al., 2017a] used [Luo and Svendsen, 1996] breakage model as it is one of the models incorporated in the computational fluid dynamics solutions which makes it one of the most used models as shown by [Raesi and Maddahian, 2022], [Cai et al., 2017b] and [Huang and Long, 2020].

Some of the solution methods implemented to solve the population balance equations numerically are discrete element modeling by [Cai et al., 2017a,b] along with homogeneous and inhomogeneous discrete methods in [Huang and Long, 2020] and [Li and Huang, 2017] respectively.

In conclusion, population balance equations have found widespread application in modeling the influence of droplet size distribution of produced water treatment. Nevertheless, a significant portion of the existing literature primarily concentrates on single-unit models, even though produced water undergoes treatment across multiple stages, as illustrated in Section (2.3) of this chapter. The subsequent section highlights the concept of Process Synthesis, which aims to develop a comprehensive flowsheet for a multi-stage process, to establish a process configuration for the treatment of produced water.

2.6 Process Synthesis

Process synthesis is a step in design where various components are arranged and interconnected with each other to create a flowsheet. By converting inputs such as materials and energy, this flowsheet produces the desired output while achieving certain objects related to the system cost, and environmental or social impacts [Nishida et al., 1981].

2.6.1 Major Approaches

The first synthesis technique is the evolutionary procedure in which the process flowsheet is improved by making sequential small changes based on engineering judgment to improve the performance of the process until no further improvements can be made. The advantage of this approach is that it maintains the good points of the current design while changing everything else to improve the overall process. However, its main drawback is it leads to local optimal as the searching space is

limited to the starting case neighborhood [Stephanopoulos and Westerberg, 1976].

To address the limitations of this technique, two more techniques were proposed by [Douglas, 1985] and [Grossmann, 1985] which are Hierarchical Decision Procedure and optimization-based methods. In the former, the design is decomposed into different layers in which certain decisions are made and the overall process is evaluated at the end of each layer. As we proceed, more decisions are made and more details are added. This procedure generates a good initial flowsheet however, it does not account for the interactions between the decision layers.

In the optimization-based approach, the process synthesis is formulated as an optimization problem in which different set of components and their interactions represents a separate flowsheet. The optimization-based approach results in multiple flowsheets from which the optimal design will be selected. The main advantage of this method over the previous one is that it accounts for the interaction between the components and can generate a flowsheet structure by considering all possible combinations. A main drawback is that it is computationally expensive and it guarantees optimality only for the considered alternatives within the problem [Grossmann, 1985]. The following section outlines the major steps of the optimization-based approach according to [Chen and Grossmann, 2017].

2.6.2 Superstructure Modeling

The method starts by representing the set of considered processes as a superstructure which is then formulated as a mathematical programming model. To find the optimal design which consists of the set of selected processes and their configuration, the model is solved using an optimization algorithm [Chen and Grossmann, 2017]. The superstructure model is formulated using linear and non-linear equations that include continuous and binary variables as shown below:

$$
\begin{aligned}
min \quad & z = f(x,y) \\
s.t. \quad & h(x,y) = 0 \\
& g(x,y) \leq 0 \\
& x \in X \subseteq R \\
& y \in 0,1
\end{aligned}
$$

Operating conditions such as heat and pressure are modeled using continuous variables x. The design specifications and operating conditions are incorporated in the model as equality constraints h. Equipment and their interconnections are selected using discrete variables y which are assigned a value of 1 in case the unit is selected and 0 otherwise. Because of this feature, the superstructure model is a mixed integer problem. Inequality constraints g represent variable bounds and system limitations such as equipment capacity. The model aims to maximize or minimize the objective function z. Based on the nature of the problem, the objective function and/or the constraints may include non-linear terms hence the problem is known as Mixed Integer Non-Linear Programming [Chen and Grossmann, 2017]. Moreover, optimization problems in which the objective functions or constraints rely on the solution of differential equations with certain initial values are known as dynamic optimization problems [Fu and Tian, 2021].

2.6.3 Water Treatment Synthesis

In water treatment synthesis, superstructure modeling has been adopted to find the optimal process configuration for various sources of water including seawater [Koleva et al., 2015], industrial wastewater from chemical plants [Zhu et al., 2017] or oil refinery [Iqbal et al., 2022]. The desalination of seawater aims at reducing the total suspended solids [Koleva et al., 2015, Zhu et al., 2017], total dissolved solids [Koleva et al., 2015] and boron [Koleva et al., 2015], while in case of industrial wastewater treatment, additional contaminants are considered which are chemical oxygen demand [Iqbal et al., 2022], ammonia [Zhu et al., 2017, Al et al., 2020]

and phenol [Zhu et al., 2017]. Various treatment processes are used for each type of source and contaminant. For example coagulation-flocculation [Koleva et al., 2015, Zhu et al., 2017], sedimentation [Koleva et al., 2015, Zhu et al., 2017], dissolved air flotation [Koleva et al., 2015, Zhu et al., 2017], multi-media filtration, microfiltration, ultrafiltration, nanofiltration, reverse osmosis [Koleva et al., 2015, Zhu et al., 2017] and activated sludge [Al et al., 2020]. These works employed an optimization-based method to design and optimize the flowsheet of the treatment process which resulted in a superstructure model aiming at minimizing the cost of the system [Koleva et al., 2015, Al et al., 2020, Iqbal et al., 2022]. Although the superstructure model is usually formulated as a mixed-integer nonlinear programming problem [Koleva et al., 2015, Zhu et al., 2017, Al et al., 2020], the model proposed by [Deng et al., 2018] was formulated as a non-linear problem and [Bozkurt et al., 2015] as a mixed-integer linear problem.

Process synthesis of produced water has also been investigated but to a lesser extent compared to other sources of water. [Onishi et al., 2017b] and [Carrero-Parreño et al., 2019] employed superstructure modeling to optimize the design of a treatment system with a main treatment unit. In the case of [Onishi et al., 2017b], the goal of the superstructure model is to find the number of effects in a Multi-Effect Evaporator/Mechanical Vapour Recompression system that results in the minimum capital and operating cost of the system. Similarly, [Carrero-Parreño et al., 2019] optimized the design of a multistage membrane by optimizing the equipment sizing and operating conditions. Both works applied the proposed models to shale gas produced water aiming at reducing the salinity of the stream. In the case of [Onishi et al., 2017b], the problem was formulated as a mixed integer nonlinear programming model where the number of selected effects is decided using binary variables. [Carrero-Parreño et al., 2019] model does not include binary variables so it is formulated as a non-linear programming problem.

Unlike [Onishi et al., 2017b] and [Carrero-Parreño et al., 2019], [Carrero-Parreno et al., 2017] and [Bagheri et al., 2018] included more treatment units in their superstructure models and aimed and removing various contaminants. [Bagheri

et al., 2018] addressed the stream coming from the oil and gas industry targeting different destination requirements for oil and grease, total suspended solids, and total dissolved solids. The treatment stages include pre-treatment, secondary, and final treatment with various technologies assigned to each stage. The problem is formulated as a mixed integer nonlinear programming model with the objective function of minimizing the total annualized cost of the system. A main drawback in the [Bagheri et al., 2018] model is that it does not account for the impact of units' sizing on the removal efficiency and unit cost. The study assumed the fixed cost, removal efficiency, and sludge production rate of each unit.

The superstructure model proposed by [Carrero-Parreno et al., 2017] addressed additional contaminants in Shale Gas produced water which are total organic carbon, calcium, magnesium, and baron for the pre-treatment of the produced water. The model considered different final destinations but with different sources of produced water. The model is formulated as a mixed-integer nonlinear programming problem aiming at minimizing the total cost of the treatment system that consists of a train of units assigned to different stages. The mathematical formulation of the problem accounts for the equipment sizing and its impact on the system cost. The limitation of this work is that the removal efficiency and sludge production rate of the units are assumed to be parameters and not functions of the unit sizing.

The previous applications of an optimization-based approach to process synthesis mainly emphasize the economic aspect as the only evaluation criterion. However, this proves insufficient considering the complex nature of design problems. Given that design problems involve multiple conflicting objectives, beyond economic considerations, the next section outlines the key differences between single and multi-objective optimization problems, particularly in the context of design problems related to produced water treatment.

2.7 Multi-objectives Optimization

2.7.1 Non-Dominated Solution Set

Unlike single-objective optimization problems, multi-objective optimization generates a set of optimal solutions that trade-off between conflicting objectives. The multi-objective optimization aims to construct a curve of non-dominated solutions in the solution space. The solution is said to be non-dominated if it can not improve one objective without worsening another one because every solution represents a trade-off between multiple objectives and there is no single solution in the space that is considered superior to others. Therefore, the best solution is subjective and depends on the preferences of the designer/decision-maker [Coello, 2006]. Figure (2.1) illustrates the non-dominated solution set curve which lies between the extreme solutions generated by optimization one objective at a time.

The general form of multi-objective optimization is expressed as follows [Ngatchou et al., 2005]:

$$\min \qquad Z = [f_1(x); f_2(x); ..f_n(x)] \tag{2.6}$$

subject to

$$h(x) = 0 \tag{2.7}$$

$$g(x) \leq 0 \tag{2.8}$$

$$x \in X \tag{2.9}$$

where Z is the vector of objective functions f, h are the equality constrain, g are the inequality constraint, x is the vector of the design variables in the space X.

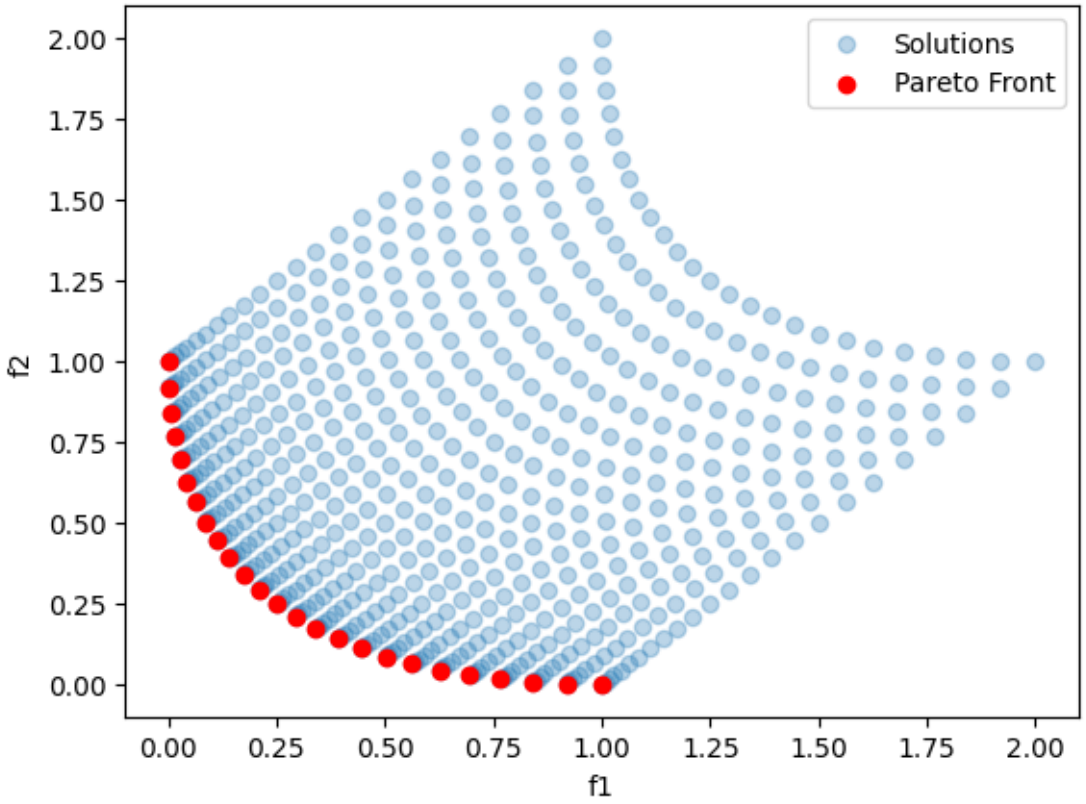

Figure 2.1: *Solution space of multi-objective optimization problem showing the set of non-dominated solutions in red and the dominated solutions in blue where f_1 is the first objective and f_2 is the second objective [Alarcon-Rodriguez et al., 2010]*

.

2.7.2 Solution Methods

2.7.2.1 Deterministic

The first method is called the classic in which the objective functions are aggregated into a single objective or convert one of the objectives into a constraint. These methods are ideal for problems where the decision maker's preference is known before solving the problem. The preference is used as a parameter to find a single solution or varied for each optimization run to generate the non-dominated solution set [Zitzler, 1999]. These methods are not suitable for non-convex problems or discontinuous problems. The following paragraphs detail these methods.

Weighted Sum: The problem is converted into a single objective by combining all objectives in one function with a weight assigned to each. The weight

represents the importance of the objective for the decision-maker. Solving the problem with the given weight results in a single solution. To generate the non-dominated solution set, the weights are changed incrementally and a new solution is obtained. Equation (2.10) shows the general form of the weighted sum method.

$$\text{Min} \qquad Z = \sum_{j=1}^{N} w_j f_j(x) \tag{2.10}$$

where

$$w_J \geq 0$$

and

$$\sum_{j=1}^{N} w_J = 1$$

Although this method is simple, it is limited in its effectiveness for non-convex problems because changes in the non-dominated solution set cannot be captured [Coello, 2000, Deb, 2001]. This is due to the fact that the linear combination of weights assigned to the objectives cannot generate points in the non-convex regions of the Pareto front, thus failing to capture all optimal solutions [Ghane-Kanafi and Khorram, 2015].

Goal Programming: In this method, for N number of objectives, the target of each objective along with its priority w are provided by the decision maker which is used as inputs to Equation (2.11) [Xiujuan and Zhongke, 2004]:

$$\text{Min} \qquad Z = \sum_{j=1}^{N} w_j |f_j(x) - T_j| \tag{2.11}$$

Equation (2.11) aims at minimizing the difference between the actual value of the objective function f_j and its target T_j.

ε-Constraint: In the epsilon constraint method, the problem is reformulated by converting one objective into a constraint bounded by ε. similar to the previous methods, the value of ε is varied to obtain the non-dominated solution set [Xiujuan and Zhongke, 2004].

Once formulated as a single objective problem, the methods applied to obtain the solution depend on the type of the problem which are: Linear Programming, Mixed Integer Linear Programming, Non-Linear Programming, Mixed Integer Non-linear Programming, and Dynamic Optimization.

2.7.2.2 Evolutionary Algorithms

Evolutionary algorithms are stochastic methods inspired by the natural evolution process in biology. These algorithms are based on two main principles: selection and variation. Just as in nature, higher-quality solutions are more likely to reproduce than lower-quality ones. Evolutionary algorithms involve randomness at various stages of the search process, making them stochastic. The process begins with a randomly initialized population to ensure diverse starting points. Mutation and crossover are then used to introduce random changes or combine existing solutions to generate new ones. In these algorithms, solution quality is measured by a value called fitness, which varies with each algorithm. The fitness value determines which solutions advance to the next iteration, with higher values indicating higher quality. Variation refers to the ability to discover new solutions by recombining fit solutions [Zitzler, 1999]. Although all Evolutionary algorithms share a common structure, they differ in how fitness is calculated, leading to different rankings of solutions. The following list briefly describes the fitness calculation methods for selected Evolutionary algorithms.

Multi Objective Genetic Algorithm: The fitness of a given solution is proportional to the number of solutions it dominates [Murata and Ishibuchi].

Non-dominated Sorting Genetic Algorithm: Solutions are classified according to their dominance. The non-dominated solutions are given a value higher than that assigned to the dominated solutions. Additionally, each solution is assigned a value called crowding distance which measures how the solutions are crowded or spaced in the solution space. The fitness value combines both the non-dominance sorting and the crowding distance and the solution [**?**].

Niched Pareto Genetic Algorithm: Two solutions are selected and each is com-

pared to a set of solutions that represents 10% of the whole population. If the solution is found to be non-dominated while the other is not, the former is chosen. However, both solutions might be dominated, therefore, depending on how similar they are, they receive a penalty that affects their fitness values and the algorithm will re-choose the solution with better fitness. In case both are non-dominated, the niching mechanism is applied which favors the more diverse solution or the one that occupies a different region in the search space [Horn et al., 1994].

Strength Pareto Evolutionary Algorithm: The algorithm starts by comparing the initial solutions in the population with each other and keeping the non-dominated ones in the archive. After the evolution process, any new solution is compared to the archive and it replaces the solution that it dominates. The strength of the solution is found by summing up the number of solutions it dominated. The fitness in this case is based on the strength value. The higher the strength the higher the fitness [Zitzler and Thiele, 1998].

Multi Objective Particle Swarm Optimization: The problem starts with a set of solutions (particles) moving in the direction of the initial optimum solution. The algorithm evaluates all particles according to their current position. Each particle has a best position which represents the minimum objective evaluation it has achieved within this iteration. The best position of all particles is compared to each other and the global best position is identified which is considered the new optimum solution. In the next iteration, all particles adjust their velocity toward the Gbest and the algorithm reevaluates the new position again to generate a new Pbest and then Gbest. The process continues till a termination criterion is met [Kennedy and Eberhart, 1995].

Evolutionary algorithms also incorporate an important aspect: maintaining a balance between exploration and exploitation, which prevents them from getting stuck in local optima. During exploration, the algorithm searches the neighborhood to refine existing solutions through crossover and mutation. Exploitation, on the

other hand, involves seeking solutions in new regions, accomplished through selection. Excessive exploration may cause the algorithm to become trapped in local minima, while excessive exploitation could waste time on poor solutions. [Pytel, 2020]. Hence, balancing these two processes is vital for effective optimization.

The main advantage of Evolutionary algorithms over deterministic methods is their ability to generate a non-dominated solution set by optimizing all objectives concurrently in a single run which makes them a better option for multi-objective optimization problems. However, their main drawbacks are they are computationally expensive and inability to guarantee global optimality [Maier et al., 2019]. Their parameters such as the number of solutions to propagate and the number of generations need to be tweaked to tailor the problem. Also, their performance is degraded with higher dimensions [von Lücken et al., 2019]. Another challenge that faces the use of these methods is to direct the search for the non-dominated solution set and how to prevent the algorithm from getting stuck in one region which leads to a less diverse population [Kazimipour et al., 2014].

Compared to deterministic methods, evolutionary algorithms are less sensitive to initialization. However, starting with a good initial population can facilitate finding the solution. On the other hand, with bad initialization, it might not be possible to find a solution, especially with large-scale optimization problems [Kazimipour et al., 2014].

2.7.2.3 Dynamic Optimization Solutions

Before solving dynamic optimization problems, they are typically reformulated using three main methods: variation, partial discretization, and full discretization [Biegler and Grossmann, 2004]. In the variation method, a new function, denoted as F, is constructed to encapsulate the behavior of the original objective function over the time domain. The derivative of F with respect to t is then found, and the resulting equation can be solved using either deterministic or stochastic methods.

Alternatively, partial discretization involves discretizing only the time domain of the differential equation, while the other variables remain continuous. On the other hand, full discretization discretizes the time interval, and the other variables

are approximated by piecewise continuous functions between these time intervals. Once the problem is reformulated, it can be solved using either a deterministic or stochastic approach.

2.7.3 Multi-objective Optimization of Produced Water Treatment

In the area of produced water multi-objective design, the available works consider the trade-off between objectives for a single processing unit. A study by [Onishi et al., 2021], proposed a new multi-objective optimization model for the treatment of shale gas produced water by single/multiple-effect evaporation systems with mechanical vapor re-compression. The model aimed to improve the system's economic and environmental performance. In this model, the economic objective function consisted of system capital and operational cost while the environmental impact was quantified using the Life-Cycle Assessment method. The model is formulated as a multi-objective non-linear programming problem and implemented in General Algebraic Modeling System (GAMS) [GAMS, 2024] using the epsilon method.

In the case of [Carrero-Parreño et al., 2017], the objectives are total annual cost and its variability, controlled by the worst-case risk management metric. The model was solved using the sample average approximation method which decomposes the original problem into a mixed integer non-linear programming model and a stochastic non-linear programming model. In [Salcedo-Díaz et al., 2017] and unlike the previous works, forward osmosis was combined with reverse osmosis to treat hyper-saline produced water and flow back water generated during shale gas production. The first objective function is the total annualized cost minimization while the second one is the minimization of freshwater consumption. The model was solved using the epsilon constraint method.

The above observations show a scarcity of research on the multi-objective optimization of produced water treatment. Existing studies concentrate exclusively on the desalination stage of produced water treatment, neglecting other treatment stages. Furthermore, in contrast to the synthesis of other water sources, which often involves considering trade-offs between objectives, as seen in the work by [Kol-

eva et al., 2016], there is currently no research addressing similar trade-offs in the context of produced water treatment.

2.8 Literature Gap

As evidenced above, numerous works have been published regarding the modeling of produced water treatment. However, previous applications of an optimization-based approach to process synthesis have mostly emphasized the economic aspect as the sole evaluation criterion, proving insufficient given the complex nature of design problems. The observations indicate a lack of research on the multi-objective optimization of produced water treatment, with existing studies only focusing on the desalination stage and overlooking other treatment stages. Notably, there is a lack of research addressing trade-offs in the context of produced water treatment. Additionally, while Population Balance Equations have been widely applied to model the impact of droplet size distribution in produced water treatment, a significant portion of the literature primarily centers on single-unit models, disregarding the fact that produced water undergoes treatment across multiple stages. The existing literature lacks a comprehensive study proposing a framework for multi-objective optimization in produced water treatment that considers the influence of particle/droplet size distribution. The gaps identified in the literature motivated the contribution of this thesis as outlined below.

2.9 Contributions

The proposed model in this research is based on the work of [Bagheri et al., 2018]. The following functionalities have been added to overcome the simplicity of the original model and to increase its generalization and applicability:

- Detailed models of the processing units are developed to quantify the impact of unit sizing on different system components such as capital cost, sludge production, and unit removal efficiencies and hence the system's overall performance.

- The impact of the change in contaminants droplets and particle size distri-

bution on the system performance is captured by incorporating the breakage and coalescence/aggregation phenomena of droplets and particles into the unit models using Population Balance Equations.

- To quantify the change in the particle/droplet size distribution on the model performance, a discrete formulation of the volume distribution was developed to generate the initial size distribution, based on the initial contaminants concentration, and to capture the volume transformation between the discrete volume classes due to the breakage and coalescence/aggregation phenomena.

- Units' removal efficiencies are modeled as continuous variables and as a function of the unit's design variables. The removal efficiency is based on the minimum droplet/particle size that can be removed by the unit which makes it a function of the change in the droplet/particle size distribution.

- A new model is developed to quantify the sludge production of the processing unit based on the unit's removal efficiency and the flowrate characteristics.

- Sludge handling is modeled as a discrete variable to choose the best option from a set of sludge handling options. The cost and environmental impact of the selected option are quantified based on the amount of Dry Matter generated by the system which is modeled as a continuous variable and as a function of the produced sludge.

- A multi-objective optimization framework is designed with the objectives of minimizing the system's total annualized cost and its environmental impact which is quantified by estimating the CO_2 emission of different system components.

Chapter 3

Methodology

3.1 Introduction

The objective of this research is to identify an economically and environmentally efficient design for a Produced Water treatment process that satisfies the quality standards of its final destination. Achieving the optimal design involves selecting and sizing treatment units from a predefined set of technologies, considering the change in the size distribution of contaminant droplets and particles. To address both economic and environmental considerations, the formulated model is structured as a multi-objective optimization. The proposed model comprises various blocks associated with treatment units, droplet/particle dynamics, treatment process, cost function, and emission function. These blocks are referred to as sub-models. The following sections provide a detailed description of the proposed model and the methods employed to solve it.

3.2 Model Development

3.2.1 Population Balance Modeling

A distribution is typically described by a continuous function. However, for design, we consider a discrete formulation based on a logarithmic discretization of the space (droplet/particle volume). This discretization is characterized by minimum and maximum diameters and a specified number of classes. The continuous distribution, typically described by a normal distribution with mean (μ) and standard

deviation (σ), is mapped to discrete space by the number of droplets present for any volume class size.

The Droplet/Particle Size Distribution does not remain constant during the treatment process due to breakage and coalescence phenomena. The mechanism behind these phenomena varies depending on the type of flow. These mechanisms do not occur in isolation of each other but they interact and overlap. Since there is no single model that captures the effect of multiple mechanisms, selected models have been adopted in this work as listed in Table (3.1) with their mathematical models detailed in Chapter (5).

The total volume of the contaminant is distributed among the n discrete volume classes in the space. The volume of the contaminant per class is determined by summing the volumes of all individual droplets/particles in that class. This can be calculated by multiplying the number of droplets or particles in the class by the volume of a single droplet or particle in that class. Since the size of the droplets or particles in each class is known from their diameter, the volume of a single droplet or particle can be calculated. Therefore, the total volume of the contaminant in the continuous phase is defined by the volume of a single droplet or particle in each class and their respective number.

The total volume of droplets is approximately conserved using discrete population balance equations. These equations capture the exchange of the volume between the discrete classes using birth and death rate equations, corresponding to the breakage and coalescence phenomena. Due to the discrete nature of the representation, in case of coalescence/aggregation, the number of new droplets of a given volume is distributed to two neighboring volume classes to ensure that the total volume overall remains approximately constant as shown in Figure (3.1).

Given the logarithmic discretization of the droplet/particle volume space, the space is discretized into n number of classes with c_i representing the class number within the space and ii and k are aliases of i. Upon coalescence/aggregation of n_i and n_{ii}, number of droplet/particle of volume v_i and v_{ii}, n_{i+ii} number of droplets/particles of volume v_{i+ii} are born. To ensure the conservation of the total contaminant vol-

Table 3.1: Breakage, coalescence, and aggregation kernels of droplets/particles in laminar and turbulent flow for selected mechanisms

Phenomena	Classification	Flow Type	Mechanism	Reference
Breakage	Droplets	Laminar	Not Applicable	Not Applicable
		Turbulent	Turbulent fluctuation and collision-drop energy	[Coulaloglou and Tavlarides, 1977, Liao and Lucas, 2009b]
	Particles	Laminar	Flow Shear-Exponential	[Jeldres et al., 2018]
		Turbulent	Flow Shear-Exponential	[Jeldres et al., 2018]
Coalescence	Droplets	Laminar	Velocity gradients and film drainage	[Friedlander, 2000, Prince and Blanch, 1990, Liao and Lucas, 2010b]
		Turbulent	Turbulent collisions and film drainage	[Prince and Blanch, 1990, Liao and Lucas, 2010b]
Aggregation	Particles	Laminar	Brownian motion, differential sedimentation and flow shear	[Song et al., 2018, Camp, 1943, Saffman and Turner, 1956, Abrahamson, 1975]
		Turbulent	Flow Shear	[Song et al., 2018, Abrahamson, 1975]

ume within the space, the total volume of the new droplets/particles $n_{i+ii}v_{i+ii}$ is distributed among class c_k and c_{k+1} such that:

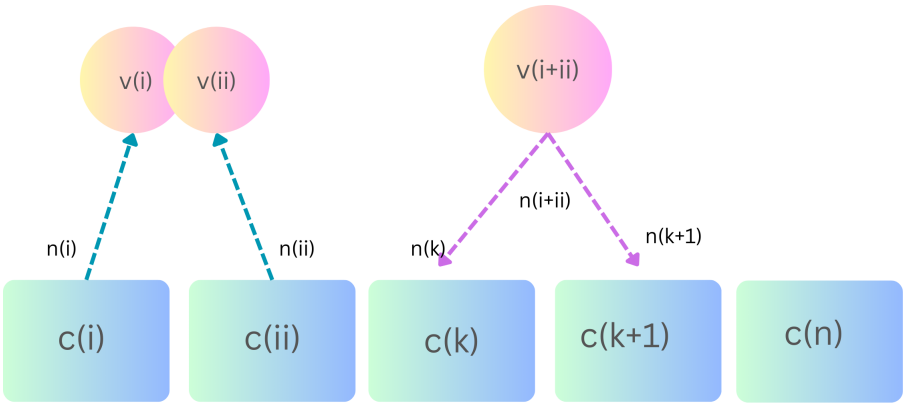

Figure 3.1: *Diagram showing the volume distribution of the new droplets/particles between the classes as a result of coalescence/aggregation. c_i represents the class number within the space and ii and k are aliases of i with n is the largest class. n_i is the number of droplets/particles of volume v_i.*

$$v_k < v_{i+ii} < v_{k+1} \tag{3.1}$$

$$n_{i+ii} = n_k + n_{k+1} \tag{3.2}$$

$$n_{i+ii} v_{i+ii} = n_k v_k + n_{k+1} v_{k+1} \tag{3.3}$$

In case of breakage, the volume of a single droplet/particle is distributed uniformly to all smaller classes in the discrete space as shown in Figure (3.2). Given n number of classes, upon breakage of a droplet/particle from class c_{i+3} with a volume of v_{i+3}, its volume is distributed uniformly into all the classes smaller than c_{i+3}.

3.2.2 Flowsheet Simulation

To find the best process configuration, the model takes the initial process parameters: the number of discrete volume classes of contaminants n_c, the mean and standard deviation std of the volume distribution. These parameters are used to generate the initial volume distribution of contaminants within the volume space. The other parameters are the initial feed flow rate of produced water ($Q_{initial}$), and

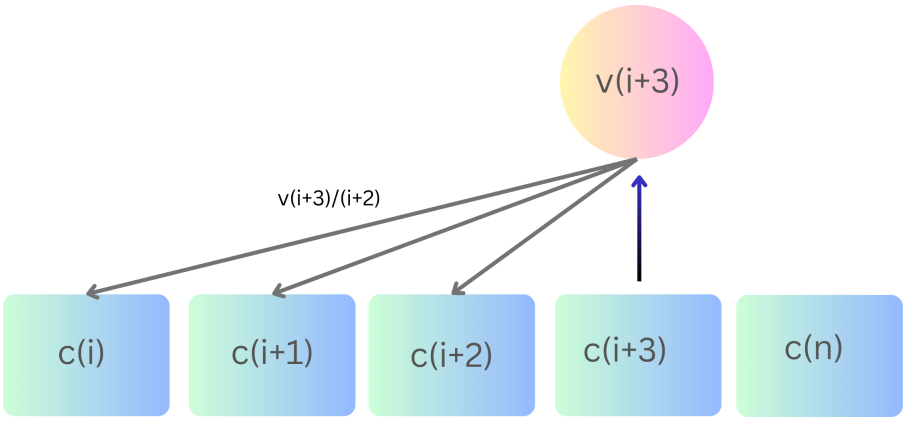

Figure 3.2: *Diagram showing the volume distribution of the new droplets/particles between the classes as a result of breakage. c_i represents the class number within the space and ii and k are aliases of i with n is the largest class. n_i is the number of droplets/particles of volume v_i.*

the initial concentration of contaminants ($C_{initial}$). Additionally, it considers the design variables: the sequence of the technologies in the process *sequence*, the number of treatment steps in the sequence n_{steps}, and a sludge handling option (slg), along with the unit's specific design variables. The first unit in the sequence receives the initial flow rate ($Q_{initial}$), contaminants' concentration ($C_{initial}$), and droplet/particle volume distribution. For each unit in the sequence, the design variables are used to calculate quantities that are passed to the various sub-models in Figure (3.3). This figure illustrates the different sub-models within the unit level that calculated the different quantities of the system cost and emission. These quantities include the unit's volume, residence time, area, and cut diameter. All sub-models in the figure represent the unit level except for the Number and Volume Generator, Population Balance Equations, and Separation sub-models, which represent the droplet/particle level.

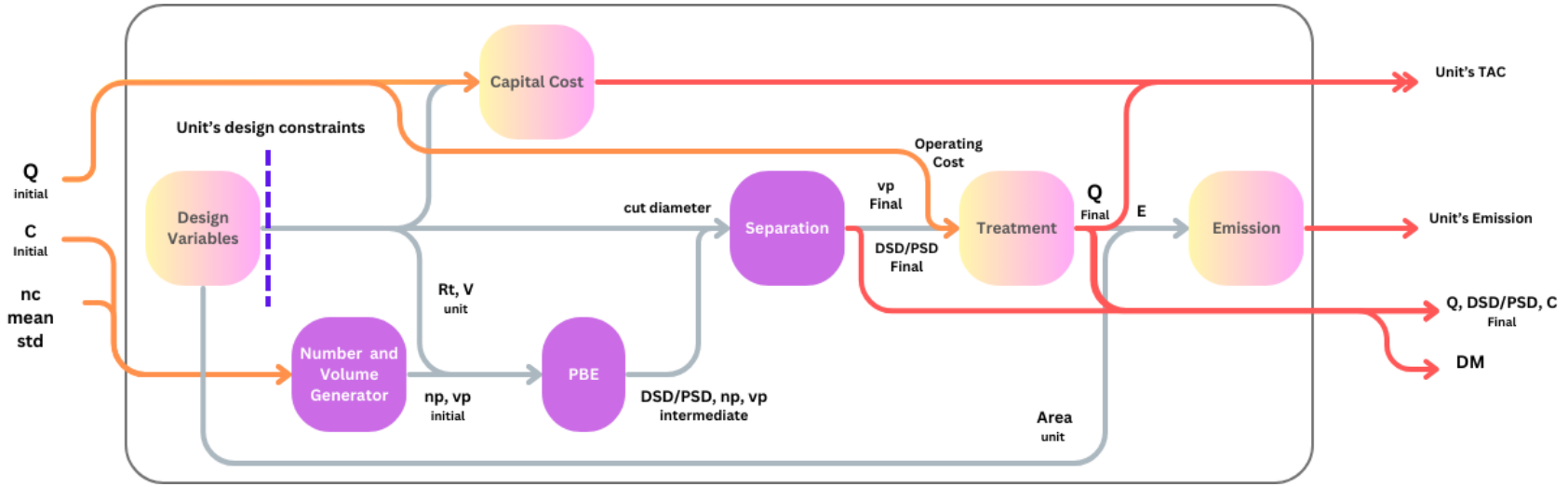

Figure 3.3: *A diagram showing the relations between sub-models representing the unit level where Q is the flowrate, C is the contaminant concentration, n_c is the number of discrete volume classes, $mean$ is the mean of the droplet/particle diameter, std is the standard deviation of droplet/particle volume distribution in the space, Rt is the residence time, V is the volume, DSD/PSD is the droplet/particle size distribution, n_p and v_p are the number and volume of particles/droplets, q_g is the gas flowrate, $Area$ is the area of the unit the requires cleaning, E is the energy consumption, DM is the amount of dry matter, TAC is the total annualized cost. The sub-models in purple represent the droplet/particle level sub-models.*

For the droplet/particle level, the Number and Volume Generator sub-model takes the initial concentration of contaminants and the initial distribution of droplets/particles, which are passed to the unit as input parameters. It returns the initial volume distribution of contaminants among the given number of classes ($vp_{initial}$) and determines the initial number of droplets/particles in each class ($np_{initial}$). These outputs, along with the unit's volume and residence time (determined using the unit's design variables), are passed to the population balance equations sub-model. The volume of the unit is used to calculate the breakage and coalescence rates of the droplets and particles (Ω_B and $\Omega_{C/A}$). Figure (3.4) shows the interactions between the breakage and coalescence/aggregation sub-models and differential equations within the population balance equations sub-model to update the number of droplets/particles within the classes and hence update the volume distribution of contaminants.

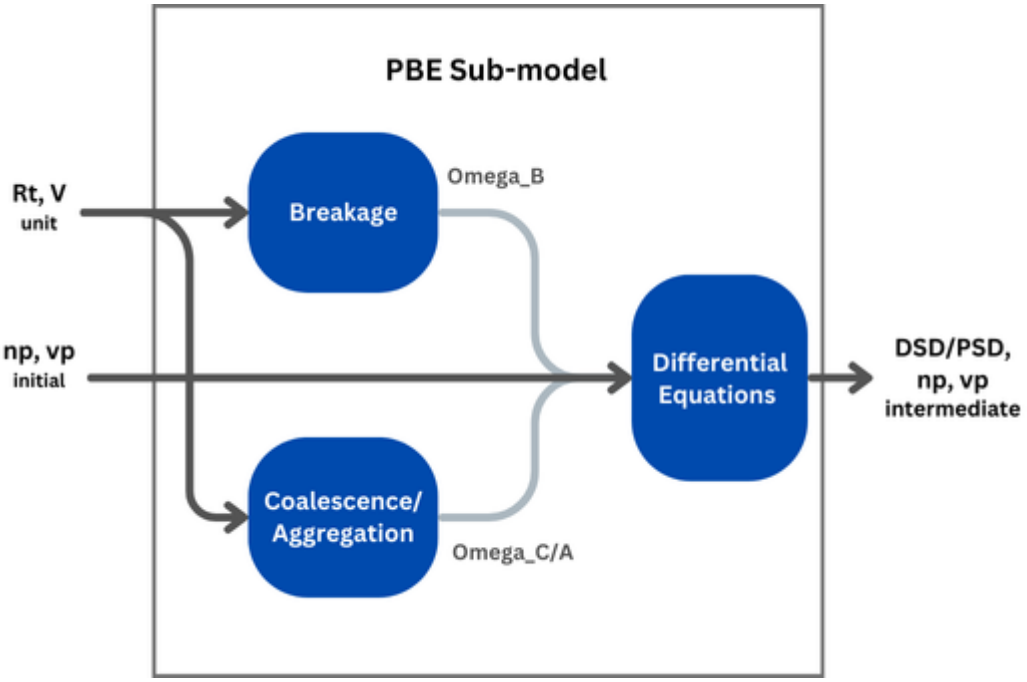

Figure 3.4: *Flow Diagram showing the dynamics within the population balance equations model which includes three sub-models; Breakage, Coalescence/Aggregation, and differential equations where n_p is the particles/droplets number, $Omega_B$ and $Omega_{C/A}$ are the breakage rate and coalescence/aggregation rate, Rt is the residence time, V is the volume of the unit, n_p and v_p are the number and volume of particles/droplets in each class.*

To find the change in the number of droplets/particles over time, the ordinary differential equations within the population balance equations sub-model use the initial number of droplets/particles from the Number and Volume Generator sub-model. They also use the breakage and coalescence rates as parameters and the unit's residence time as the time span for the differential equations. The population balance equations sub-model returns the updated number of droplets/particles in each volume class after considering the impact of breakage, coalescence, and aggregation. Based on these numbers, the updated volume distribution is found along with the updated number of droplets/particles and contaminant volume per class. The outputs of the population balance equations sub-model are then passed to the Separation sub-model, which performs the separation based on the cut diameter of the unit, a design variable. The outputs from the population balance equations sub-model in Figure (3.3) are referred to as 'intermediate' to distinguish them from the 'final' values that result after the separation process.

At the unit level, the capital cost sub-model calculates the capital cost using the flow rate and unit design variables, adjusting to the 2023 value. The operating cost and emissions are calculated through the Treatment and Emission sub-models. The Treatment sub-model uses the final contaminant volume distribution from the Separation sub-model to calculate the output concentration of contaminants, output flow rate of produced water, energy consumption of the unit, amount of dry matter generated by the unit, and the unit's operating cost. The latter is combined with the capital cost to form the unit's total annualized cost. The energy consumption and the produced water output flow rate are then passed to the Emission sub-model to determine the unit's emissions.

At the process level, the interactions between the unit and droplet/particle levels are repeated for each unit in the sequence. Figure (3.5) shows the link between the model input parameters, processing units, sludge handling, and the model outputs and how the n_{tech} number of technologies assigned to the steps within the process configuration. The units are interconnected by passing updated values of flow rate, contaminant volume distribution, and contaminant concentration from one unit

to the next. The capital and operating costs, emissions, and dry matter are accumulated across all units in the sequence to provide totals for a given sequence. These values are represented by the blue shape in Figure (3.5). The total dry matter is then passed to the selected sludge handling option, where the cost and emission of the sludge handling are calculated and added to the total unit costs and emissions, resulting in the total annualized cost and environmental impact of the system.

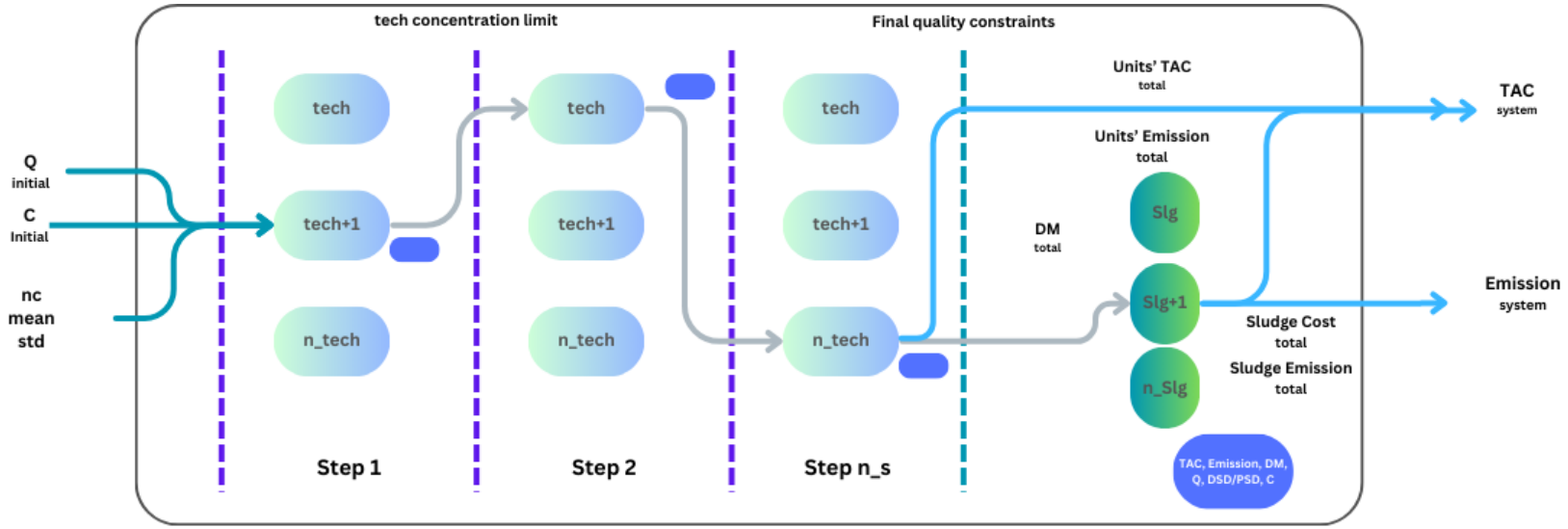

Figure 3.5: *Diagram showing the link between the model input parameters, processing steps, sludge handling, and model outputs, highlighting the flow of calculated quantities between the steps. Arrows indicate the flow of data and water stream between the units, while dotted lines represent constraints related to design variables and final quality constraints. In the diagram, tech represents a technology or processing unit, Q is the flowrate, C is the contaminant concentration, n_c is the number of volume classes, mean is the mean of droplet/particle diameter within the volume space and std is the standard deviation, slg is the sludge handling option, DM is the amount of dry matter, and TAC is the total annualized cost.*

The total annualized cost of the system TAC_{system} and system total emission $Emission_{system}$, along with any constraint violations, are returned for a given design. Constraints are related to the upper and lower bounds of the design variables, the maximum allowable inlet concentration of contaminant for each technology, and the final contaminant concentration levels, which must meet the requirements of the produced water's final destination, are represented by the vertical dotted line in Figure (3.3 and 3.5). By evaluating different flowsheets, those with the lowest cost and emissions and meet the model constraints are identified as part of the non-dominated solution set. The selection process for the best solutions using the Fresa solver is detailed in Chapter (3).

The solver proposes a sequence that includes all units in different positions within the process, using the n_{step} variable to determine the number of steps that are included in the process. For example, the solver proposes a sequence that includes all the available technologies using the *sequence* variable which assigns technologies to steps and then decides how many steps are needed from that sequence using the n_{step} variable. As shown in Figure (3.5), at the first step, any available technology can be assigned. For the remaining steps, technologies already assigned in previous steps cannot be reused. This constraint, along with the non-linear relationships within the cost and unit models, classifies the problem as mixed integer non-linear programming. Additionally, the presence of ordinary differential equations necessitates a dynamic optimization approach, making the model a Mixed Integer Dynamic Optimization problem.

3.2.3 Multi-objectives Optimization

Two objective functions are identified to assess the performance of the system: Total Annualised Cost per year and the Environmental Impact per year. The values of the objective functions are estimated as follows:

Total Annualized Cost: It consists of the total cost of building and running the system for one year which is cascaded down to capital and operating costs. The initial capital cost of the purchased equipment is estimated according to 2010 data and then scaled up to 2023. The operating cost of each unit con-

sists of the following components: cost of energy and cost of chemicals in addition to specific technology-related costs such as the cost of gas in the case of and the cost of cleaning and back-washing in the case of Nutshell filters and Microfiltration membrane. Another cost component that contributes significantly to the process operating cost is the cost of the sludge handling option.

Environmental Impact: It is measured by summing up the CO_2 emitted from the system as a result of the unit's operations and sludge handling. The considered sources of CO_2 emitted in this study are the energy consumption, use of chemicals for unit operation and cleaning, use of fresh water, and use of methane to operate induced gas flotation in addition to the emission from the sludge disposal.

In addition to the objective functions, the problem is bounded by technical constraints related to unit dimensions and inlet flow concentration limits of contaminants which are detailed under each unit's model in Chapter (4).

3.3 Problem Description

According to the above, the design problem can be formulated as follows:

Assumptions: In addition to the assumptions showed in Chapter (4 and 5) for each sub-model, it is also assumed that two contaminants to be removed from the produced water stream which is *Oil and Grease* ($O\&G$) and *Total Suspended Solids* (TSS).

Given the input parameters: In addition to the cost and emission data in Appendix (A), the following are the main model parameters that will vary to create different case studies:

- Correspondent minimum and maximum logarithmic values of the droplet/particle volume- $\log V_{cont}^{min}$ and $\log V_{cont}^{max}$. They represent the minimum and maximum volume of droplets/particles in the water stream.

- Number of the discrete volume classes of the contaminants droplet/particle in the volume distribution (n_c).
- Mean μ and standard deviation σ of the droplet/particle volume distribution of contaminants in the feed flow rate.
- Initial inlet mass flow rate of the produced water stream in ton/hr (Q).
- Initial concentration of the contaminants ($cont$) in the initial produced water stream in mg/L (C^{in}_{cont}).
- Final concentration of the contaminants ($cont$) in the produced water stream that needs to be achieved by the treatment system in mg/L (C^{f}_{cont}).

The pool of technologies includes the following units: Horizontal Separator, also known as American Petroleum Institute (API) separator, Corrugated Plates Interceptor (CPI), Hydro-cyclone (HC), Induced Gas Flotation (IGF), Nutshell Filter (NF), Centrifuge separator (CF) and Micro-filtration membrane (MF). The working principles of these units are explained in Section (2.3) and their mathematical models can be found in Section (4.2). The sludge handling options are machine thickening, machine thickening and incineration, and machine thickening and melting.

Determine the design variables: The design problem aims to determine the sequence of treatment technologies, the number of stages, the values of the design variables for each technology, along the sludge handling option. The design variables are listed in Table (3.2).

Subject to constraints: The constraints are classified into three categories which are:

- Unit-specific constraints related to the units' dimensions that can be found in Section (4.2).
- Upper and lower bounds of the design variables. Refer to the constraints section under each model in Chapter (4).

Table 3.2: List of the optimization problem design variables

Design Variable	Description
$CD_{API,OnG}$	Cut diameter of Oil & Grease ($O\&G$) by American Petroleum Institute (API) separator in μm
d_{API}	Depth of the American Petroleum Institute (API) separator in m
w_{API}	Width of the American Petroleum Institute (API) separator in m
$CD_{CPI,OnG}$	Cut diameter of Oil & Grease ($O\&G$) by Corrugated Plate Interceptors (CPI) in μm
L_{CPI}	Length of the Corrugated Plate Interceptors (CPI) plate in m
w_{CPI}	Width of the Corrugated Plate Interceptors (CPI) plate in m
h_{CPI}	Distance between Corrugated Plate Interceptors (CPI) plates in m
n_{HC}	Number of parallel hydro-cyclones (HC)
d_{HC}	Diameter of the hydro-cyclone (HC) in m
n_{IGF}	Number of Induced Gas Flotation (IGF) cells
r_{IGF}	Radius of Induced Gas Flotation (IGF) cell in m
h_{IGF}	Height of the Induced Gas Flotation (IGF) cell in m
q_g	Methane gas flowrate in m^3/sec
L_{bed}	Length of the Nutshell Filter (NF) bed in m
L_{NF}	Length of the Nutshell Filter (NF) unit without the bed in m
r_{NF}	Radius of the Nutshell Filter (NF) unit in m
$r_{CF,outer}$	Outer radius of Centrifuge (CF) unit in m
L_{CF}	Length of the Centrifuge (CF) unit in m
n_{MF}	Number of Microfiltration (MF) unit
r_{MF}	Radius of Microfiltration (MF) unit in m
L_{MF}	Length of Microfiltration (MF) unit in m
slg	Sludge handling option
$sequence$	Sequence of treatment units in the configuration
n_{steps}	Number of steps in the configuration

- Final quality requirements constraints for the produced water output which represent the final level of contaminant concentration in the output stream.

So as to minimize the objective functions: The objective functions in the current model are the Total Annualized Cost (TAC) as shown in Eq.(3.4). The second objective function is the Environmental Impact (IE) Eq.(3.5) of the system.

$$\min \quad TAC \tag{3.4}$$

$$\min \quad EI \tag{3.5}$$

3.4 Model Implementation

3.4.1 Model Generalization

The model's generalization and applicability were assessed by examining its performance across different aspects. The impact of discretization of the droplets/particles volume space is assessed by running the model with different numbers of volume classes. In addition to the variation in the objective values and obtained configurations, the conservation of volume due to the discretization is also investigated. The model is assessed also for its ability to handle different process initial conditions such as the flow rate and the contamination concentrations by varying these inputs. Likewise, different droplet/particle size distributions and volume ranges are attempted.

Considering that existing breakage and coalescence models in the literature are tailored to particular mechanisms within the continuous phase, various models related to diverse droplet/particle interaction mechanisms are assessed. This aims to explore how different mechanisms affect system performance and to measure the proposed model's ability to accommodate various breakage and coalescence models.

3.4.2 Solution Methods

The multi-objectives optimization problem was solved using an evolutionary algorithm called Fresa [Fraga, 2021] which is a nature-inspired algorithm based on the propagation of strawberries. Fresa mimics the strawberry in search of soil and nutrients [Salhi and Fraga, 2011] by sending a few long runners to explore areas with more water and nutrients and more short runners to areas with more of these resources.

These two strategies are known as diversification and intensification of algorithm search. They allow the search for the optimal solutions using intensification while diversification prevents the search from being trapped at the local optimum and hence search for a global optimum solution. Due to this feature, a balance between these conflicting characteristics is important for the algorithm to succeed. Initially, the algorithm was used to solve single objective function problems and then it was extended to applications of multiple objectives [Rodman et al., 2018] which motivated using it in this study.

Fresa takes the number of iterations or cycles that will run before it terminates which is known as the number of generations. Also, it takes the number of solutions within each iteration that will be selected to reproduce new solutions for the next generation which is known as the number of solutions to propagate. At each generation, each population sends runners with termination criteria g_{max} to explore a better solution. The number and distance the runner is sent to is inversely proportional to the fitness value.

The fitness value is determined using the fitness function which helps the algorithm in evaluating and ranking solutions in a population. The ranking assigned to the solutions acts as a guide to improving solutions over generations. For a single objective function, the fitness equals the normalized and reversed value of the objective function which results in the best solution having a fitness value closer to 1 and closer to zero for the less good solution. For multi-objective problems, another method is used to calculate the fitness which is called a Hadamard product of individual criteria rankings which is computationally less expensive than the for-

mer method and results in a broader Pareto front [Salhi and Fraga, 2011, Fraga and Amusat, 2016].

$$f = 1 - \frac{I_1 \odot I_2 \odot .... \odot I_{n_c}}{n_p^{n_c}} \tag{3.6}$$

In Eq. (3.6), $\odot$ is the Hadamard product of two vectors. I_j, j = 1,... n_c, is a vector that represents the index assigned to a point based on its position when sorted according to criterion j, n_p is the total number of points, and n_c is the number of criteria. The fitness value, denoted by f and constrained to the range $[0, 1)$, indicates the quality of the solution, with higher values reflecting better fitness.

The proposed model was implemented in Julia, chosen for its proficiency in handling complex mathematical models. Julia's support for parallel computing and multiple dispatch enables the utilization of diverse function arguments [Bezanson et al., 2017, Julia Language, 2024]. Within Julia, the DifferentialEquations package was used to solve the ordinary differential equations [Rackauckas and Nie, 2017]. This method's arguments are the function to be evaluated, the problem's initial conditions, and the time span. In our case, the function is the population balance equations sub-model, with breakage and coalescence rates as function parameters. The initial condition corresponds to the initial number of droplets/particles, while the time span is defined as the unit residence time R_t. For our dynamic optimization solution, we adopted a partial discretization method, discretizing the residence time of the unit R_t while maintaining continuity for other variables.

To solve the ordinary differential equations, a composite algorithm combining two solvers is used: Tsit5 and Rosenbrock23 [Team, 2022]. Tsit5 uses a fifth-order singly diagonally implicit Runge-Kutta method, while Rosenbrock23 is based on the Rosenbrock method. Both solvers estimate the derivatives of the solutions by computing several intermediate stages within the time span. In Tsit5, the process begins with explicit methods like straightforward calculations based on known information, such as the previous solution and the derivative function. Subsequently, implicit methods refine the initial estimation obtained from the explicit method. The intermediate stages are then combined to derive the final derivative estimate at the

current time step, which is utilized for the subsequent time step. Depending on the error estimate threshold, the time step may be adjusted for the next iteration. This process repeats for each time step until reaching the end of the time interval or meeting a termination criterion [Tsitouras, 2011]. In contrast, Rosenbrock23 only uses implicit methods for stage calculation, solving the ordinary differential equations at the intermediate stage directly [Benner and Mena, 2013].

The composite algorithm employs multiple evaluation criteria to select the appropriate solver for each time step [Team, 2022]. One of these criteria is the stiffness of the problem, indicating rapid changes in one direction of space and slower changes in others. In such cases, explicit methods are unsuitable as they require small time steps to maintain accuracy. Therefore, Tsit5 may not be the optimal choice, while Rosenbrock can offer greater efficiency [Klooster, 2021, Benner and Mena, 2013]. By integrating both methods, the algorithm can adapt the step size and choose the most suitable solver based on the evolving behavior of the solution, thus leveraging the strengths of each method.

3.5 Proposed Approach

The conceptual framework adopted in this work is illustrated in Figure (3.6). The design is governed by the level of contamination concentration for the produced water final destinations. The design problem takes the number of volume classes, mean, and standard deviation to generate the initial droplet/particle size distribution along with the initial feed flow rate and contamination concentrations as inputs for the entire model.

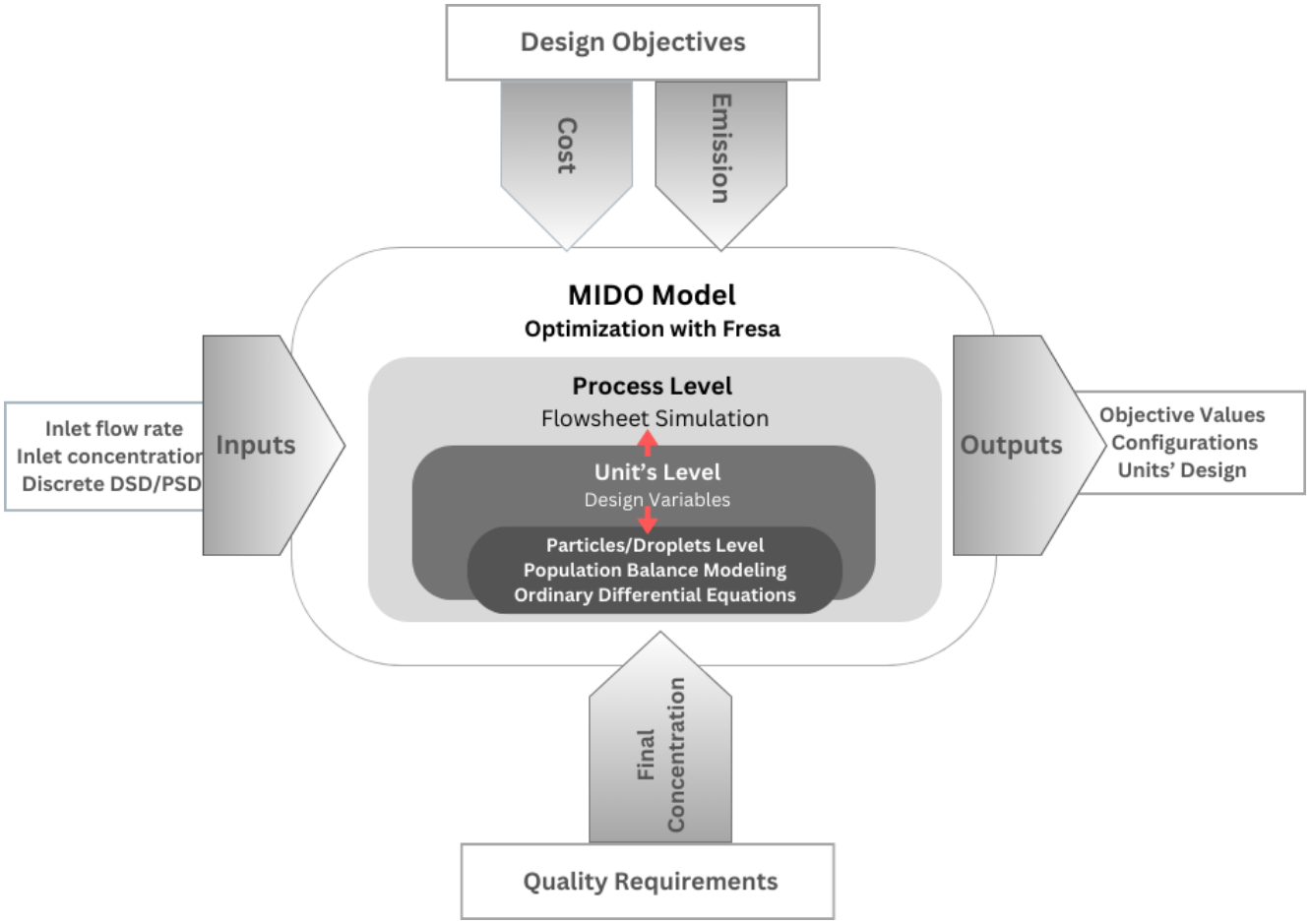

Figure 3.6: *Conceptual framework of the proposed methodology showing the interaction between the different levels of the model, process, unit, and particles in addition to the model inputs, outputs, objective functions, and the governing constraints where MIDO is mixed-integer dynamic optimization, DSD is droplet size distribution and PSD is particle size distribution.*

The interaction between the droplet/particle level and the process optimization level is illustrated through the impact of design variables on the evolution of the volume distribution of contaminants over time and the separation of droplets and particles. At the process level, the sequence of technologies within the process design, along with the values of the units' design variables, defines the breakage and coalescence rates at the particle/droplet level. These rates affect the distribution of droplets/particles within the volume classes, resulting in changes to the volume distribution of contaminants within the volume space.

The change in the volume distribution of contaminants significantly influences the performance of the units. The volume distribution within the classes, which is a function of the unit volume, and the cut diameter of the unit, which is also a function of the unit design variables, determine the volume of contaminants that will be removed by the unit. Since the unit cost and emissions are functions of the design variables, the impact of these variables on the droplet/particle level extends to the removal efficiency. This, in turn, affects the overall system cost and environmental impact. Thus, the design variables influence the evolution of droplets/particles, removal efficiency, and, consequently, the cost and emissions of the system.

The formulated model represents a mixed integer dynamic optimization problem, solved using a nature-inspired solver, Fresa. Designs are selected based on two objectives: total annualized cost and environmental impact, measured by CO_2 emission from the system. The objective functions rely on the solution of the ordinary differential equations, capturing the evolution of the contaminant droplet/particle size distribution across treatment stages. The proposed model is applied to different case studies exploring the impact of the volume space discretization, model parameters, droplet/particle breakage, and coalescence kernels.

3.6 Conclusion

This chapter presents the steps taken to develop and evaluate the model aiming to find the optimal design of the produced water treatment system. The proposed methodology combines different levels of modeling; the process level which aims

at finding the optimal value of the unit's design variables and process configuration and the droplet/particle levels where the impact of the change in the size distribution is quantified and linked to the process level. The case studies to assess the model applicability have also been discussed along with the solution methods for the ordinary differential equations and the multi-objective optimization model. The mathematical formulation of the sub-models is detailed in the following two chapters.

Chapter 4

Mathematical Formulation of Treatment Process

4.1 Introduction

In this chapter, the mathematical formulation of all treatment processes and units is detailed. The sub-models are categorized into two sections to facilitate their presentation. All treatment units' models can be found under Section (4.2) of this chapter while the treatment, cost, and environmental impact sub-models and process simulation sub-models can be found in Section (4.3). The parameters and variables of each model are listed under the Nomenclature of each section.

The sub-models presented in this chapter are derived from various sources in the literature, with different aspects drawn from the works of different authors. References indicating the sources from which each equation is derived are provided for clarity alongside each equation. Otherwise, the equations are developed by the author of this work.

The indices, set, and common parameters associated with the proposed models are listed below. The values of the parameters can be found in Table (A.1) of Appendix (A).

Nomenclature

Indices

$tech$	Treatment technology

cont	Contaminant to be removed from produced water
chem	Chemical consumed during the treatment process

Sets

Tech	Set of technologies
Contaminants	Set of contaminants to be removed from produced water
Chemicals	Set of chemicals consumed during treatment process

Parameters

Q	Flow rate of the inlet water in ton/hr
g	Gravitational acceleration in m/s^2
$d_{conv.}$	Conversion factor from μm to m for droplet/particle size in
$f_{conv.}$	Conversion factor to convert flowrate from ton/hr to m^3/s in m^3/s
ρ_c	Density of the continuous phase (water) in kg/m^3
ρ_d	Density of the dispersed phase (oil) in kg/m^3
ρ_{TSS}	Density of the total suspended solids (TSS) in kg/m^3
ρ_{CH_4}	Density of the methane gas (CH_4) in kg/m^3
ρ_{PW}	Density of produced water (PW) in kg/m^3
ρ_{sludge}	Density of sludge in kg/m^3
σ	Interracial tension between oil and water in N/m
μ_d	Viscosity of the dispersed phase (oil) in $kg/m.s$
μ_c	Water viscosity in $kg/m.s$
C_{SK}	Cost of belt oil skimmer unit in $/unit
μ_{PW}	Absolute viscosity of produced water (PW) at temperature = 50° in $kg/m.s$

4.2 Treatment Unit Models

4.2.1 American Petroleum Institute Separator

The working principle of the American Petroleum Institute Separator can be found in Section (2.3) of the Literature Review chapter.

4.2.1.1 Assumptions

- The number of channels in the American Petroleum Institute Separator is 2. This ensures the continuity of operation when one channel is out of service due to cleaning and repair [American Petruelem Institute, 1990, Odiete and Agunwamba, 2019].
- The length of the baffle is 75% of the tank depth and its width is the same as the tank width.
- The removal efficiency of droplet/particle larger than the cut diameter of the American Petroleum Institute Separator is 100%.
- The American Petroleum Institute Separator including the baffles is made of carbon steel.
- The flow in the American Petroleum Institute Separator is assumed to be laminar due to the existence of the baffles that reduce the flow to laminar [Enviro Tech Systems, 2024].
- The American Petroleum Institute Separator unit design considers the cut diameter of the Oil & Grease ($O\&G$) to be a design variable while the cut diameter of the Total Suspended Solids (TSS) is a dependent variable.

4.2.1.2 Nomenclature

The values of the input parameters for the American Petroleum Institute Separator model are listed in Table (A.2) of Appendix (A).

Parameters

n_{API}	Number of American Petroleum Institute Separator (API) channels
r^{e}_{API}	Specific energy consumption of American Petroleum Institute Separator (API) unit in kwh/ton
TH_{BF}	American Petroleum Institute Separator (API) baffle thickness in m
Cts_{Mtr}	Baffle material cost in $\$/ton$

Variables

$CD_{API,OnG}$	Cut diameter of Oil & Grease ($O\&G$) by American Petroleum Institute Separator (API) separator in μm
d_{API}	Depth of the American Petroleum Institute Separator (API) separator in m
w_{API}	Width of the American Petroleum Institute Separator (API) separator in m

4.2.1.3 Equations

Terminal rise velocity of the oil droplet in the American Petroleum Institute Separator (API) in (m/s) is calculated according to the Stock's Law as per Eq. (4.1) [American Petruelem Institute, 1990, Odiete and Agunwamba, 2019]:

$$Vt_{API,OnG} = \frac{g\, CD^{2}_{API,OnG}\,(\rho_C - \rho_D)}{18\,\mu_C} \tag{4.1}$$

While the horizontal velocity of the droplet is determined by the smaller of thee values of v_h according to (4.2) [American Petruelem Institute, 1990, Odiete and Agunwamba, 2019] in (m/s):

$$Vh_{API,OnG} = 15\,Vt_{API,OnG} \leq 0.01524 \tag{4.2}$$

The minimum vertical cross-sectional area of the separator in (m^2) is calcu-

lated using Eq.(4.3) [American Petruelem Institute, 1990, Odiete and Agunwamba, 2019]:

$$A_c = \frac{Q f_{Conversion}}{V h_{API,OnG}} \tag{4.3}$$

API separator length in (m) is given by Eq.(4.4) [American Petruelem Institute, 1990, Odiete and Agunwamba, 2019]:

$$L_{API} = \frac{F V h_{API,OnG} d_{API}}{V t_{API,OnG}} \tag{4.4}$$

Where F is the turbulence and short-circuiting factor given by Eq.(4.5) and (4.6) [American Petruelem Institute, 1990, Odiete and Agunwamba, 2019]:

$$Ft = 0.0228 \left(\frac{V h_{API,OnG}}{V t_{API,OnG}} \right) + 1.0137 \tag{4.5}$$

$$F = 1.2 Ft \tag{4.6}$$

Therefore, the tank volume for the American Petroleum Institute Separator (API) separator in (m^3) given its dimensions is:

$$Vol_{API} = L_{API} d_{API} n_{API} w_{API} \tag{4.7}$$

The residence time of oil droplets OnG in (sec) is the time taken by the droplet to reach the surface of the tank as per Eq.(4.8) [Odiete and Agunwamba, 2019]:

$$Rt_{API} = \frac{d_{API}}{V t_{API,OnG}} \tag{4.8}$$

The settling velocity of the Total Suspended Solids (TSS) in (m/s) is the distance traveled by the TSS particle from the top of the tank to the bottom within the residence time [American Petruelem Institute, 1990]:

$$V s_{API,TSS} = \frac{d_{API}}{Rt_{API}} \tag{4.9}$$

From the settling velocity and according to Stokes's law, the cut diameter in μm of the Total Suspended Solids (TSS) by American Petroleum Institute Separator (API) separator is given by Eq.(4.10) [American Petruelem Institute, 1990, Odiete and Agunwamba, 2019]. The quantity is multiplied by 10^6 to convert it from m to μm:

$$CD_{API,TSS} = 10^6 \left(\frac{18\,\mu_C V s_{API,TSS}}{\rho_{TSS} - \rho_C} \right)^{0.5} \tag{4.10}$$

The power consumption per unit (kWh) of the separator is a function of the flow rate of the inlet feed Q [Bagheri et al., 2018]:

$$Power_{API} = r^e_{API}\, Q \tag{4.11}$$

The rate at which kinetic energy is converted into other forms of energy (such as heat) within the separator (energy dissipation rate) in (m^2/s^3) is a function of the power per mass of the flow rate [Schubert, 1999]. The $Power_{API}$ is multiplied by 1,000 to convert (kwh) to (wh):

$$\varepsilon_{API} = \frac{1000\,Power}{\rho_C\, Vol_{API}} \tag{4.12}$$

Since the American Petroleum Institute Separator (API) has two baffles that divide the tanks into three compartments, the cost of the baffles is calculated by multiplying the number of baffles by the cost of their materials by the baffle volume. Assuming the baffle is 75% of the tank depth, the volume can be found by multiplying the baffle length by width, which is the same as the tank's width, by the thickness. The total cost of baffles in ($) is then given by Eq.(4.13):

$$C_{BF} = 2\,Cts_{Mtr}\,(0.75\,d_{API}\,w_{API}\,TH_{BF}) \tag{4.13}$$

The Capital Cost of the American Petroleum Institute Separator (API) unit is the sum of the tank, oil skimmer unit, and baffles costs ($) [Towler and Sinnott,

2012]:

$$CCost_{API} = 5,800 + 1,600\,Vol_{API}^{0.7} + C_{SK} + C_{BF} \tag{4.14}$$

4.2.1.4 Constraints

The width of the separator typically ranges from 6 to 20 feet (1.8 to 6 m) to confirm the standard dimensions for flight scraper shaft lengths for sludge removal [American Petruelem Institute, 1990, Odiete and Agunwamba, 2019]:

$$1.8 \leq w_{API} \leq 6 \tag{4.15}$$

To minimize the effect of the inlet and outlet turbulence on the separator channel by providing a more uniform distribution, it is suggested that the length be at least five times the width. Therefore, American Petroleum Institute Separator (API) length-to-width ratio is [American Petruelem Institute, 1990, Odiete and Agunwamba, 2019]:

$$L_{API} \geq 5\,w_{API} \tag{4.16}$$

Based on operating experience with oil-water separators, the ratio of separator depth to separator width typically ranges from 0.3 to 0.5 in refinery service [American Petruelem Institute, 1990, Odiete and Agunwamba, 2019]:

$$0.3 \leq \frac{d_{API}}{w_{API}} \leq 0.5 \tag{4.17}$$

To minimize turbulence caused by oil/sludge flight scrapers and high flow and to account for the need for additional depth for installing flight scrapers equipment, it is recommended for the depth of the American Petroleum Institute Separator (API) separator to range from 3 to 8 feet (0.9 to 2.4 m) [American Petruelem Institute, 1990, Odiete and Agunwamba, 2019]:

$$0.9 \leq d_{API} \leq 2.4 \tag{4.18}$$

Given the above design considerations of the American Petroleum Institute

Separator (API) tank, it is difficult for $O\&G$ droplets smaller than 150 μm to be removed given their very low rise velocity. Therefore, the cut diameter of the American Petroleum Institute Separator (API) separator for $O\&G$ in μm should be higher than 150 μm [Stewart and Arnold, 2011]:

$$CD_{API,OnG} \geq 150 \tag{4.19}$$

4.2.2 Corrugated Plates Interceptor

The working principle of the Corrugated Plates Interceptor can be found in Section (2.3) of the Literature Review chapter.

4.2.2.1 Assumptions

- The width of the Corrugated Plates Interceptor unit is the same as the width of the tank that contains it.
- The Corrugated Plates Interceptor unit design considers the cut diameter of the Oil & Grease ($O\&G$) to be a design variable while the cut diameter of the Total Suspended Solids (TSS) is a dependent variable.

4.2.2.2 Nomenclature

The values of the input parameters for the Corrugated Plates Interceptor model are listed in Table (A.3) of Appendix (A).

Parameters

C_{CPI}	Corrugated Plates Interceptor (CPI) unit cost in $\$/m^3$
r^e_{CPI}	Specific energy consumption of Corrugated Plates Interceptor (CPI) unit in kwh/ton

Variables

$CD_{CPI,OnG}$	Cut diameter of Oil & Grease ($O\&G$) by Corrugated Plates Interceptor (CPI) separator in μm

L_{CPI}	Length of the Corrugated Plates Interceptor (CPI) plate in m
w_{CPI}	Width of the Corrugated Plates Interceptor (CPI) plate in m
h_{CPI}	Distance between Corrugated Plates Interceptor (CPI) plates in m

4.2.2.3 Equations

Terminal rise velocity of the oil droplet in the Corrugated Plates Interceptor (CPI) separator in (m/s) is calculated according to the Stock's Law as per Eq.(4.20) [Odiete and Agunwamba, 2019]:

$$Vt_{CPI,OnG} = \frac{g\, CD^2_{CPI,OnG}\, (\rho_C - \rho_D)}{18\, \mu_C} \tag{4.20}$$

The required separation area for the Corrugated Plates Interceptor (CPI) unit (m^2) [Okam, 2008]:

$$A_s = \frac{Q\, f_{Conversion}}{Vt_{CPI,OnG}} \tag{4.21}$$

Corrugated Plates Interceptor (CPI) plate area in (m^2) is a function of the unit design variables [Okam, 2008]:

$$A_p = L_{CPI}\, w_{CPI} \tag{4.22}$$

The total number of plates required for a given plate dimension and for a given flow capacity is obtained by Eq. (4.23) [Okam, 2008]:

$$n_{CPI} = \frac{A_s}{A_p} \tag{4.23}$$

The height of the Corrugated Plates Interceptor (CPI) separator can be found from the number of plates and the distance between them (m) according to Eq. (4.24) [Okam, 2008]:

$$H_{CPI} = (n_{CPI} - 1)\, h_{CPI} \tag{4.24}$$

Therefore, the volume of the separator (m^3) can be calculated from its dimensions:

$$Vol_{CPI} = H_{CPI}\, l_{CPI}\, w_{CPI} \tag{4.25}$$

The residence time of the Corrugated Plates Interceptor (CPI) unit in (sec) is the time needed for a droplet to travel from the bottom of the channel to the top:

$$Rt_{CPI} = \frac{h_{CPI}}{Vt_{CPI,OnG}} \tag{4.26}$$

The settling velocity of the total suspended solids (TSS) in (m/s) is the distance traveled by the Total Suspended Solids (TSS) particle from the top of the Corrugated Plates Interceptor (CPI) channel to the bottom within the residence time:

$$Vs_{CPI,TSS} = \frac{h_{CPI}}{Rt_{CPI}} \tag{4.27}$$

From the settling velocity and according to Stoke's law [Odiete and Agunwamba, 2019], the cut diameter in μm of the Total Suspended Solids (TSS) by Corrugated Plates Interceptor (CPI) separator is given by Eq.(4.28). The quantity is multiplied by 10^6 to convert it from m to μm:

$$CD_{CPI,TSS} = 10^6 \left(\frac{18\, \mu_C\, Vs_{CPI,TSS}}{\rho_{TSS} - \rho_C} \right)^{0.5} \tag{4.28}$$

The tanks are generally sized to contain the plates. Therefore, the length of the Corrugated Plates Interceptor (CPI) tank in (m) including the length of the forebay area, the section where the flow enters before it passes through the corrugated plates, and the afterbay area is the section of the Corrugated Plates Interceptor (CPI) unit located immediately after the main separation zone (where the corrugated plates are located) and before the effluent discharge point [Pangestu et al., 2021] is:

$$L_{tank} = \frac{12\, L_{CPI}}{5} \tag{4.29}$$

Similarly, in addition to the calculated separator height, 0.45 (m) was added

to allow for sludge settling and head space above the plate packs. Therefore, the high of the tank containing the Corrugated Plates Interceptor (CPI) separator in (m) [Pangestu et al., 2021] is:

$$H_{tank} = H_{CPI} + 0.45 \tag{4.30}$$

Based on the assumption made earlier, the width of the Corrugated Plates Interceptor (CPI) tank in (m) is: [Pangestu et al., 2021]:

$$W_{tank} = w_{CPI} \tag{4.31}$$

Therefore, the volume of the tank containing the Corrugated Plates Interceptor (CPI) separator in (m^3) can be found from its dimensions:

$$Vol_{tank} = H_{tank} L_{tank} w_{tank} \tag{4.32}$$

The power consumption per unit (kW) of the separator is a function of the flow rate [Bagheri et al., 2018] :

$$Power_{CPI} = r^{e}_{CPI} Q \tag{4.33}$$

The rate at which kinetic energy is converted into other forms of energy (such as heat) within the separator (energy dissipation rate) in (m^2/s^3) is a function of the power per mass of the flow rate [Schubert, 1999]. The $Power_{CPI}$ is multiplied by 10^3 to convert (kwh) to (wh):

$$\varepsilon_{CPI} = \frac{10^3 \, Power_{CPI}}{\rho_C \, Vol_{CPI}} \tag{4.34}$$

Fluid velocity in m/s can be obtained by dividing the volumetric flowrate by the cross-sectional area of the separator [Okam, 2008]:

$$u_{CPI} = \frac{Q \, f_{conv}}{h_{CPI} \, w_{CPI} \, n_{CPI}} \tag{4.35}$$

Reynolds number Rehm et al. [2008]:

$$Re_{CPI} = \frac{u_{CPI}\,\rho_c\,h_{CPI}}{\mu_c} \tag{4.36}$$

The total Capital Cost of the unit including the Corrugated Plates Interceptor (CPI) unit (plates), tank, and the oil skimmer in ($) is [Towler and Sinnott, 2012]:

$$CCost_{CPI} = 5,800 + 1,600\,Vol_{tank}^{0.7} + C_{CPI}\,Vol_{CPI} + C_{SK} \tag{4.37}$$

4.2.2.4 Constraints

The upper and lower bounds of the design variables are given in Eq.(4.38 to 4.42).

The Cut diameter of Oil & Grease ($O\&G$) by Corrugated Plates Interceptor (CPI) separator (μm) is established based on operational experiences with water separation [Stewart and Arnold, 2011]:

$$CD_{CPI,OnG} \geq 40 \tag{4.38}$$

Similarly, the distance between Corrugated Plates Interceptor (CPI) plates (m) is recommended to be within the following range [Pangestu et al., 2021]:

$$0.0127 \leq h_{CPI} \leq 0.508 \tag{4.39}$$

Length of the Corrugated Plates Interceptor (CPI) plate (m) [Pangestu et al., 2021]:

$$0.5 \leq l_{CPI} \leq 4.49 \tag{4.40}$$

Width of the Corrugated Plates Interceptor (CPI) plate (m) [Pangestu et al., 2021]:

$$1.828 \leq w_{CPI} \leq 6.09 \tag{4.41}$$

The value of Reynolds number of Corrugated Plates Interceptor (CPI) should

be less than 2,000 to ensure the flow is laminar [Pangestu et al., 2021]:

$$Re_{CPI} \leq 2,000 \tag{4.42}$$

4.2.3 Hydrocyclone Separator

The working principle of the Hydrocyclone can be found in Section (2.3) of the Literature Review chapter.

4.2.3.1 Assumptions

In the case of parallel Hydrocyclone (HC), it is assumed the flow rate is distributed equally among n_{HC} hydrocyclones [Rietema, 1961].

4.2.3.2 Nomenclature

The values of the input parameters for the hydrocyclone model are listed in Table (A.4) of Appendix (A).

Parameters

r^e_{HC}	Specific energy consumption of the hydrocyclone (HC) unit in kwh/ton

Variables

n_{HC}	Number of parallel hydrocyclones (HC)
d_{HC}	Diameter of the hydrocyclone (HC) in m

4.2.3.3 Equations

The volumetric flowrate per hydrocyclone q_{HC} in (m^3/sec) is calculated by dividing the inlet flow rate (Q) by the number of the parallel hydrocyclone (HC) according to Eq.(4.43) where f_{Conv} is a conversion factor:

$$q_{HC} = \frac{Q\, f_{Conv}}{n_{HC}} \tag{4.43}$$

The design of the hydrocyclone adopted in this work is based on the model

proposed by Lapple [Gimbun et al., 2005, Taiwo et al., 2016].

Hydrocyclone (HC) inlet height a in (m):

$$a = 0.5\, d_{HC} \tag{4.44}$$

Hydrocyclone (HC) inlet width b in (m):

$$b = 0.25\, d_{HC} \tag{4.45}$$

Hydrocyclone (HC) cylinder height h in (m):

$$h = 2\, d_{HC} \tag{4.46}$$

Hydrocyclone (HC) total height H in (m):

$$H = 2\, d_{HC} + h \tag{4.47}$$

The cut diameters CD_{cont} in μm of Oil & Grease ($O\&G$) and Total Suspended Solids (TSS) by the hydrocyclone (HC) are given by Eq.(4.48) and (4.49) [Silva et al., 2008]:

$$CD_{OnG} = \left[\frac{9\mu b}{2\pi N_e V_i(\rho_C - \rho_D)}\right] \tag{4.48}$$

$$CD_{TSS} = \left[\frac{9\mu b}{2\pi N_e V_i(\rho_{TSS} - \rho_C)}\right] \tag{4.49}$$

Where N_e is the number of turns inside the hydrocyclone (HC) and V_i are the inlet velocity (m/s) which are calculated using Eq.(4.50) [Gimbun et al., 2005] and (5.20):

$$N_e = \frac{1}{a} \times \left[h + \frac{H-h}{2}\right]^{(0.5)} \tag{4.50}$$

$$V_i = \frac{4\,q_{HC}}{\pi\,d_{HC}^2} \tag{4.51}$$

Therefore, the removal efficiencies η_{cont} of the Oil & Grease ($O\&G$) droplets and Total Suspended Solids (TSS) particle by the hydrocyclone (HC) are given by Eq.(4.52) and (4.53) where dp is the diameter in μm of a given droplet/particle [Gimbun et al., 2005]:

$$\eta_{OnG} = \frac{1}{1+\left(\frac{CD_{OnG}}{dp}\right)^2} \tag{4.52}$$

$$\eta_{TSS} = \frac{1}{1+\left(\frac{CD_{TSS}}{dp}\right)^2} \tag{4.53}$$

The residence time Rt_{HC} of the flow inside the hydrocyclone (HC) is given by dividing the path length of the droplet/particle by the velocity of the feed as shown in Eq.(4.54):

$$Rt_{HC} = \frac{\pi\,d_{HC}\,N_e}{V_i} \tag{4.54}$$

The volume Vol_{HC} in (m^3) and cost $CCost_{HC}$ in (\$/unit) of a single hydrocyclone (HC) are given by Eq.(4.55) and (4.56) [Carrero-Parreno et al., 2017] while the total cost $CCost_{HC,tot}$ in (\$) is given by Eq.(4.57)

$$Vol_{HC} = 1.096\,d_{HC} - 0.346 \tag{4.55}$$

$$CCost_{HC} = 4,590\,Vol_{HC} + 15,495 \tag{4.56}$$

Therefore, the total cost of all parallel hydrocyclones (HC) is given by:

$$CCost_{HC,tot} = CCost_{HC}\,n_{HC} \tag{4.57}$$

The power consumption $Power_{HC}$ in (kW) of all hydrocyclones (HC) is a function of the flow rate [Bagheri et al., 2018]:

$$Power_{HC} = r^{e}_{HC} Q \tag{4.58}$$

The rate at which kinetic energy ε_{HC} is converted into other forms of energy (such as heat) within the hydrocyclone (HC) (energy dissipation rate) in (m^2/s^3) is a function of the power per mass of the flow rate [Schubert, 1999]. The $Power_{HC}$ is multiplied by 10^3 to convert (kw) to (w):

$$\varepsilon_{HC} = \frac{10^3 \, Power_{HC} r^{e}_{HC}}{\rho_C Vol_{HC}} \tag{4.59}$$

Reynolds number Re_{HC} of the hydrocyclone (HC) separator [Overcamp and Scarlett, 1993]:

$$Re_{HC} = \frac{V_i \rho_c d_{HC}}{\mu_c} \tag{4.60}$$

4.2.3.4 Constraints

According to industry practices in water separation, hydrocyclone (HC) is recommended for handling droplets and particles ranging from 5 to 200 μm [Tarleton and Wakeman, 2007]. Consequently, the inlet droplet/particle diameter d_p should be less than 200 μm:

$$d_p \leq 200 \tag{4.61}$$

Similarly, the cut diameter CD_{cont} of con in μm by hydrocyclone (HC) is larger than 5 (μm):

$$CD_{cont} \geq 5 \tag{4.62}$$

The minimum body diameter d_{HC} of the hydrocyclone (HC) in (m) is set to be consistent with the volume equation (4.55), while the upper bound is recommended to be around 2.5 (m) according to industry practices in water separation [Cilliers, 2000]:

$$0.4535 \leq d_{HC} \leq 2.5 \tag{4.63}$$

4.2.4 Induced Gas Flotation

The working principle of the Induced Gas Flotation can be found in Section (2.3) of the Literature Review chapter.

4.2.4.1 Assumptions

- The cut diameter of Oil & Grease and Total Suspended Solids by Induced Gas Flotation are given parameters.
- Methane gas is used to generate the bubbles in the tank [Piccioli et al., 2020].
- The Induced Gas Flotation tank is cylindrical.
- The unit consists of multiple cells.

4.2.4.2 Nomenclature

The values of the input parameters for the Induced Gas Flotation model are listed in Table (A.5) of Appendix (A).

Parameters

C_{RS}	Rotor and stator cost in $\$/unit$
γ	Surface tension of Water in contact with Air in N/m
k_p	mass transfer coefficient in min^{-1}
r^e_{IGF}	specific energy consumption of Induced Gas Flotation unit in kwh/ton

Variables

n_{IGF}	number of Induced Gas Flotation (IGF) cells
r_{IGF}	radius of Induced Gas Flotation (IGF) cell in m
h_{IGF}	high of the Induced Gas Flotation (IGF) cell in m
q_g	methane gas flowrate in m^3/sec

4.2.4.3 Equations

Given the Induced Gas Flotation (IGF) cell tank is cylindrical, the volume of a single cell Vol_{IGF} in (m^3) is:

$$Vol_{IGF} = \pi r_{IGF}^2 h_{IGF} \tag{4.64}$$

The total volume of all Induced Gas Flotation (IGF) cells (m^3)

$$Vol_{IGF}^{tot} = n_{IGF} Vol_{IGF} \tag{4.65}$$

The residence time rt_{IGF} of the stream within the Induced Gas Flotation (IGF) cell in (sec). The flow is multiplied by $f_{Conversion}$ to convert it from (ton/hr) to (m^3/sec):

$$rt_{IGF} = \frac{Vol_{IGF}}{Q f_{Conv.}} \tag{4.66}$$

The velocity of the fluid u_{IGF} entering the unit in m/s:

$$u_{IGF} = \frac{Q f_{conv}}{\pi r_{IGF}^2} \tag{4.67}$$

Reynolds number Re_{IGF} [Overcamp and Scarlett, 1993]:

$$Re_{IGF} = \frac{u_{IGF} \rho_c r_{IGF}}{\mu_c} \tag{4.68}$$

Induced Gas Flotation (IGF) cost $CCost_{IGF}$ in ($) consists of the cost of a single cell and the rotor and stators multiplied by the number of cells [Towler and Sinnott, 2012]

$$CCost_{IGF} = n_{IGF} (5800 + 1600 Vol_{IGF}^{0.7} + C_{RS}) \tag{4.69}$$

The power consumption $Power_{IGF}$ of the separator including all cells in (kW) is a function of the flow rate [Bagheri et al., 2018]:

$$Power_{IGF} = r_{IGF}^e Q \tag{4.70}$$

The rate at which kinetic energy is converted into other forms of energy (such as heat) within the separator (energy dissipation rate ε_{Max}) at the generation zone in (m^2/s^3) is a function of the power per mass of the flow rate [Schubert, 1999]:

$$\varepsilon_{Max} = \frac{1000\,Power_{IGF}}{\rho_C\,Vol_{IGF}} \tag{4.71}$$

The energy dissipation rate ε_{IGF} in (m^2/s^3) at the collection zone is [Schubert, 1999]:

$$\varepsilon_{IGF} = \frac{\varepsilon_{Max}}{30} \tag{4.72}$$

The diameter of the methane gas bubbles (d_b) in (m) is [Yoon et al., 2016]:

$$d_b = \left(\frac{2.11\,\gamma}{\rho_C\,\varepsilon_{Max}^{0.66}}\right)^{0.6} \tag{4.73}$$

The removal efficiency per unit E in (%) is found using Eq (4.74 and 4.75) [Stewart and Arnold, 2009]. The flow is multiplied by $f_{Conversion}$ to convert it from (ton/hr) to (m^3/sec) and k_p is divided by 60 to convert it from $1/min$ to $1/sec$:

$$K = 6\,\pi\left(\frac{k_p}{60}\right)\frac{r_{IGF}^2\,h_{IGF}\,q_g}{Q\,f_{Conversion}\,d_b} \tag{4.74}$$

$$E = \frac{K}{Q\,f_{Conversion} + K} \tag{4.75}$$

The overall removal efficiency Et_{cont} in (%) for each contaminant, Oil & Grease $(O\&G)$ and Total Suspended Solids (TSS), is given by Eq.(4.76) [Stewart and Arnold, 2009]:

$$Et_{cont} = 1 - (1-E)^{n_{IGF}} \qquad \forall\ cont \tag{4.76}$$

4.2.4.4 Constraints

According to industry practices in water separation, the ranges of the design variables are recommended to be within the ranges given in Eq.(4.77 to 4.81).

The inlet concentrations in mg/L of Oil & Grease $(O\&G)$ for Induced Gas

Flotation (IGF) cell should not exceed the following limits as the unit underperforms at inlet concentration higher than this limit [Saththasivam et al., 2016, Shen et al., 2022]:

$$Conc_{in,OnG} \leq 1,000 \tag{4.77}$$

Number of Induced Gas Flotation (IGF) cells n_{IGF} [Stewart and Arnold, 2009]:

$$1 \leq n_{IGF} \leq 4 \tag{4.78}$$

The radius of Induced Gas Flotation (IGF) cells r_{IGF} in (m) [Piccioli et al., 2020]:

$$1.5 \leq r_{IGF} \leq 3.5 \tag{4.79}$$

The high of Induced Gas Flotation (IGF) cells h_{IGF} in (m) [Piccioli et al., 2020]:

$$0.5 \leq h_{IGF} \leq 7.5 \tag{4.80}$$

The gas flowrate q_g of the methane gas to generate the bubbles in $(m^3 s^{-1})$ [Sarkar et al., 2010]:

$$q_g \leq 0.00001 \tag{4.81}$$

4.2.5 Nutshell Filter

The working principle of the Nutshell Filter can be found in Section (2.3) of the Literature Review chapter.

4.2.5.1 Assumptions

- The separation of the Nutshell Filter is assumed to be 100% for the droplets/particles larger than the cut diameter.
- The cut diameters of Nutshell Filter for Oil & Grease ($O\&G$) and Total Suspended Solids (TSS) are parameters.
- The filtration medium is made out of walnut granular.

4.2.5.2 Nomenclature

The values of the input parameters for the Nutshell Filter model are listed in Table (A.6) of Appendix (A).

Parameters

Cts_{medium}	Cost of the walnut granular in $\$/ton$
ρ_{NF}	Density of the walnut granular medium in kg/m^3
BW^{r}_{NF}	Backwash rate of Nutshell Filter (NF) in $m^3/m^2.min$
BW^{fre}_{NF}	Frequency of backwash of Nutshell Filter (NF) in hr^{-1}
BW^{d}_{NF}	Duration of backwash of Nutshell Filter (NF) in min
$porosity$	Filtration bed porosity
α	Empirical fitting factor
A_h	Hamker constant
K_B	Boltzmann constant in j/k
T	Absolute temperature in K
d_{col}	Collector diameter in m
r^{e}_{NF}	Specific energy consumption of Nutshell Filter (NF) unit in kwh/ton

Variables

L_{bed}	The length of the Nutshell Filter bed in m
L_{NF}	The length of the Nutshell Filter (NF) unit without the bed in m
r_{NF}	The radius of the Nutshell Filter (NF) unit in m

4.2.5.3 Equations

Assuming the tank is cylindrical. Nutshell Filter (NF) tank volume in m^3 is:

$$Vol_{NF} = \pi r^2_{NF} (L_{bed} + L_{NF}) \tag{4.82}$$

The power consumption $Power_{HC}$ in per unit (kW) of the Nutshell Filter (NF)

is a function of the flow rate [Bagheri et al., 2018].

$$Power = r^{e}_{NF}\, Q \tag{4.83}$$

The rate at which kinetic energy ε_{NF} is converted into other forms of energy (such as heat) within the Nutshell Filter (NF) (energy dissipation rate) in (m^2/s^3) is a function of the power per mass of the flow rate [Schubert, 1999]. The $Power_{NF}$ is multiplied by 10^3 to convert $(kwatt)$ to $(watt)$:

$$\varepsilon_{NF} = \frac{10^3\, Power}{\rho_C\, Vol_{NF}} \tag{4.84}$$

The filtration bed area A_{NF} in m^2 is:

$$A_{NF} = \pi\, r^2_{NF} \tag{4.85}$$

The volume of the backwash tank of Nutshell Filter $Vol_{BWT,NF}$ in (m^3) is calculated based on the frequency BW^r_{NF} and duration BW^d_{NF} of the backwash and the filtration area A_{NF}:

$$Vol_{BWT,NF} = BW^r_{NF}\, A_{NF}\, BW^d_{NF} \tag{4.86}$$

Therefore, the backwash tank cost $Cost_{BWT,NF}$ in ($) is [Towler and Sinnott, 2012]:

$$Cost_{BWT,NF} = 5,800 + 1,600\, Vol^{0.7}_{BWT,NF} \tag{4.87}$$

The Nutshell Filter (NF) equipment cost $Cost_{NF}$ in ($) including the filtration medium and the backwash tank is [Towler and Sinnott, 2012]:

$$Cost_{NF} = 5800 + 1600\, Vol^{0.7}_{NF} + \frac{Cts_{medium}\, \rho_{NF}}{10^3}\, \pi\, r^2_{NF}\, L_{bed} + Cost_{BWT} \tag{4.88}$$

The $medium_{cost}$ is multiplied by $(\rho_{NF}/10^3)$ to convert the cost to $(\$/m^3)$.

The residence time Rt_{NF} of the flow in the filtration tank in (sec) is:

$$Rt_{NF} = \frac{Vol_{NF}}{Q\, f_{Conversion}} \tag{4.89}$$

The flow is multiplied by $f_{Conversion}$ to convert it from (ton/hr) to (m^3/sec).

The removal efficiency of the Nutshell Filter (NF) is based on the work of [Lawler and Nason, 2006] as shown in Eq. (4.90 to 4.103).

The superficial velocity V_0 of the stream in (m/s):

$$V_0 = \frac{Q\, f_{Conversion}}{\pi\, r_{NF}^2} \tag{4.90}$$

Parameter A_s from Happel's flow mode:

$$p = (1 - porosity)^{\frac{1}{3}} \tag{4.91}$$

$$A_s = \frac{2(1-p^5)}{(2-3p+3p^5-2p^6)} \tag{4.92}$$

Van der Waals number N_{vdw}:

$$N_{vdw} = \frac{A_h}{k_B\, T} \tag{4.93}$$

The particle diffusion coefficient Dp_{cont}:

$$Dp_{cont} = \frac{K_B\, T}{3\,\pi \mu_C\, d_{cont}\, d_{conversion}} \qquad \forall\ cont \tag{4.94}$$

Where d_{cont} is the diameter of particle/droplet of contaminant $cont$.

Peclet number Pe_{cont} of contaminant $cont$ droplets and particles:

$$Pe_{cont} = \frac{V_0\, d_{col}}{Dp_{cont}} \qquad \forall\ cont \tag{4.95}$$

Gravity number NG_{cont} of contaminant $cont$ droplets and particles is:

$$NG_{cont} = \frac{(\rho_C - \rho_D)\, g\, (d_{OnG}\, d_{Conversion})^2}{18\, \mu_W\, V_0} \qquad \forall\ cont \tag{4.96}$$

Attraction number NA_{cont} of contaminant *cont* droplets and particles is:

$$NA_{cont} = \frac{A_h}{3\,\pi\mu_W\,(d_{cont}\,d_{Conversion})^2\,V_0} \qquad \forall\ cont \tag{4.97}$$

Aspect ratio NR_{cont} of contaminant *cont* droplets and particles is:

$$NR_{cont} = \frac{d_{cont}\,d_{Conversion}}{d_{col}} \qquad \forall\ cont \tag{4.98}$$

The removal efficiencies Br_{cont} of contaminant *cont* droplets and particles by Brownian motion is:

$$Br_{cont} = 2.4\,A_s^{\frac{1}{3}}\,Pe_{cont,i}^{-0.715}\,NR_{cont,i}^{-0.081}\,N_{vdw}^{0.052} \qquad \forall\ cont \tag{4.99}$$

The removal efficiencies I_{cont} of contaminant *cont* droplets and particles by interception is:

$$I_{cont} = 0.55\,A_s\,NR_{cont,i}^{1.675}\,NA_{cont}^{0.125} \qquad \forall\ cont \tag{4.100}$$

The removal efficiencies GS_{cont} of contaminant *cont* droplets and particles by gravity sedimentation is:

$$GS_{cont} = 0.22\,NR_{cont}^{-0.24}\,NG_{cont}^{1.11}\,N_{vdw}^{0.053} \qquad \forall\ cont \tag{4.101}$$

The summation of all removal efficiencies $\sum R_{cont}$ for contaminant *cont* droplets and particles is:

$$\sum R_{cont} = Br_{cont} + I_{cont} + GS_{cont} \qquad \forall\ cont \tag{4.102}$$

The total removal efficiency $\eta filter_{cont}$ contaminant *cont* droplets and particles is:

$$\eta filter_{cont} = 1 - exp\left(\frac{-3\,(1-porosity)\,\alpha\,\sum R_{cont}\,L_{bed}}{2\,d_{col}}\right) \qquad \forall\ cont \tag{4.103}$$

The velocity of the fluid u_{NF} entering the tank in m/s is:

$$u_{NF} = \frac{Q f_{conv}}{A_{NF}} \tag{4.104}$$

Reynolds number of the flow inside the tank is [Rehm et al., 2008]:

$$Re_{NF} = \frac{u_{NF} \rho_c r_{NF}}{\mu_c} \tag{4.105}$$

4.2.5.4 Constraints

According to industry practices in water separation, the ranges of the design variables are recommended to be within the ranges given in Eq (4.106 to 4.110).

The inlet concentrations $C_{in,cont}$ in mg/L of Oil and Grease ($O\&G$) and Total Suspended Solids (TSS) for Nutshell Filter (NF) should not exceed the following limit [CECO Environmental, 2023]:

$$C_{in,cont} \leq 50 \qquad \forall\ cont \tag{4.106}$$

The inlet droplet/particle diameter dp_{cont} is less than 5 μm [CECO Environmental, 2023]:

$$dp_{cont} \leq 5 \tag{4.107}$$

The depth of filtration media L_{bed} in (m) is [Moo-Young, 2011]:

$$0.5 \leq L_{bed} \leq 2.5 \tag{4.108}$$

The radius of the Nutshell Filter (NF) r_{NF} unit in (m) is [CECO Environmental, 2023] :

$$0.5 \leq r_{NF} \leq 4.26 \tag{4.109}$$

The height of the Nutshell Filter (NF) h_{NF} unit in (m) is [CECO Environmental, 2023]:

$$0.381 \leq h_{NF} \leq 2.25 \tag{4.110}$$

4.2.6 Centrifuge Separator

The working principle of the centrifuge separator can be found in Section (2.3) of the Literature Review chapter.

4.2.6.1 Nomenclature

The values of the input parameters for the centrifuge separator model are listed in Table (A.7) of Appendix (A).

Parameters

r^{e}_{CF}	Specific energy consumption of centrifuge (CF) separator in kwh/ton
$speed$	centrifuge (CF) separator rotational speed in RPM

Variables

$r_{CF,outer}$	Outer radius of centrifuge (CF) separator in m
L_{CF}	Length of the centrifuge (CF) separator in m

4.2.6.2 Equations

The cost of centrifuge separator $CCost_{CF}$ in (\$) is [Towler and Sinnott, 2012]:

$$CCost_{CF} = 63,000 + 280,000\, r^{0.7}_{CF,outer} \tag{4.111}$$

The angular velocity ω of the centrifuge separator bowel in rad/s is [Kumar et al., 2020]:

$$\omega = \left(\frac{2\pi\, speed}{60}\right) \tag{4.112}$$

ω is divided by 60 to convert the speed rotation per second.

The inner diameter of centrifuge bowl $r_{CF,inner}$ in (m) is [Berk, 2009] :

$$r_{CF,inner} = 0.35\, r_{CF,outer} \tag{4.113}$$

Reynolds number Re_{CF} of the flow inside the bowel is [Doran, 2013a]:

$$Re_{CF} = \frac{\pi \rho_{PW}\, \omega r_{CF,inner}^2}{\mu_{PW}} \tag{4.114}$$

The volume of the centrifuge separator bowel Vol_{CF} in (m^3) is [Berk, 2009]:

$$Vol_{CF} = \pi \left(r_{CF,outer}^2 - r_{CF,inner}^2\right) L_{CF} \tag{4.115}$$

The power consumption $Power_{CF}$ in (kW) of the centrifuge (CF) separator is a function of the flow rate [Bagheri et al., 2018]:

$$Power_{CF} = r_{CF}^e\, Q \tag{4.116}$$

The rate at which kinetic energy ε_{CF} is converted into other forms of energy (such as heat) within the centrifuge (CF) separator (energy dissipation rate) in (m^2/s^3) is a function of the power per mass of the flow rate [Schubert, 1999]. The $Power_{CF}$ is multiplied by 10^3 to convert $(kwatt)$ to $(watt)$:

$$\varepsilon_{CF} = \frac{10^3\, Power\, r_{CF}^e}{\rho_C\, Vol_{CF}} \tag{4.117}$$

Residence time Rt_{CF} of the flow inside the centrifuge (CF) separator in (sec) is [Magdi Abadir, 2018]:

$$Rt_{CF} = \frac{Vol_{CF}}{Q\, f_{Conv}} \tag{4.118}$$

The cut diameter of contaminant $cont$ droplets and particles by centrifuge (CF) separator $DC_{CF,OnG}$ in μm is [Berk, 2009]:

$$DC_{CF,cont} = \left(\frac{18\,\mu_C}{Rt_{CF}\left(\rho_C - \rho_{cont}\right)\omega^2}\, ln\frac{r_{CF,outer}}{r_{CF,inner}}\right)^{0.5} d_{Conv} \qquad \forall\ cont \tag{4.119}$$

The fraction of particles of size d_{cont} recovered by the centrifuge (CF) separator

$G_{CF,cont}$ [Maybury et al., 1998] is given by equations (4.120):

$$G_{CF,cont} = 1 - \exp^{-0.865\left(\frac{d_{cont}\, d_{Conv}}{DC_{CF,cont}}\right)^{2.08}} \qquad \forall\ cont \tag{4.120}$$

4.2.6.3 Constraints

According to industry practices in water separation, the ranges of the centrifuge specifications and design variables are recommended to be within the ranges given in Eq (4.121 to 4.124).

The inlet droplet/particle diameter dp_{cont} is less than 100 μm [Tarleton and Wakeman, 2007]:

$$dp_{cont} \leq 100 \qquad \forall\ cont \tag{4.121}$$

The ratio between the centrifuge (CF) separator diameter $CF,outer$ and length L_{CF} is [Tarleton and Wakeman, 2007]:

$$4 \leq \frac{r_{CF,outer}}{L_{CF}} \leq 8 \tag{4.122}$$

The bounds of the outer radius $r_{CF,outer}$ of the centrifuge (CF) separator (m) [Tarleton and Wakeman, 2007, Sabbagh et al., 2015]

$$0.025 \leq r_{CF,outer} \leq 0.5 \tag{4.123}$$

The bounds of the length of the centrifuge (CF) separator L_{CF} are based on the aspect ratio limits in Eq (4.122) (m):

$$0.2 \leq L_{CF} \leq 8 \tag{4.124}$$

4.2.7 Microfiltration Membrane

The working principle of the microfiltration membrane can be found in Section (2.3) of the Literature Review chapter.

4.2.7.1 Assumptions

- The separation of the microfiltration is assumed to be 100% for all the droplets/particles smaller than the cut diameter of the microfiltration.
- The cut diameter of microfiltration for Oil & Grease ($O\&G$) and Total Suspended Solids (TSS) are parameter.
- The inlet flowrate Q is equally distributed among the number of microfiltration units n_{MF}

4.2.7.2 Nomenclature

The values of the input parameters for the microfiltration model are listed in Table (A.8) of Appendix (A).

Parameters

Cts_{area}	Cost per area of the microfiltration membrane in $\$/m^2$
BW^{r}_{MF}	Backwash rate of microfiltration membrane (MF) in $m^3/m^2.hr$
BW^{fre}_{MF}	Frequency of backwash of microfiltration membrane (MF) in hr^{-1}
BW^{d}_{MF}	Duration of backwash of microfiltration membrane (MF) in min
r^{e}_{MF}	Specific energy consumption of microfiltration membrane (MF) in kwh/m^3
Cln^{fre}_{MF}	Frequency of chemical cleaning of microfiltration membrane (MF) in hr^{-1}
$porosity_{MF}$	porosity of the microfiltration membrane (MF)

Variables

n_{MF}	Number of microfiltration membrane (MF)
r_{MF}	Radius of microfiltration membrane (MF) in m
L_{MF}	Length of microfiltration membrane (MF) in m

4.2.7.3 Equations

Given that there are multiple units of microfiltration membrane (MF), the flowrate per MF unit q_{MF} in (ton/hr) is given by Eq.(4.125):

$$q_{MF} = \frac{Q}{n_{MF}} \tag{4.125}$$

The area $Area_{MF}$ in (m^2) of the microfiltration membrane (MF) is found using Eq.(4.136)

$$Area_{MF} = \pi r_{MF}^2 \tag{4.126}$$

The cost of all microfiltration membrane (MF) units $Cost_{MF}$ in ($) is:

$$Cost_{MF} = area_{MF}\, Cost_{area}\, n_{MF} \tag{4.127}$$

Pump cost $Cost_{pump}$ in ($) [Towler and Sinnott, 2012] is:

$$Cost_{pump} = 8,000 + 240\,(10^{-3} \times Q\, f_{Conversion})^{0.9} \tag{4.128}$$

The flow is multiplied by $f_{Conversion}$ to convert it from (ton/hr) to (m^3/sec). Since the cost of the pump is given per L/sec, the cost is multiplied by 10^{-3}.

Backwash tank volume $Vol_{BWT,MF}$ in (m^3) is calculated based on the duration BW_{MF}^d and frequency of backwash BW_{MF}^r of microfiltration membrane (MF) area $Area_{MF}$. The volume is divided by 60 to convert the rate from hr to min:

$$Vol_{BWT,MF} = \frac{BW_{MF}^r\, Area_{MF}\, BW_{MF}^d}{60} \tag{4.129}$$

Therefore, the backwash tank cost in ($) is [Towler and Sinnott, 2012]:

$$Cost_{BWT,MF} = 5,800 + 1,600\, Vol_{BWT,MF}^{0.7} \tag{4.130}$$

Total cost of microfiltration membrane (MF) system including all parts

$TCost_{MF}$ in (\$) is:

$$TCost_{MF} = Cost_{MF} + Cost_{pump} + Cost_{BWT,MF} \tag{4.131}$$

Microfiltration membrane (MF) volume Vol_{MF} in (m^3) is:

$$Vol_{MF} = Area_{MF}\, L_{MF} \tag{4.132}$$

The power consumption $Power_{MF}$ in ($kwatt$) of all microfiltration membrane (MF) is a function of the flow rate [Bagheri et al., 2018]:

$$Power_{MF} = r^{e}_{MF}\, Q \tag{4.133}$$

The rate at which kinetic energy of microfiltration membrane (MF) ε_{MF} is converted into other forms of energy (such as heat) within the microfiltration membrane (MF) (energy dissipation rate) in (m^2/s^3) is a function of the power per mass of the flow rate [Schubert, 1999]. The $Power_{MF}$ is multiplied by 10^3 to convert ($kwatt$) to ($watt$):

$$\varepsilon_{MF} = \frac{10^3\, Power_{MF}}{\rho_C\, Vol_{MF}} \tag{4.134}$$

Residence time of the flow inside the microfiltration membrane (MF) Rt_{MF} in (sec) is:

$$Rt_{MF} = \frac{Vol_{MF}}{q_{MF}\, f_{Conversion}} \tag{4.135}$$

The effective area of the microfiltration membrane (MF) unit $Area^{eff}_{MF}$ in (m^2) is [Abbasgholipourghadim et al., 2016]:

$$Area^{eff}_{MF} = porosity_{MF}\, Area_{MF} \tag{4.136}$$

The velocity of the flow entering the microfiltration membrane (MF) unit u_{MF}

in (m/s) is:

$$u_{MF} = \frac{Q\, f_{conv}}{Area_{MF}^{eff}} \tag{4.137}$$

Reynolds number Re_{MF} of the flow inside the microfiltration membrane (MF) unit is [Rehm et al., 2008]:

$$Re_{MF} = \frac{u_{MF}\, \rho_c\, r_{MF}}{\mu_c} \tag{4.138}$$

4.2.7.4 Constraints

According to industry practices in water separation, the ranges of the microfiltration membrane (MF) specifications and design variables are recommended to be within the ranges given in Eq (4.139 to 4.141).

The inlet concentrations $C_{in,cont}$ in (mg/l) of contaminant *cont* for microfiltration membrane (MF) unit should not exceed the following limit [Tarleton and Wakeman, 2007]:

$$C_{in,cont} \leq 100 \qquad \forall\ cont \tag{4.139}$$

The radius of microfiltration membrane (MF) unit r_{MF} in (m) is:

$$0.0564 \leq r_{MF} \leq 0.0798 \tag{4.140}$$

The length of microfiltration membrane (MF) unit L_{MF} in (m) is [Aqua Free, 2024]:

$$0.1 \leq L_{MF} \leq 1.5 \tag{4.141}$$

4.3 Process Models

4.3.1 Capital Cost Estimation

The capital cost estimation in this model is based on the Factorial Estimation Techniques where the cost of purchased equipment is estimated and then other costs are estimated as factors of the equipment cost [van Amsterdam, 1918].

4.3.1.1 Assumptions

The cost estimation is based on 2010 values and updated to 2023 using the cost index of 2023.

4.3.1.2 Nomenclature

The values of input parameters of the Capital Cost Estimation model are listed in Table (A.15) of Appendix (A).

Parameters

f_p	installation factor for piping
f_{er}	installation factor for equipment erection: foundation and structural work
f_{el}	installation factor for electrical work: power and lighting
f_i	installation factor for instrumentation and process control: automatic process control system
f_c	installation factor for civil engineering work: site preparation and roads
f_s	installation factor for structures and buildings
f_l	installation factor for lagging, insulation, or paint of pipes
f_m	materials cost factors relative to plain carbon steel
P	working capital: cost needed to maintain plant operations such as the cost of inventories of feed, products, and spare parts.
OS	the cost of off-sites: cost of additions to site infrastructure to accommodate the new plant such as firefighting equipment, laboratories, electrical substations, cooling towers (outside the plant location)
DE	the design and engineering cost: include the cost of engineering design, construction supervision, and project management

X	the contingency cost: cost added to the project to allow for variation in the original cost estimation
2023_{Index}	cost index in year 2023
2010_{Index}	cost index in year 2010
$Cts^{cp}_{j,tech}$	capital cost of $tech$ in $\$/yr$

4.3.1.3 Equations

Cost of purchased equipment C^{eqp}_{tech} in carbon steel in ($) is:

$$C^{eqp}_{tech} = Cts^{cp}_{j,tech}\left(\frac{(1+f^p)+(f^{er}+f^{el}+f^i+f^c+f^s+f^l)}{f^m}\right) \qquad \forall\ tech \quad (4.142)$$

Total fixed capital cost C^{fc}_{tech} including equipment, operations, engineering, and contingency costs ($) is:

$$C^{fc}_{tech} = C^{eqp}_{j,tech}(1+OS)(1+DE+X) \qquad \forall\ tech \quad (4.143)$$

Capital cost $Cts^{cp,2023}_{tech}$ for unit $tech$ in the year 2023 in ($) is:

$$Cts^{cp,2023}_{tech} = C^{fc}_{tech}\left(\frac{Index_{2023}}{Index_{2010}}\right) \qquad \forall\ tech \quad (4.144)$$

4.3.2 Treatment

This model describes the produced water treatment process which includes the addition of chemicals, consuming energy, and generating sludge.

4.3.2.1 Assumptions

- The operation of the system is continuous.
- Fossil fuel is the only source of power used to run the system.
- The fraction of water in the sludge stream is 0.5.

4.3.2.2 Nomenclature

The values of input parameters of the treatment model are listed in Table (A.16) of Appendix (A).

Parameters

Cst_{elc}	Cost of electricity to run the system in ($\$/kwh$)
Cst_{CH4}	Cost of methane gas used to generate gas bubbles for induced gas flotation unit in ($\$/ton$)
rc_{acid}	Acid concentration per area in (mg/m^2)
Cst_{acid}	Cost of acid used for backwash of microfiltration in ($\$/mg$)
rc_{base}	Base concentration per area in (mg/m^2)
Cst_{base}	Cost of base used for backwash of microfiltration in ($\$/mg$)
Cst_{w}	Cost of fresh water used to backwash microfiltration and nutshell filter units in ($\$/m^3$)
r^{e}_{tech}	Specific energy consumption for the treatment technologies in (kWh/ton)
$r^{c}_{tech,chem}$	Fraction of chemicals for each $tech$ in (mg/l)
ρ_{chem}	Density of chemical $chem$ in (kg/m^3)
Cts_{chem}	Cost of chemical $chem$ used in the treatment process in ($\$/ton$)
BW^{r}_{tech}	Backwash rate of technology $tech$ in ($m^3/m^2.min$)
BW^{fre}_{tech}	Frequency of backwash of technology $tech$ in (h^{-1})
Cln^{fre}_{tech}	Frequency of chemical cleaning $tech$ in (h^{-1})
BW^{d}_{tech}	Backwash duration of technology $tech$ in (min)
$Cost_{slg}$	Cost of sludge handling system slg ($\$/t_{DM}$)
$area_{tech}$	Area of technology $tech$ in (m^2)
q^{in}_{tech}	Inlet water flow rate at technology $tech$ in (m^2/s^3)
no_{tech}	Number of units of technology $tech$
$V^{total,out}_{tech,cont}$	Total volume for each $cont$ after the separation in (m^3)
$C^{in}_{tech,cont}$	Inlet concentration of contaminate $cont$ at technology $tech$ in (kwh/ton)

qg_{tech}	Gas flowrate in technology $tech$ in (m^3/sec)
$volume_{tech}$	Volume of the technology $tech$ in (m^3)

4.3.2.3 Equations

The amount consumed chemicals by unit $tech$ q_{tech}^{Chem} in (ton/hr) is given in Eq. (4.145) [Bagheri et al., 2018]:

$$q_{tech}^{Chem} = \sum_{chem} \frac{10^3 \, r_{tech,chem}^{c} \, q_{tech}^{in}}{10^6 \, \rho_{chem}} \qquad \forall \; tech \tag{4.145}$$

Since the fraction of chemicals is given in mg/L, the equation is multiplied by $\frac{10^3}{10^6 \rho_{chem}}$ to obtain the chemical flowrate in ton/hr.

The mass flowrate of contaminant $cont$ in the feed stream in (ton/hr) can be found given the initial concentration $C_{tech,cont}^{in}$:

$$q_{tech,cont}^{in} = C_{tech,cont}^{in} \, q_{tech}^{in} \, \rho_{PW} \left(\frac{10^3}{10^6} \right) \qquad \forall \; tech, cont \tag{4.146}$$

Since the initial concentration of contaminant in the flowrate $C_{tech,cont}^{in}$ is given in mg/L, the equation is multiplied by $\frac{10^3 \rho_{PW}}{10^6}$ to obtain the flowrate in ton/hr.

Therefore, the composition of the contaminant $cont$ in the feed stream q_{tech}^{in}:

$$X_{tech,cont}^{in} = \frac{q_{tech,cont}^{in}}{q_{tech}^{in}} \qquad \forall \; tech, cont \tag{4.147}$$

The total mass balance equation for each treatment unit:

$$q_{tech}^{out} = (q_{tech}^{in} + q_{tech}^{Chem} - q_{tech}^{Sludge}) \qquad \forall \; tech \tag{4.148}$$

The partial mass balance equation for each treatment unit:

$$q_{tech}^{out} X_{tech,cont}^{out} = (q_{tech,cont}^{in} X_{tech,cont}^{in} + q_{tech}^{Chem} - q_{tech,cont}^{slg} X_{tech,cont}^{slg}) \qquad \forall \; tech, cont \tag{4.149}$$

Since half of the sludge stream consists of water, the remaining consists of Oil & Grease and Total Suspended Solids:

$$0.5 = X^{slg}_{tech,OnG} + X^{slg}_{tech,TSS} \qquad \forall\ tech \tag{4.150}$$

The composition of contaminant *cont* in the output stream $X^{out}_{tech,cont}$ can be calculated from the volume of the contaminants after the separation:

$$X^{out}_{tech,cont} = \frac{V^{total,out}_{tech,cont}\,\rho_{cont}}{10^3\,q^{out}_{tech,tech,}} \qquad \forall\ tech, cont \tag{4.151}$$

The equation is multiplied by $\frac{\rho_{cont}}{10^3}$ to convert the volume flowrate $V^{total,out}_{tech,cont}$ to mass flowrate in ton/hr.

The concentration of contaminant *cont* in the outlet stream $C^{out}_{tech,cont}$ of technology *tech* in (mgl^{-1}) is:

$$C^{out}_{tech,cont} = \frac{V^{total,out}_{cont}\,\rho_{cont}\rho_{PW}}{10^3\,q^{out}_{tech,cont}} \qquad \forall\ tech, cont \tag{4.152}$$

The outlet feed flow rate q_{out} is multiplied by 10^3 to convert it from (ton) to (kg).

The flow rate of the dry matter in (ton/hr) is the fraction of the Total Suspended Solids (TSS) in the sludge stream:

$$q^{DM}_{tech} = X^{slg}_{tech,cont}\,q^{Sludge}_{tech} \qquad \forall\ tech \tag{4.153}$$

The amount of energy consumed in each technology *tech* in kwh/hr:

$$E_{tech} = \frac{r^{e}_{tech}\,volume_{tech}\,\rho_{PW}\,no_{tech}}{10^3} \qquad \forall\, tech \tag{4.154}$$

The outlet feed flow rate r^{e}_{tech} is divided by 10^3 to convert it from (kwh/ton) to (kwh/kg).

Cost of energy of technology $tech$ in $\$/hr$:

$$Cst^{e}_{tech} = E_{tech} Cst^{elc} \qquad \forall\ tech \tag{4.155}$$

The cost of consumed chemicals in ($\$/hr$) is given in Eq.(4.156) [Bagheri et al., 2018]:

$$Cst^{Chem}_{tech} = \sum_{chem} \frac{10^3\, Cost_{chem}\, r^{c}_{tech,chem}\, q^{in}_{tech}}{10^6\, \rho_{chem}} \qquad \forall\ tech \tag{4.156}$$

Since the fraction of chemicals is given in mg/L, the equation is multiplied by $\frac{10^3}{10^6\,\rho_{chem}}$ to obtain the chemical flowrate in ton/hr.

Cost of methane gas to run technology $tech$ in $\$/hr$. Only applicable for Induced Gas Flotation (IGF). The gas flowrate is multiplied by 3,600 to convert it from *sec* to *hr*:

$$Cst^{g}_{tech} = 3,600\, q^{g}_{tech}\, Cst_{CH4} \tag{4.157}$$

Cost of membrane cleaning in $\$/hr$. Only applicable to microfiltration membrane (MF):

$$Cst^{cln}_{tech} = (rc_{acid}\, Cst_{acid} + rc_{base}\, Cst_{base})\, Cln^{fre}_{tech}\, area_{tech}\, no_{tech} \tag{4.158}$$

Cost of backwash $\$/hr$. Only applicable to microfiltration membrane (MF) and nutshell filter (NF) :

$$Cst^{BW}_{tech} = Cst^{w}_{tech}\, BW^{r}_{tech}\, BW^{d}_{tech}\, BW^{frq}_{tech}\, area_{tech}\, no_{tech} \qquad \forall\ tech = NF, MF \tag{4.159}$$

Cost of the sludge handling option ($\$/hr$):

$$Cst^{slg}_{tech} = q^{DM}_{tech}\, Cost_{slg} \qquad \forall\ tech \tag{4.160}$$

Total units operating cost in ($/hr)

$$Cst^{op}_{tech} = Cst^{Chem}_{tech} + Cst^{e}_{tech} + Cst^{g}_{tech} + Cst^{cln}_{tech} + Cst^{BW}_{tech} + Cst^{slg}_{tech} \qquad \forall\ tech \tag{4.161}$$

4.3.3 CO_2 Emission

The purpose of this model is to quantify the amount of CO_2 emitted from the system.

4.3.3.1 Assumptions

The system uses energy generated from oil.

4.3.3.2 Nomenclature

The values of input parameters of the Emission model are listed in Table (A.18) of Appendix (A).

Parameters

F_{chem}	Emission factor of chemical *chem* in ($kgCO_2e/kg$)
F^{g}	Emission factor of methane gas in ($kgCO_2e/kg$)
F^{elect}	Emission factor of electricity in ($kgCO_2e/kwh$)
F^{w}	Emission factor of treating water in ($kgCO_2e/kg$)
$rc_{tech,chem}$	Fraction of chemicals for each $tech$ in (mg/l) and in (mg/m^2) for the acid and base
ρ_g	Density of methane gas in (kg/m^3)
ρ_{chem}	Density of chemical *chem* in (kg/m^3)
BW^{r}_{tech}	Backwash rate of technology $tech$ in ($m^3/m^2.m$)
BW^{fre}_{tech}	Frequency of backwash of technology $tech$ in (h^{-1})
BW^{d}_{tech}	Backwash duration of technology $tech$ in (min)
Cln^{fre}_{tech}	Frequency of chemical cleaning $tech$ in (h^{-1})
no_{tech}	Number of units of technology $tech$
E_{tech}	Energy consumption by technology $tech$ in (kwh/hr)
q^{in}_{tech}	Water flow rate and technology $tech$ in (m^2/s^3)
q^{g}_{tech}	Gas flowrate of technology $tech$ in (m^3/s)

$area_{tech}$	Area of technology $tech$ in (m^2)
F_{slg}	Emission factor of sludge option slg in $(kgCO_2e/ton_{DM})$
q_{tech}^{DM}	Flow rate of dry matter produced by technology $tech$ in (ton/hr)

4.3.3.3 Equations

The CO_2 emissions are calculated from the following sources:

- The consumption of electricity to run the unit EMS_{tech}^{elec} in $(kgCO_2e/hr)$:

$$EMS_{tech}^{elec} = no_{tech} E_{tech} F^{elect} \qquad \forall\ tech \tag{4.162}$$

- The consumption of the chemicals used to run the unit EMS_{tech}^{cm} in $(kgCO_2e/hr)$:

$$EMS_{tech}^{cm} = \sum_{chem=1}^{4} \left(\frac{rc_{tech,chem}\, q_{tech}^{in} F_{chem}}{10^3\, \rho_{chem}} \right) \qquad \forall\ tech \tag{4.163}$$

  The equation is divided by 10^3 to convert the flowrate from ton/hr to kg/hr.

- The consumption of methane gas EMS_{IGF}^{g} used to run the unit in $(kgCO_2e/hr)$ if applicable. This source of emission is specific for the Induced Gas Flotation (IGF) unit and it is zero for all other units. The gas flowrate is multiplied by 3,600 to convert it from (m^3/sec) to (m^3/hr):

$$EMS_{tech}^{g} = 3{,}600\, q_{tech}^{g} F^{g} \rho_g \qquad \forall\ tech \tag{4.164}$$

- The consumption of chemicals used for backwash EMS_{tech}^{cln} in $(kgCO_2e/hr)$. This emission is specific for the Microfiltration unit (MF) unit and it is zero

for all other units:

$$EMS^{cln}_{tech} = no_{tech} Cln^{fre}_{tech} \sum_{chem=5}^{6} \left(\frac{rc_{tech,chem} area_{tech} F_{chem}}{10^6} \right) \qquad \forall\ tech \tag{4.165}$$

The rc_{chem} is divided by 10^6 to convert it from (mg/m^2) to (kg/m^2). *chem* 5 and 6 are the acid and base used for cleaning.

- The consumption of water used for backwash EMS^{BW}_{tech} in $(kgCO_2e/hr)$. This emission is specific for the Nutshell Filter (NF) and Microfiltration (MF) units and it is zero for all other units:

$$EMS^{BW}_{tech} = no_{tech} BW^{fre}_{tech} area_{tech} F_w BW^{r}_{tech} BW^{d}_{tech} \qquad \forall\ tech = NF, MF \tag{4.166}$$

- The emission from the sludge handling system EMS_{slg} in $(kgCO_2e/hr)$:

$$EMS^{slg}_{tech} = DM_{tech} F_{slg} \qquad \forall\ tech \tag{4.167}$$

The total CO_2 emissions from each unit EMS_{tech} in $(kgCO_2e/hr)$:

$$EMS_{tech} = EMS^{elec}_{tech} + EMS^{cm}_{tech} + EMS^{g}_{tech} + EMS^{cln}_{tech} + EMS^{BW}_{tech} + EMS^{slg}_{tech} \qquad \forall\ tech \tag{4.168}$$

4.3.4 Process Simulation

This model includes the equations that calculate the total cost and emission of the system.

4.3.4.1 Nomenclature

The values of input parameters of the process simulation sub-model are listed in Table (A.19) of Appendix (A).

Parameters

H_{op}	operating hours per year in *hr*

$C^{out}_{tech,cont}$	inlet concentration of contaminant *cont* into technology *tech* in mg/L
C^{final}_{cont}	maximum allowable outlet concentration of *cont* in mg/L
$Cts^{cp,2023}_{tech}$	capital cost as of 2023 of technology *tech* in $\$/hr$

Variables

n_{steps}	number of steps in the treatment process
sequence	sequence of technology *tech* in the treatment process

4.3.4.2 Equations

For a given sequence of n_{steps} number of steps, the Total Annualized Cost (TAC) of the system in ($\$/yr$) consists of the operating and capital costs of all the units:

$$TAC = \sum_{tech} Cst^{op}_{tech} H_{op} + Cts^{cp,2023}_{tech} \tag{4.169}$$

Similarly, the emission of the system *EMS* in ($kgCO_2e/yr$) consists of the emission of all the units in the sequence:

$$EMS = H_{op} \sum_{tech} EMS_{tech} \tag{4.170}$$

The outlet concentration $C^{out}_{tech,cont}$ at n_{steps} of *sequence* should meet the requirements of the final destination C^{final}_{cont} for each contaminant *cont*:

$$C^{out}_{tech,cont} \leq C^{final}_{cont} \qquad \forall\ cont \tag{4.171}$$

4.4 Summary

This chapter outlines the mathematical formulation of the treatment process and unit-level sub-models, illustrating the connection between the unit's design variables and the separation efficiency of produced water contamination, along with

their influence on the objective function values. Additionally, it introduces the modeling of sludge and dry matter production within the Treatment sub-model, a key contribution of this thesis. Finally, the process simulation sub-model is detailed, reflecting the approach outlined in the previous chapter to achieve the optimal solution. The subsequent chapter presents the modeling of droplet/particle level dynamics.

Chapter 5

Mathematical Formulation of Droplet/Particle Dynamics

5.1 Introduction

Droplets and particles coexist within the continuous phase, each possessing distinct properties. Droplets typically appear as spherical liquid entities, while particles exhibit a variety of shapes and compositions determined by their origin. Although both entities coexist in the same medium, they display distinct behaviors owing to their differing characteristics. In this study, Oil and Grease contaminants exist in the form of droplets while Total Suspended Solids are in the form of particles.

This chapter presents the mathematical formulation related to Droplet/Particle Dynamics. Section (5.2) details the equations utilized to establish the initial size distribution of droplets and particles, aligning with the proposed volume discretization method introduced in this study. Subsequently, Section (5.3) addresses the determination of the updated volume and number of droplets and particles for each unit. Sections (5.4) to (5.7) present the breakage and coalescence/aggregation kernels, including alternative ones to be implemented in Chapter (6). The discrete Population Balance Equations sub-model is outlined in Section (5.8), followed by the modeling of droplet and particle separation in Section (5.9).

The sub-models presented in this chapter are derived from various sources in the literature, with different aspects drawn from the works of other authors. Ref-

erences indicating the sources from which each equation is derived are provided for clarity alongside each equation. Otherwise, the equations are developed by the author of this work.

The indices, set, and common parameters associated with the proposed models are listed below. The values of the parameters can be found in Table (A.1) of Appendix (A).

Nomenclature

Indices

$tech$	Treatment technology
$cont$	Contaminant to be removed from produced water
i, ii, k	Volume class, where ii and k are aliases of i (i=1,2,..n_c)

Parameters

Q	Flow rate of the inlet water in ton/hr
g	Gravitational acceleration in m/s^2
$d_{conv.}$	Conversion factor from μm to m for droplet/particle size in
$f_{conv.}$	Conversion factor to convert flowrate from ton/hr to m^3/s in m^3/s
ρ_c	Density of the continuous phase (water) in kg/m^3
ρ_d	Density of the dispersed phase (oil) in kg/m^3
ρ_{TSS}	Density of the total suspended solids (TSS) in kg/m^3
ρ_{PW}	Density of produced water (PW) in kg/m^3
σ	Interracial tension between oil and water in N/m
μ_d	Viscosity of the dispersed phase (oil) in $kg/m.s$
μ_c	Water viscosity in $kg/m.s$
μ_{PW}	Absolute viscosity of produced water (PW) at temperature = 50° in $kg/m.s$

5.2 Initial Particles/Droplets Volume Distribution

The purpose of this model is to generate the initial droplet and particle volume distribution and size distribution of droplets and particles given the initial concentration of the contaminants.

Contaminants exist in droplets and particles. In this work, it is assumed that there are n number of volume classes, with droplets or particles in each class having the same size, measured by diameter. The volume of contaminant in each class is given by the volume of one droplet or particle multiplied by their number in that class. Thus, the total volume of contaminants in the continuous phase can be found by summing the volumes of all classes. Consequently, the number of droplets or particles in each class determines how the volume is distributed among the classes. Due to coalescence and breakage phenomena, the number of droplets or particles in each class fluctuates, affecting the volume distribution within the space, although the total volume is approximately conserved.

The number of droplets or particles in each class plays a crucial role in selecting the separation process needed to meet the final requirements for Produced Water. For example, if more droplets or particles are concentrated in the smaller classes, a higher separation efficiency and cost are required to meet the final requirements. In contrast, a higher number of droplets or particles in the larger classes requires less efficiency and cost to achieve the final requirements.

5.2.0.1 Assumptions

- Oil & Grease droplets and Total Suspended Solids particles have the same initial volume distribution.
- Droplets and particles have a spherical shape.

5.2.0.2 Nomenclature

The values of the input parameters depend on each case study.

Parameters

$\log V_{min}^{cont}$	Log of minimum $cont.$ volume

$\log V_{max}^{cont}$	Log of maximum *cont*. volume
n_c	Number of discrete size classes of droplet/particles in the volume space

5.2.0.3 Equations

The step size for the discretization of the droplet/particle size for each *cont* (δ_{cont}^{V}) is given by Eq.(5.1):

$$\delta_{cont}^{V} = \frac{logV_{cont}^{max} - logV_{cont}^{min}}{n_c - 1} \qquad \forall\ cont \tag{5.1}$$

The log of contaminant *cont* droplet/particle volume of class (i) is:

$$logV_{cont,i} = logV_{cont}^{min} + (i-1)\ \delta_{cont}^{V} \qquad \forall\ i, cont \tag{5.2}$$

The volume of the droplet/particle size for each contaminant of class i in m^3 is:

$$v_{cont,i} = 10^{logV_{cont,i}} \times 10^{-27} \qquad \forall\ i, cont \tag{5.3}$$

The equation is multiplied by 10^{-27} to convert the volume from nm^3 to m^3.

The diameter of droplet/particle for class i in μm:

$$d_{cont,i} = \left(\frac{6V_{cont,i}}{\pi}\right)^{1/3} \times 10^{6} \qquad \forall\ i, cont \tag{5.4}$$

The equation is multiplied by 10^6 to convert the diameter from m to μm.

5.3 Droplets/Particles Number and Volume

The purpose of this sub-model is to generate the number and volume of droplets/particles for each class.

5.3.0.1 Assumptions

The volume distribution of droplets/particles follows a normal distribution with mean (μ), standard deviation (σ), and a total of (nc) classes. To ensure that the distribution is properly defined, the volumes are calculated and normalized so that the total volume equals one.

5.3.0.2 Nomenclature

The values of the input parameters for this model depend on each case study except for $v_{cont,i}$ which is a calculated variable.

Parameters

C^{in}_{OnG}	Initial concentration of Oil & Grease ($O\&G$) in the inlet stream mg/L
C^{in}_{TSS}	Initial concentration of Total Suspended Solids (TSS) in the inlet stream mg/L
μ	Mean value for the normal distribution function μm
σ	Mean value for the normal distribution function
nc	Number of volume classes
$v_{cont,i}$	Volume of a single droplet/particle of $cont$ at class i in m^3. Refer to Eq.(5.3)

5.3.0.3 Equations

The initial total volume of contaminant ($V^{init,total}_{cont}$) in m^3:

$$V^{init,total}_{cont} = \frac{C^{initial}_{cont} q_{feed}}{\rho_{cont}\,\rho_{PW}} \qquad \forall\ cont \tag{5.5}$$

The particle/droplet size distribution for each contaminant $cont$:

$$PSD_{cont,i} = Normal(\mu, \sigma, nc) \qquad \forall\ i, cont \tag{5.6}$$

The volume per class for each contaminant *cont* in m^3:

$$V^{c}_{cont,i} = V^{init,total}_{cont}\ PSD_{cont,i} \qquad \forall\ i, cont \tag{5.7}$$

The number of droplets/particles in class i for each contaminant *cont*:

$$n_{cont,i} = \frac{V^{c}_{cont,i}}{v_{cont,i}} \qquad \forall\ i, cont \tag{5.8}$$

5.4 Droplets Breakage

The purpose of this model is to calculate the breakage rate of droplets based on the type of flow in the treatment unit.

5.4.0.1 Assumptions

- The breakage of the droplets is due to the turbulent fluctuation and collision where the breakage takes place when the turbulent kinetic energy of the drop exceeds a critical value.
- The daughter droplet distribution after breakage follows a uniform distribution.

5.4.0.2 Nomenclature

The values of the input parameters for the breakage model are listed in Table (A.9) of Appendix (A).

Parameters

C_3	Constant
C_4	Constant
α_d	Volume fraction of the dispersed phase Oil & Grease ($O\&G$)
$d_{OnG,k}$	Diameter of Oil & Grease ($O\&G$) droplet of class k in μm
ε	Energy dissipation rate of the unit in m^2/s^3
k_g	constant

β constant

5.4.0.3 Equations

Laminar Flow: Based on the Grace curve which represents the relation between the critical Capillary number and the viscosity ratio where the former represents the ratio between shear stress and the interfacial tension between oil and water while the latter is the ratio between the viscosity of the two phases. Below the curve, the interfacial tension between phases is so strong that the breakup can not take place. Above the curve, the shear stress is stronger, and hence droplets can break. However, for a viscosity ratio above 3, a breakup does not occur no matter how much shear stress is applied which is the case in our model. Therefore, there is no breakage of droplets in the laminar flow [Mehrabian et al., 2015].

Turbulence Flow: The droplet breakage model adopted in this study is the one proposed by [Coulaloglou and Tavlarides, 1977, Liao and Lucas, 2009a].

Breakage rate of droplets in class k

$$\Omega_{B,OnG,k} = C_3 \frac{\varepsilon^{1/3}}{(1+\alpha_d)\, d_{OnG,k}^{2/3}} \exp\left[\frac{-C_4\, \sigma\, (1+\alpha_d)^2}{\rho_d\, \varepsilon^{2/3}\, d_{OnG,k}^{5/3}}\right] \qquad \forall\ k \qquad (5.9)$$

In the alternative model, the breakage kernel is proposed by [MARTÍNEZ-BAZÁN et al., 1999].

$$\Omega_{B,OnG,k} = K_g \frac{\sqrt{\beta\, (\varepsilon\, d_k)^{2/3} - 12\, \sigma/(\rho_c\, d_k)}}{d_k} \qquad \forall\ k \qquad (5.10)$$

Daughter droplet size assumed that droplet of class i will break uniformly into all the classes smaller than i. Therefore, the volume will be distributed among (i-1) number of classes, each class is represented as k. Thus, the fraction of

droplet i that will be added to class k is given by:

$$\Gamma_{i,k} = \frac{1}{i-1} \qquad \forall\ i,k \tag{5.11}$$

5.5 Droplets Coalescence

5.5.0.1 Assumptions

- The collision frequency between droplets i and k in a uniform laminar flow is assumed to happen due to the velocity gradients of the flow according to the model proposed by [Friedlander, 2000].

- The collisions of the droplets in turbulent flow are due to the fluctuating turbulent velocity of the surrounding liquid.

5.5.0.2 Nomenclature

The values of the input parameters for the droplet coalescence model are listed in Table (A.10) of Appendix (A).

Parameters

$d_{OnG,k}$	Diameter of Oil & Grease ($O\&G$) droplet of class k in μm
ε_{tech}	Energy dissipation rate of the unit $tech$ in m^2/s^3
c	Constant
C_{12}	Constant
C_{13}	Constant
C_{VM}	Constant

5.5.0.3 Equations

Laminar Flow: The radius of the Oil & Grease ($O\&G$) droplets for i/k class in μm:

$$r_{OnG,i/k} = \frac{d_{OnG,i/k}\, d_{Conv}}{2} \qquad \forall\ i/k, cont \tag{5.12}$$

The collision frequency between droplets i and k [Friedlander, 2000]:

$$h_{tech,OnG,i,k} = \frac{4}{3}(r_{OnG,i} + r_{OnG,k})^3 G_{tech} \qquad \forall\ i,k,tech \tag{5.13}$$

The absolute velocity gradient [Liao and Lucas, 2010b]:

$$G_{tech} = \sqrt{\frac{\varepsilon_{tech}}{v_{PW}}} \qquad \forall\ tech \tag{5.14}$$

The equivalent radius of droplet formed due to coalescence between droplets of classes i and k in m [Prince and Blanch, 1990]:

$$req_{OnG,i,k} = 0.5 \left(\frac{1}{r_{OnG,i}} + \frac{1}{r_{OnG,k}} \right)^{-1} \qquad \forall\ i,k \tag{5.15}$$

The kinematic viscosity of the liquid in m^2/s:

$$v_{PW} = \frac{\mu_{PW}}{\rho_{PW}} \tag{5.16}$$

The coalescence efficiency of droplets i and k [Prince and Blanch, 1990]:

$$\lambda_{OnG,i,k} = exp \left(\frac{-2.3\, \rho_C^{0.5}\, req_{OnG,i,k}^{5/6}\, \varepsilon^{1/3}}{\sigma^{0.5}} \right) \qquad \forall\ i,k \tag{5.17}$$

The coalescence frequency of droplets of classes i and k to form a new droplet [Liao and Lucas, 2010b]:

$$OmegaC_{OnG,i,k} = \lambda_{OnG,i,k}\, h_{OnG,i,k} \qquad \forall\ i,k \tag{5.18}$$

For the alternative kernel, the collision frequency is calculated according to [Friedlander, 2000, Prince and Blanch, 1990].

$$h_{i,k} = \frac{\pi}{4}(d_i + d_k)^2 |u_i - u_k| \qquad \forall\ i,k \tag{5.19}$$

$$u_{i/k} = (2.14\,\sigma/\rho_c\,d_i + 0.505\,g\,d_i)^{0.5} \qquad \forall\ i/k \tag{5.20}$$

Coalescence efficiency according to the energy model [Sovova, 1981]

$$\lambda_{i,k} = \lambda_{1,i,k} + \lambda_{2,i,k} - \lambda_{1,i,k}\lambda_{2,i,k} \qquad \forall\ i,k \tag{5.21}$$

$$\lambda_{1,i,k} = exp\left(-C_{12}\,\frac{\mu_c\,\rho_c\,\varepsilon}{\sigma^2}\left(\frac{r_i\,r_k}{r_i + r_k}\right)^4\right) \qquad \forall\ i,k \tag{5.22}$$

$$\lambda_{2,i,k} = exp\left(-C_{13}\,\frac{\sigma}{\rho_d\,\varepsilon^{\frac{2}{3}}}\,\frac{(r_i^2 + r_k^2)\,(r_i^3 + r_k^3)}{r_i^3 r_k^3 (r_i^{\frac{2}{3}} + r_k^{\frac{2}{3}})}\right) \tag{5.23}$$

Turbulent Flow: The radius of the Oil & Grease ($O\&G$) droplets for i/k class in μm

$$r_{OnG,i/k} = \frac{d_{OnG,i/k}\,d_{Conv}}{2} \qquad \forall\ i/k \tag{5.24}$$

The equivalent radius of droplet formed due to coalescence between droplets of classes i and k in (m) [Prince and Blanch, 1990]

$$req_{OnG,i,k} = 0.5\left(\frac{1}{r_{OnG,i}} + \frac{1}{r_{OnG,k}}\right)^{-1} \qquad \forall\ i,k \tag{5.25}$$

The collision frequency of droplets of classes i and k [Prince and Blanch, 1990]

$$h_{OnG,i,k} = c\left(d_{OnG,i} \times 10^6 + d_{OnG,k} \times 10^6\right)^2 \left((d_{OnG,i} \times 10^6)^{2/3} + (d_{OnG,k} \times 10^6)^{2/3}\right)^{0.5} \varepsilon^{1/3} \qquad \forall\ i,k \tag{5.26}$$

The diameter is multiplied by 10^6 to convert it from m to μm.

The coalescence efficiency of droplets i and k [Prince and Blanch, 1990]

$$\lambda_{OnG,i,k} = exp\left(\frac{-2.3\,\rho_C^{0.5}\,req_{OnG,i,k}^{5/6}\,\varepsilon^{1/3}}{\sigma^{0.5}}\right) \qquad \forall\ i,k \tag{5.27}$$

The coalescence frequency of droplets of classes i and k to form a new droplet [Liao and Lucas, 2010b]

$$OmegaC_{OnG,i,k} = \lambda_{OnG,i,k}\,h_{OnG,i,k} \qquad \forall\ i,k \tag{5.28}$$

For the alternative kernel, [Kamp et al., 2001] model for the coalescence efficiency will be used instead of the one by [Prince and Blanch, 1990].

$$h_{i,k} = exp\left(\frac{-\sqrt{3}}{2\,\pi}\frac{\rho_c^{2/3}\,u_{rel}\,d_{eq,i,k}}{\sigma^{0.5}\,C_{VM}^{0.5}}\right) \tag{5.29}$$

$$d_{eq,i,k} = \frac{2\,d_{OnG,i}\,d_{OnG,k}}{d_{OnG,i} + d_{OnG,k}} \tag{5.30}$$

$$u_{rel,i,k} = max(1.414\varepsilon^{\frac{1}{3}}(d_{OnG,i}\,d_{OnG,k}\,(10^{-}6)^2)^{\frac{1}{6}}, |u_{OnG,k} - u_{OnG,k}|) \tag{5.31}$$

where $u_{OnG,i/k}$ is calculated in Equation (5.20) above. The quantity is multiplied by $(10^{-}6)^2$ to convert both diameters from μm to m

5.6 Particle Aggregate Breakage

5.6.0.1 Assumptions

- The breakage in this model refers to the breakage of an aggregate of particles assuming it has a spherical shape.
- The daughter droplet distribution after breakage follows a uniform distribution.

5.6.0.2 Nomenclature

The values of the input parameters of the particle breakage model are listed in Table (A.11) of Appendix (A).

Parameters

B	Fitting parameter that represents the critical force needed for the breakage of aggregates
$d_{TSS,k}$	Diameter of Total Suspended Solid (TSS) particle of class k in μm
$v_{TSS,k}$	Volume of Total Suspended Solid (TSS) particle of class k in m
ε	Energy dissipation rate in m^2/s^3

5.6.0.3 Equations

Laminar Flow: The aggregate breakage model in laminar flow is the one proposed by [Jeldres et al., 2018].

The breakage rate of particle i of contaminants *cont* is given by Eq.(5.32):

$$\Omega_{b_{TSS,i}} = \left(\frac{4}{15\pi}\right)^{\frac{1}{2}} \left(\frac{\varepsilon}{v_{PW}}\right)^{\frac{1}{2}} exp\left(\frac{-\varepsilon^{cr}_{TSS,i}}{\varepsilon}\right) \qquad \forall\ i \tag{5.32}$$

The critical energy dissipation rate that causes the breakage:

$$\varepsilon^{cr}_{TSS,i} = \frac{B}{\left(\frac{d_{TSS,i}}{2}\right)} \qquad \forall\ i \tag{5.33}$$

The kinematic viscosity of the liquid in m^2/s

$$v_{PW} = \frac{\mu_{PW}}{\rho_{PW}} \tag{5.34}$$

Daughter particle size assumed that particle aggregate of class i will break uniformally into (i-1) classes, therefore, the fraction of particle aggregate i

breaking into k class is given by:

$$\Gamma_{TSS,i,k} = \frac{1}{i-1} \qquad \forall\ i \tag{5.35}$$

Turbulent flow: According to [Flesch et al., 1999], the same model proposed by [Jeldres et al., 2018] applies to turbulent flow.

For the alternative kernel, the power law empirical model proposed by [Pandya and Spielman, 1983] will be used:

$$\Omega_{b_{TSS,i}} = 9 \times 10^{-7}\, G^{0.71}\, v_{TSS,i}^{0.33} \qquad \forall\ i \tag{5.36}$$

The shear rate in (sec^{-1}):

$$G = \frac{\varepsilon}{v_{PW}} \tag{5.37}$$

5.7 Particle Aggregation

5.7.0.1 Assumptions

Upon aggregation, the particle aggregate is assumed to have a spherical shape.

5.7.0.2 Nomenclature

The values of the input parameters of the particle aggregation model are listed in Table (A.12) of Appendix (A).

Parameters

k_B	Boltzmann constant in J/K
T	Fluid temperature in $^\circ$
k_f	fluid properties parameter
H	Hamaker constant representing van der Walls force in J
$d_{TSS,k}$	Diameter of Total Suspended Solid (TSS) particle of class k in μm
ε	Energy dissipation rate in m^2/s^3

5.7.0.3 Equations

Laminar flow: In the laminar flow, the collision frequency between particles is governed by three mechanisms: Brownian motion h^{BM}, differential sedimentation h^{DS} and flow shear h^{SL} [Song et al., 2018].

The radius of the Total Suspended Solid (TSS) particle for i/k class in μm:

$$r_{TSS,i/k} = \frac{d_{TSS,i/k}}{2} \qquad \forall\ i/k \tag{5.38}$$

The equivalent radius of particle aggregate formed due to coalescence between particles of classes i and k in (m):

$$req_{TSS,i,k} = \frac{d_{TSS,i}\, d_{TSS,i} \times 10^6}{d_{TSS,i} + d_{TSS,k}} \qquad \forall\ i,k \tag{5.39}$$

The equation is multiplied by 10^6 to convert the diameters from μm to m.

$$h^{BM}_{TSS,i,k} = \frac{2 k_B T \left(r_{TSS,i} + r_{TSS,k}\right)^2}{3 \mu_C\, r_{TSS,i}\, r_{TSS,k}} \qquad \forall\ i,k \tag{5.40}$$

$$h^{DS}_{TSS,i,k} = \frac{\pi}{4}(r_{TSS,i} + r_{TSS,j})^2 |V_{TSS,i} - V_{TSS,j}| \qquad \forall\ i,k \tag{5.41}$$

The settling velocity of the particle of class i/k:

$$V_{TSS,i/k} = 347.5602 r^{1.54}_{TSS,i/k} \qquad \forall\ i/k \tag{5.42}$$

$$h^{SL}_{TSS,i,k} = \frac{4}{3} G \frac{\left(r_{TSS,i} + r_{TSS,j}\right)^3}{8} \qquad \forall\ i,k \tag{5.43}$$

The absolute velocity gradient:

$$G = \sqrt{\frac{\varepsilon}{\nu_{PW}}} \tag{5.44}$$

The kinematic viscosity of the liquid in m^2/s:

$$v_{PW} = \frac{\mu_{PW}}{\rho_{PW}} \tag{5.45}$$

The total collision frequency is given by:

$$h^{TOL}_{TSS,i,k} = h^{BM}_{i,k} + h^{DS}_{i,k} + h^{SL}_{TSS,i,k} \qquad \forall\ i,k \tag{5.46}$$

The coalescence efficiency is given by:

$$\lambda_{TSS,i,k} = k_f\, e^{0.18}_{TSS,i,k} \qquad \forall\ i,k \tag{5.47}$$

Where e is a parameter that represents the relation between van der Walls force and flow shear force.

$$e_{TSS,i,k} = \frac{H}{36\pi\mu_C Greq_{TSS,i,k}} \qquad \forall\ i,k \tag{5.48}$$

Therefore, the agglomeration efficiency is given by:

$$\Omega A_{TSS,i,j} = h^{TOL}_{TSS,i,k}\lambda_{TSS,i,k} \qquad \forall\ i,k \tag{5.49}$$

Turbulent flow: In the case of turbulent flow, the only difference from the laminar case is in the collision frequency where the only mechanism contributing to the collision between the particles is the flow shear [Song et al., 2018].

$$h^{SL}_{TSS,i,k} = \sqrt{\frac{8\pi}{15}}\, G\, \frac{(r_{TSS,i} + r_{TSS,j})^3}{8} \qquad \forall\ i,k \tag{5.50}$$

5.8 Population Balance Equations

The purpose of this sub-model is to find the differential equation that describes the rate of change of droplets and particles. To find this equation, the birth and death of droplets and particles due to the breakage and coalescence are modeled.

The general form of the Population Balance Equations is based on the work of [Kumar and Ramkrishna, 1996], however, some equations have been added to fit the proposed discretization of the volume space.

5.8.0.1 Assumptions

- The breakage at the smallest class will not result in droplets of new class sizes therefore no breakage takes place at this class.
- No coalescence/aggregation takes place at $k = n_c$, the largest class size.

5.8.0.2 Nomenclature

The values of input parameters of the PBEs model are listed in Table (A.13) of Appendix (A).

Parameters

$n_{cont,k}$	initial number of droplets of class i
$v_{cont,k}$	volume of droplet/particle of contaminant $cont$ and class k in m^3
$A_{i,j}$	coalescence rate between droplets of class i and $k-i$ in μm
G_i	breakage rate of droplets of class i in μm
$\Gamma_{i,k}$	probability density function (PDF) of droplets breaking from class i to k in m^2/s^3

5.8.0.3 Equations

Given the logarithmic discretization of the droplet/particle volume space, the space is discretized into n_c number of classes with i representing the class index and ii and k are aliases of i. Upon coalescence/aggregation of n_i and n_{ii} number of droplet/particle of volume v_i and v_{ii}, droplets/particles of volume v_{i+ii} are born.

$$n_{cont,i+ii} = \Omega^{B/A}_{cont,i,ii} n_{cont,i} n_{cont,ii} \qquad \forall\, cont,\ i < n_c, ii < n_c, i \leq ii \tag{5.51}$$

To ensure the conservation of the total contaminant volume within the space,

the total volume of the new droplets/particles $n_{i+ii}\,v_{i+ii}$ is distributed among class k and $k+1$ such that:

$$v_k < v_{i+ii} < v_{k+1} \tag{5.52}$$

$$n_{i+ii} = n_k + n_{k+1} \tag{5.53}$$

$$n_{i+ii} v_{i+ii} = n_k v_k + n_{k+1} v_{k+1} \tag{5.54}$$

Birth of droplet/particle due to coalescence: the number of droplets/particles of class k generated due to coalescence is given by Eq. (5.55):

$$Bc_{cont,k} = \sum_{i=1}^{n_c-1} \sum_{ii=1,ii\geq i}^{n_c-1} n_{cont,k} \qquad \forall\ cont,\ k \tag{5.55}$$

The number of droplets/particles of class k disappeared due to coalescence is given by [Kumar and Ramkrishna, 1996]:

$$Dc_{cont,k} = n_{cont,k} \sum_{i=1}^{n_c-1} \Omega^{B/A}_{cont,i,k}\, n_{cont,k} \qquad \forall\ k \neq n_c, cont \tag{5.56}$$

The number of droplets/particles of class k generated due to breakage is given by [Kumar and Ramkrishna, 1996]:

$$Bb_{cont,k} = \sum_{i>k}^{i=n_c} \Omega^{B}_{cont,k} \Gamma_{i,k}\, n_{cont,i}\, \frac{v_{cont,i}}{v_{cont,k}} \qquad \forall\ k \neq n_c, cont \tag{5.57}$$

The number of droplets/particles of class k disappeared due to breakage is given by [Kumar and Ramkrishna, 1996]:

$$Db_{cont,k} = \Omega^{B}_{cont,k}\, n_{cont,k} \qquad \forall\ k \neq 1, cont \tag{5.58}$$

Therefore, the rate of change of droplets/particles of class k of contaminant *cont* is given by the following differential equation:

$$\frac{d}{dt}n_{k,cont} = Bc_{cont,k} - Dc_{cont,k} + Bb_{cont,k} - Db_{cont,k} \qquad \forall\ k, cont \tag{5.59}$$

5.9 Separation

This model presents how the separation of droplets and particles, based on their size, takes place given the cut diameter and the updated droplet/particle size distribution of Oil & Grease ($O\&G$) and Total Suspended Solid (TSS) that results from the population balance equations model.

5.9.0.1 Nomenclature

The values of input parameters of the separation model are listed in Table (A.14) of Appendix (A).

Parameters

$d_{cont,i}$	Initial number of droplets of class i in μm
$CD_{tech,cont}$	Cut diameter of $cont$ by $tech$ in μm
$V^{c,in}_{cont,i}$	Initial total volume per class i for each $cont$ in m^3
$Rv_{tech,cont,i}$	Removal efficiency of technology $tech$ for each class i of contaminant $cont$ in %

5.9.0.2 Equations

The separation of particles/droplets takes place if the droplet/particle's diameter is greater than the cut diameter for the chosen technology $tech$:

$$d_{i,cont} \geq CD_{tech,cont} \qquad \forall\ i, cont, tech \tag{5.60}$$

The total volume per class i for each $cont$ in m^3 after the separation:

$$V^{c,out}_{cont,i} = V^{c,in}_{cont,i}(1 - Rv_{tech,cont,i}) \qquad \forall\ i, cont, tech \tag{5.61}$$

The total volume for each *cont* in m^3 after the separation:

$$V_{cont}^{tot,out} = \sum_{i=1}^{i=n_c} V_{cont,i}^{c,out} \qquad \forall\ cont \tag{5.62}$$

The normalized droplet/particle size distribution after the separation is:

$$PSD_{cont,i}^{out} = \frac{V_{cont,i}^{c,out}}{V_{cont}^{tot,out}} \qquad \forall\ i, cont \tag{5.63}$$

5.10 Summary

This chapter presents the mathematical formulation of sub-models about the establishment and update of droplet/particle size distribution, according to the proposed volume discretization method introduced herein. It also presents the modeling phenomena contributing to size distribution changes, including breakage and coalescence/aggregation, across various flow types. These sub-models are integrated with discrete Population Balance Equations to compute the rate of change of droplets/particles. Subsequently, the separation sub-model utilizes the outcomes of the PBEs to update the size distribution, yielding the final distribution post-separation. The subsequent chapter shows the implementation results of these sub-models alongside those from the preceding one.

Chapter 6

Case Studies

In this chapter, the proposed sub-models from Chapter (4 and 5) are applied to various case studies to show the proposed model's versatility and practicality. The insights gained from each case study are used to inform the next one. Starting by Section (6.1), Fresa parameters shown in Table (6.1) are varied to examine their impact on the obtained solutions. From there, their values will be fixed to run the subsequent case studies. In Section (6.2), the impact of volume space discretization on the process design is tested by solving the model for a different number of classes. Based on the volume conservation of the contaminants after the discretization, the number of classes will be determined to solve the model in Section (6.3). In this section, the model parameters that define the stream characteristics, Table (6.2), are varied. Finally, different breakage and coalescence kernels are used to solve the population balance equations in Section (6.4).

Fresa is written in Julia. Julia was chosen due to its parallel processing feature which distributes the processing over multiple cores and hence results in a higher performance than single processing [Julia Language, 2024]. For the proposed problem, a computer system with 36 cores has been used.

6.1 Fresa Performance

For the given case study below, Fresa was run with the parameter values given in Table (6.1) which are varied to test their impact on the obtained solutions. According to the values in the table, Fresa will go through 2,500 iterations during the

Table 6.1: Fresa parameter values used to solve the first case study

Parameter	Value
Number of Solutions to Propagate	10
Number of Generations	2,500
Similarity Index ε	10,000

optimization process. At each iteration, 10 solutions will be selected to create new individuals for the next iteration based on their fitness value. For two solutions to be included in the non-dominated set, the distance between their values is more than 10^4.

6.1.1 Illustrative example

Produced water from an offshore facility of an oil and gas industry is treated to meet discharge requirements. The main contaminants to be removed from the feed stream are *Oil and Grease* (*O&G*) and *Total Suspended Solids* (*TSS*). The water stream characteristics used to solve this problem are listed in Table (6.2) and the discharge requirements of the contaminants are in Table (6.3).

Table 6.2: Model initial parameters used to create the initial size distribution where $logV^{min}$ and $logV^{max}$ are the logarithmic corresponding values of the smallest and largest diameter in the volume space of contaminant droplets and particles, n_c is the number of discrete volume classes, μ is mean of diameters for the size distribution, σ is the standard deviation values for the volume distribution, Q is the initial mass flowrate of the inlet stream

Parameter	Value	Unit
$logV^{min}$	10.6	-
$logV^{max}$	16	-
n_c	10	-
μ	10	μm
σ	100	-
Q	250	ton/hr

The resulting inlet size distribution of *Oil and Grease* droplets and *Total Suspended Solids* particles follow a normal distribution, as shown in Figure (6.1), and are represented by the discrete mapping shown in Table (6.4) with droplets/particles diameters ranging from 4.5 to 267.3 μm.

Table 6.3: Target contaminants and their desired values in (mg L^{-1}) for the discharge option. C^{in}_{cont} is the initial concentration of the contaminant in the water stream and C^{f}_{cont} is the final concentration requirements [Bagheri et al., 2018]

Cont	C^{in}_{cont}	C^{f}_{cont}
O&G	1,500-2,200	40
TSS	189	30

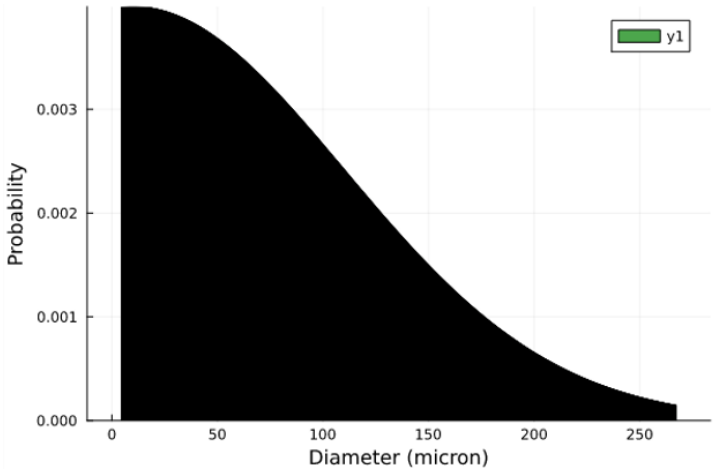

Figure 6.1: *Probability distribution of droplets and particles over the volume space range obtained using the parameters in Table (6.2)*

6.1.2 Results and Analysis

Number of Solutions to Propagate: The number of solutions to propagate at each generation was increased from 10 to 20, and 30. Figure (6.2) shows the set of non-dominated solutions obtained by solving the case study for different values of solutions to propagate. A higher number of solutions to propagate did not result in a denser, more diverse, or higher number of solutions in our case which is in line with the literature [de Jonge and van den Berg, 2020]. This means 30 solutions to propagate did not result in a better solution compared with 20 especially with computational time significantly increasing from 23 hours for 20 solutions to 31 hours for 30 solutions. Figure (6.3) shows the computational time for each value of the number of solutions to propagate.

Number of Generations: The number of generations was increased from 500 to

Table 6.4: The initial normalized droplets/particles size distribution of Oil & Grease ($O\&G$) and Total Suspended Solids (TSS) in the produced water inflow based on the parameters in Table (6.2) where i is the class number, d_i is the diameter of the droplet/particle is class i, and PD_i is the normalized probability distribution of droplets/particles in volume class i

i	d_i	PD_i
1	4.5	0.1291
2	7.1	0.1293
3	11.2	0.1293
4	17.7	0.1290
5	27.8	0.1275
6	43.8	0.1227
7	68.8	0.1098
8	108.2	0.0812
9	170.1	0.0367
10	267.3	0.0047

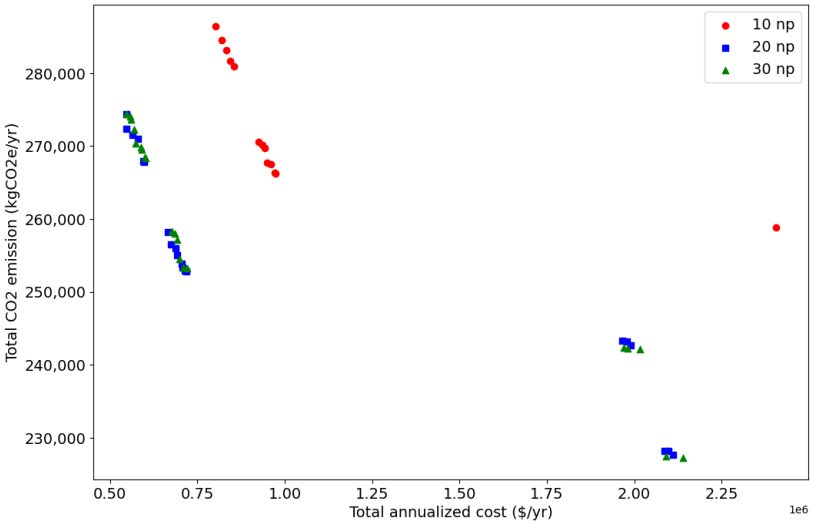

Figure 6.2: *Set of non-dominated solutions obtained by solving the case study with parameters in Table (6.2 and 6.3) for different values of the number of solution to propagate n_p, 2,500 generations and $\varepsilon = 10^4$*

2,500. Figure (6.4) displays the set of non-dominated solutions obtained for each value of generation number. 1,000 generations appear to be sufficient to give confidence that a good solution has been obtained while ensuring that the computational demands are not excessive. Although the 2,000 generations appear to obtain a slightly better solution, it requires more computation compared with the 1,000 generations.

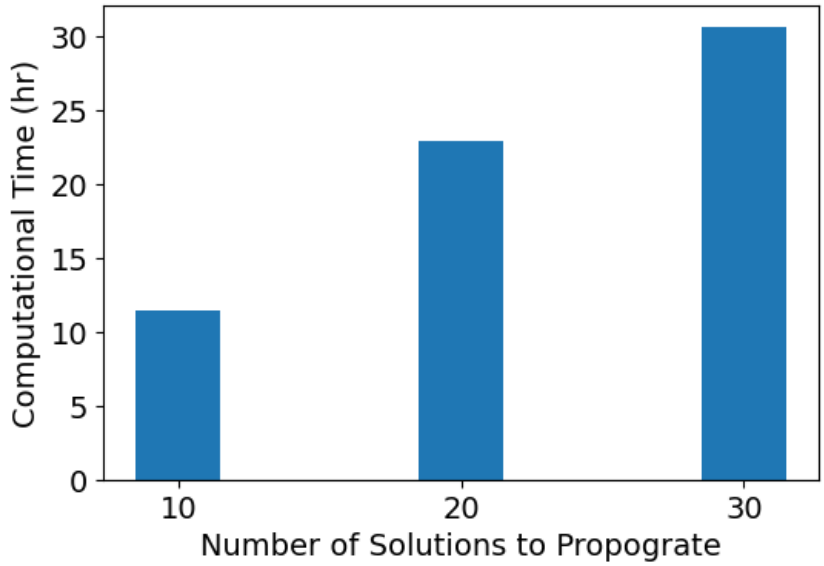

Figure 6.3: *Computational time taken for solving the multi-objective optimization problem for 2,500 generations and different values of a number of solutions to propagate n_p.*

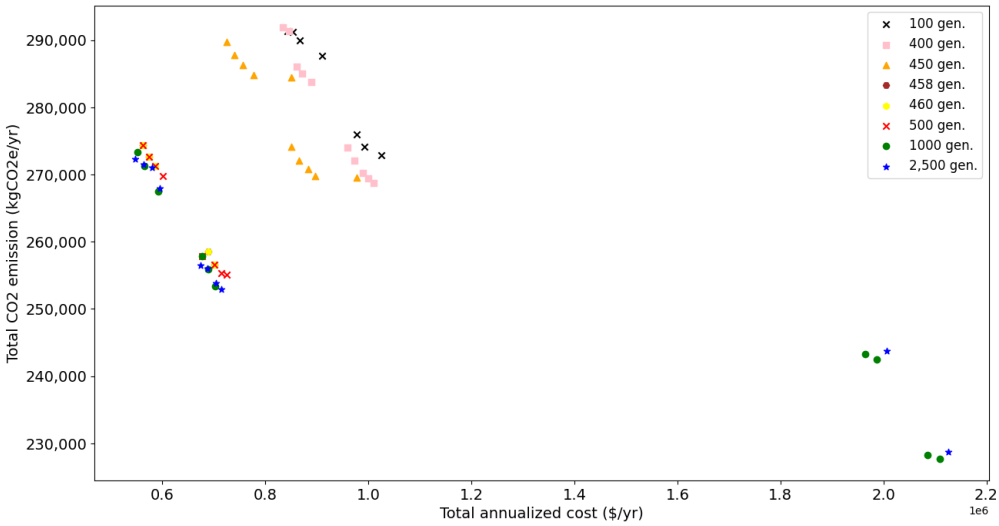

Figure 6.4: *Set of non-dominated solutions obtained for different generations showing how the solution evolved*

Given that Fresa solver uses heuristic methods to solve optimization problems, they find approximate solutions that are close to the best one quickly and easily compared with the classic methods. Heuristic methods achieve that by trading optimality and accuracy for speed however, there is no guarantee that the optimal solution can be achieved. Although the solutions obtained by

these methods are not optimal, they are still considered valuable given that they can be found in a relatively short time [Desale et al., 2015].

As an evolutionary algorithm, Fresa incorporates a crucial aspect: maintaining a balance between exploration and exploitation to avoid getting stuck in local optima. Exploration involves searching the neighborhood to refine existing solutions through crossover and mutation. In contrast, exploitation focuses on seeking solutions in new regions, achieved through selection [Pytel, 2020].

Solution Evolution Over Time: Running the optimization over 2,500 generations resulted in 68,285 objective function evaluations. The best solution found by Fresa was at 60,280 function evaluations. The rapid decrease in the objective function value can be seen in Figure (6.4) from 459 to 458 generations. After that, the improvement in the solution becomes smaller with a significant increase in the computational time.

Impact of Similarity Index: To ensure the diversity of the returned solutions, the population was pruned using "similarz" function that eliminates solutions that have similar values of the objective functions. In our case, the similarity index ε was varied from 10^4 to 2×10^4 and then 3×10^4 to ensure different configurations are obtained as demonstrated in Figure (6.5). 10^4 resulted in better solutions compared with 2×10^4 and 3×10^4.

Impact of Solution Initialization: To assess the influence of initialization on the resulting Pareto-front, the problem was solved with two initial solutions, each representing a different system design. As displayed in Figure (6.6), the non-dominated solution sets generated from these varied initializations are similar. This slight variation observed can be attributed to the stochastic nature of the solution method rather than sensitivity to the initial conditions. These findings imply that the Fresa algorithm is consistent in solving this design problem.

Multiple Runs: Due to the stochastic nature of Fresa, the design problem was solved 10 times to determine whether the stochastic aspects affect the quality

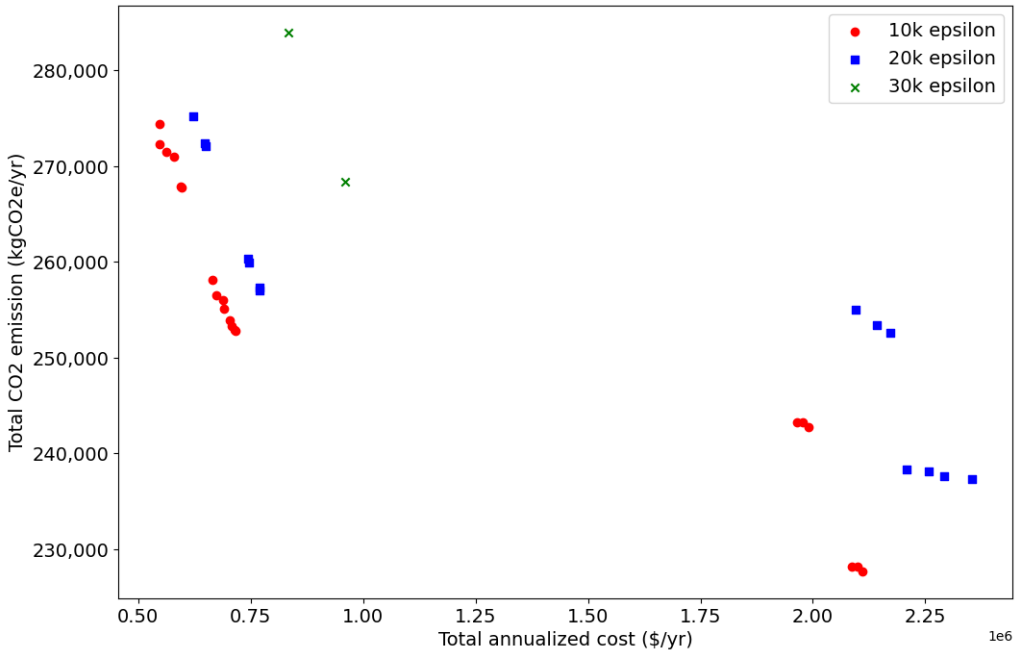

Figure 6.5: *Set of non-dominated solutions obtained by solving the multi-objective optimization problem for different ε with 2,500 generations and 20 solutions to propagate*

of designs obtained, with the settings described above. In all cases, the obtained non-dominated solutions sets look similar with slight variation due to the stochastic nature of the algorithm as shown in Figure (6.7).

Number of Generated Solutions: On average, Fresa produces 2.5 new solutions for every member of the population propagated per generation, leading to approximately 62,500 process designs being evaluated in the search.

Model Verification: The model has been with another method (Genetic Algorithm) for verification [Fraga, 2022]. The solutions obtained by Fresa after the evaluation of around 62,000 designs are better than those obtained using a genetic algorithm for 100,000 function evaluations.

Solution Clusters: The obtained solutions appear in two clusters due to the use of the Hadamard product fitness function to rank the solutions by Fresa which emphasizes points that are towards the ends of the approximation to the Pareto frontier leading to a broader and more diverse solution set [Fraga, 2021]. Fig-

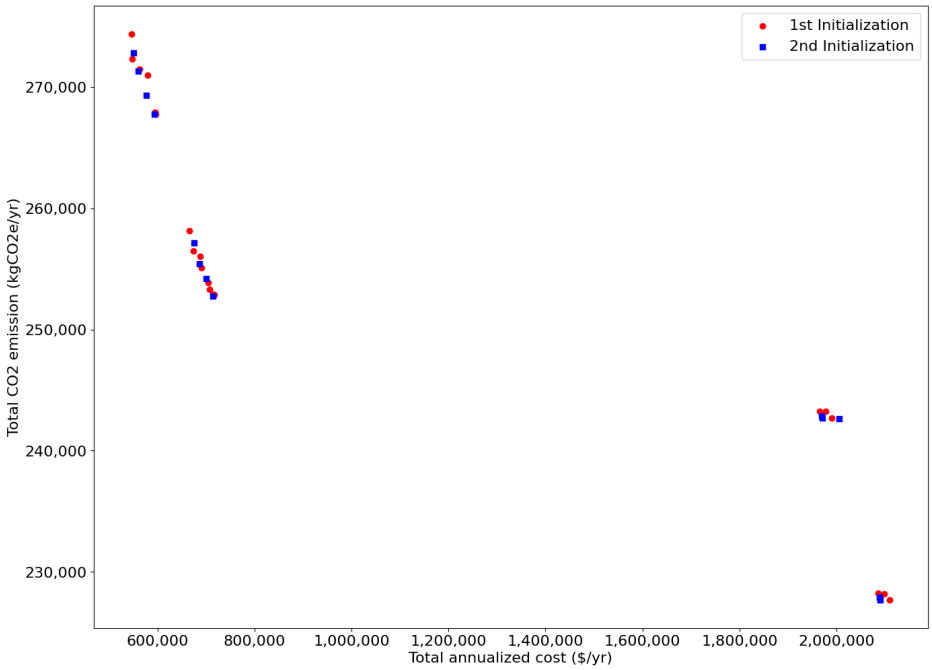

Figure 6.6: *Sets of non-dominated solutions obtained by solving the multi-objective optimization problem for different initialization*

ure (6.8) shows the designs of key flowsheets obtained by solving the original case study. The first flowsheet consists of Corrugated Plate Interceptors followed by Centrifuge. This flowsheet falls in the cluster to the upper left of the graph indicating higher cost and lower emission while the second flowsheet, Corrugated Plate Interceptors followed by Hydrocyclone falls in the lower right cluster representing the lower emission and higher cost flowsheet.

Optimal Solution: The above graphs display a set of non-dominated solutions that illustrate the trade-off between two objectives. At this stage, no solution can be considered the overall optimal solution since both objectives are equally important. The selection of the best solution depends on the decision maker's preferences, based on which objective is prioritized. Additionally, methods such as multi-criteria decision analysis can be integrated with multi-objective optimization to provide a more comprehensive framework for selecting the best design.

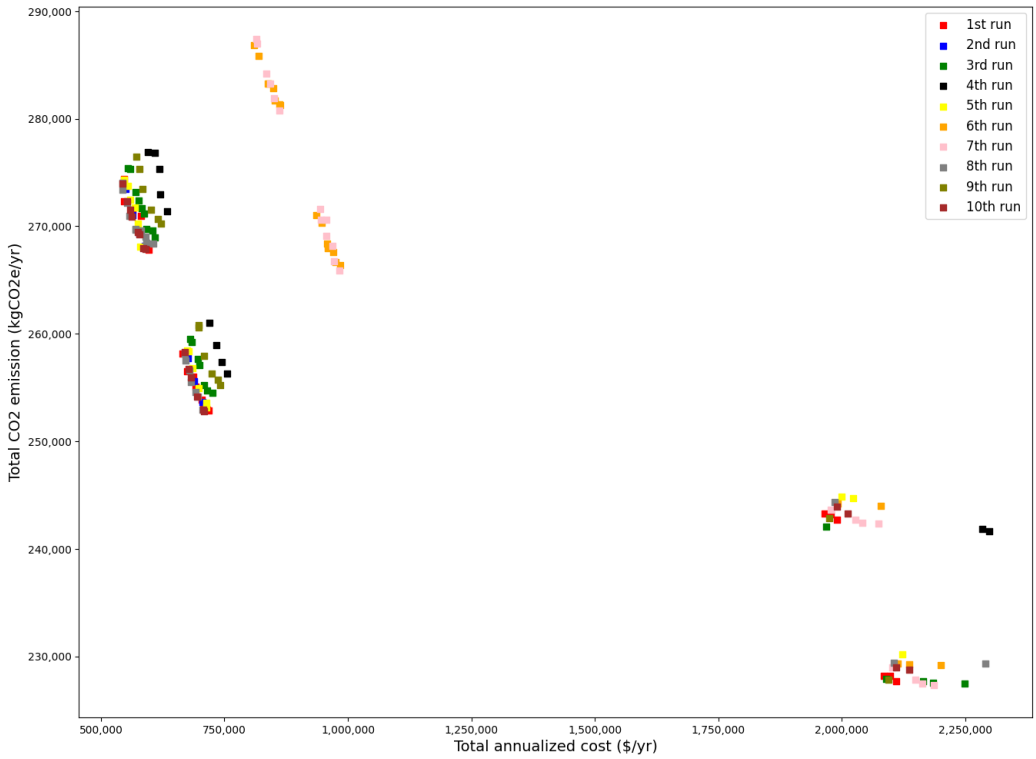

Figure 6.7: *Sets of non-dominated solutions obtained by solving the multi-objective optimization problem for 10 runs*

6.1.3 Conclusion

From the above, we can conclude that the Fresa algorithm is suitable for solving this design problem and can obtain good solutions with an acceptable computational demand with 1,000 generations, 20 solutions to propagate, and a 10^4 similarity index. These parameters will be used to solve all the subsequent case studies.

6.2 Impact of Volume Classes Discretization on Process Design

The impact of discretization of the droplet/particle size distribution on the process design was tested by varying the number of classes from 5 to 20. The volume of the smallest and largest droplets remains the same for all cases. However, the volume of the classes in between varies with the number of classes. Compared to the original case with 10 classes, the performance of the model and the design outputs have varied as described below.

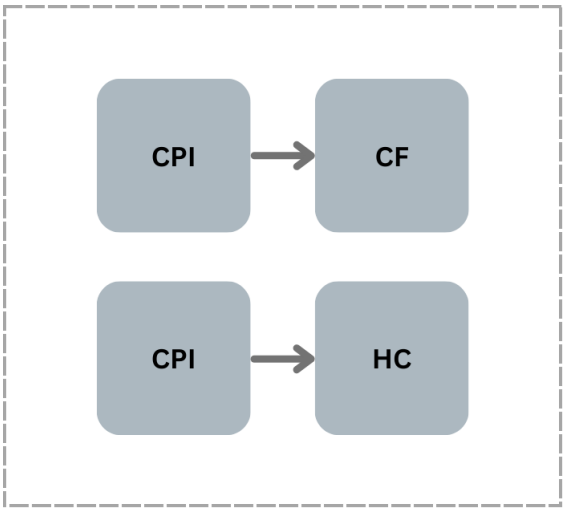

Figure 6.8: *Flowsheets obtained by solving the original case study for 1000 generations, 20 solutions to propagate, 10^4 similarity index where CPI is Corrugated Plate Interceptors, CF is Centrifuge and HC is Hydrocyclone.*

6.2.1 Illustrative Example

Produced water from an offshore facility of an oil and gas industry is treated to meet discharge requirements. The main contaminants to be removed from the feed stream are *Oil and Grease* and *Total Suspended Solids*. The water stream characteristics used to solve this problem are listed in Table (6.2), on page 146, except for the number of volume classes n_c that is varied from 5 to 20 classes. The initial concentration and the discharge requirements of the contaminants are in Table (6.3) on page 146.

6.2.2 Results and Analysis

6.2.2.1 Computational Time

The time taken to run the model with the same machine for a different number of classes has varied. The larger the number of class sizes the longer the computational time. This is because of the increase in the time needed for solving the differential equations for the change in the number of droplets/particles due to the breakage and coalescence. Table (6.5) shows the increase in the computational time for each number of classes.

Table 6.5: Computational time to obtain the set of non-dominated solutions for different number of classes n_c in hours

n_c	Time (hr)
5	0.95
10	9.38
15	39.05
20	71.39

6.2.2.2 Non-dominated Solution Set

13 non-dominated solutions were obtained when the number of classes n_c is 5 and 10, 19 solutions for 15 classes, and 14 solutions for 20 classes. Figure (6.9) shows the set of non-dominated solutions obtained for solving the multi-objective optimization model for different numbers of classes. A discrete curve is obtained rather than smooth due to discrete design choices. Table (6.6) displays the most cost-effective solution and the most environmentally friendly solution obtained for each value of the number of classes with the remaining solutions varying between these two solutions in the space. The variation in the cost is the highest in the case of 15 classes where the cost is almost 13 times higher in the most environmentally friendly compared with the most cost efficient. On the other hand, the variation is the lowest 24 % only between the most cost-effective and environmentally friendly solutions in the case of 5 classes. The variation in the emission is lower compared with the cost as the maximum is only 17 % higher in the case of 5 classes and the lowest is 6% different in the case of 20 classes.

Table 6.6: The most cost-effective and environmentally friendly solutions for each number of classes n_c

n_c	Cost ($\$/yr$)	Emission ($KgCO_2e/yr$)
5	596,298	273,483
	2,220,000	226,809
10	802,288	286,459
	2,405,650	258,829
15	547,128	276,451
	7,254,404	255,012
20	811,933	290,342
	1,007,954	271,836

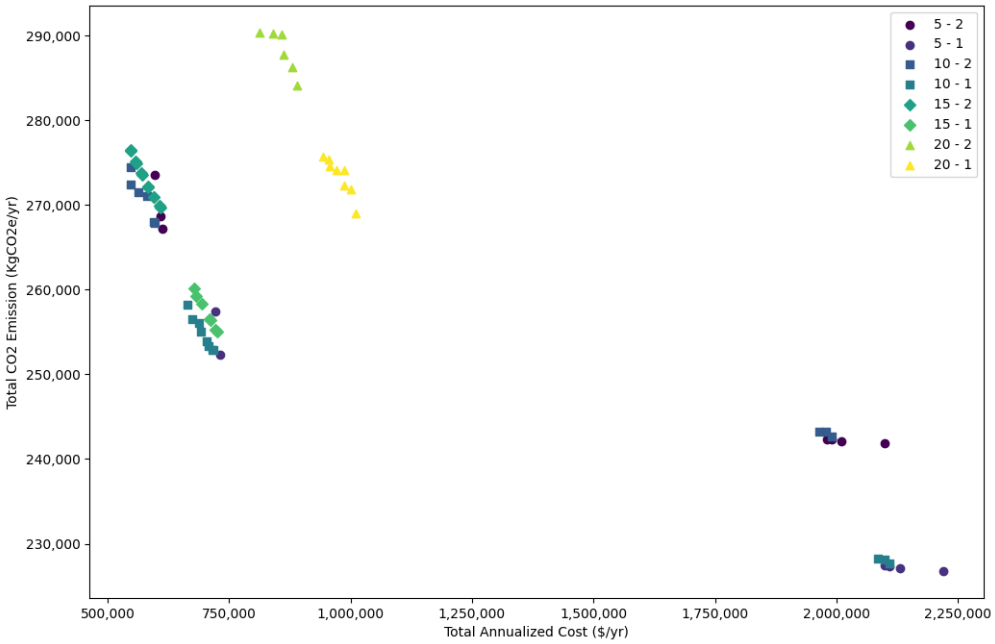

Figure 6.9: *Set of non-dominated solutions obtained for different number of classes n_c classified by the selected sludge option where the legend represents the pair of class number n_c and sludge option slg (n_c- slg)*

The variation in the number of classes resulted in different configurations and also the final concentrations of the oil & grease and total suspended solids have varied with the number of volume classes as displayed in the parallel coordinates plot in Figure (6.10). The vertical axes in the diagram represent the number of classes n_c and the final output concentration of oil & grease and total suspended solids in mg/L. Each connected line across all the axes represents a different design. The designs obtained by solving the optimization problem for a given number of classes have the same color. For example, one of the designs obtained for 20 classes, where the line color is purple, resulted in an output stream with a concentration of 0.0029 mg/L for oil & grease and around 18.5 mg/L for the total suspended solids.

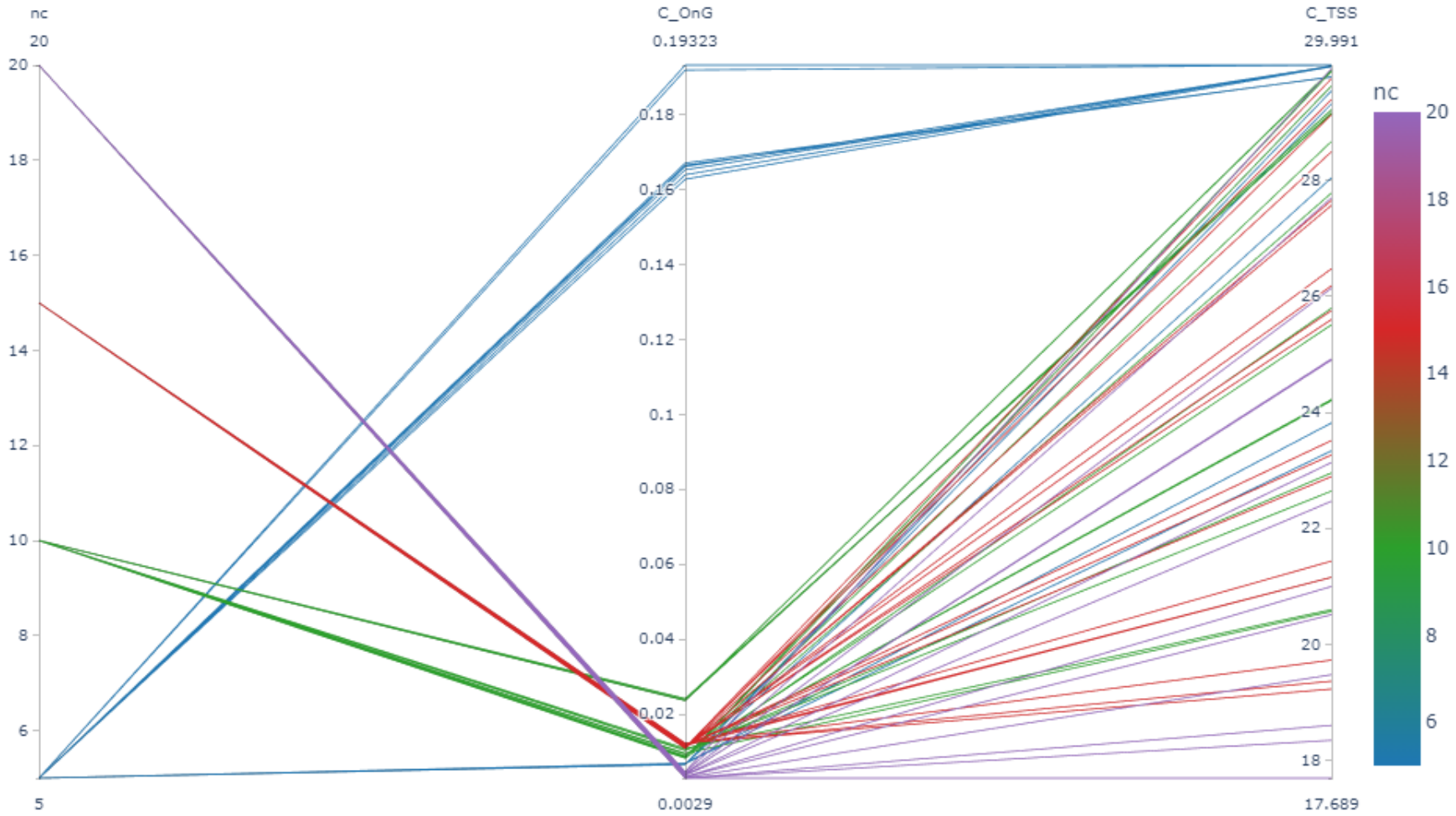

Figure 6.10: *Parallel Coordinates plot showing the variation in the Oil & Gas (O&G) and Total Suspended Solid (TSS) final concentration with the number of volume classes n_c*

Figure (6.10) reveals two notable observations. The first one is related to the difference in the concentration levels of oil & grease and total suspended solids. The second is the spread of the output concentration for the number of classes. The variation in the stream specifications between the different number of classes can be attributed to the impact of breakage and coalescence on the droplet/particle size distribution. To understand the reasons behind this variation, two designs from the non-dominated solution set for 5 classes are chosen for illustration. Table (6.7) presents the final concentrations obtained for oil & grease and total suspended solids for these two solutions.

Table 6.7: Values of the final oil & grease ($O\$G$) and total suspended solids (TSS) concentration for two designs and using 5 volume classes

Design	$O\&G\ (mg/L)$	$TSS\ (mg/L)$
1	0.0068	23.3
2	0.0065	29.5

The first observation is that the output concentration of oil & grease is lower than that of total suspended solids although the initial concentration of the former is 1,850 and 189 mg/L for the latter. This is attributed to the difference in the size distribution between oil & grease and total suspended solids. Figure (6.11 (a)) shows the obtained distribution for oil & grease and total suspended solids as a result of the breakages and coalescence. We can observe from the figure that the volume of oil & grease has been shifted to classes 4 and 5. In the case of total suspended solids, the volume has been shifted to class 1. For oil & grease, the coalescence has an impact on the droplet while there is no breakage taking place resulting in droplets becoming larger and hence shifting to the larger classes. In the case of the total suspended solids, the breakage rate of particles exceeds the aggregation resulting in smaller droplets. The reasons behind this dynamic are attributed to the selection of the breakage and coalescence kernels which will be discussed in detail in Section (6.4) of this chapter.

This shift in the size distribution affects the removal efficiency of droplets and particles. Figure (6.11 (b)) shows the removal efficiency of oil & grease and total

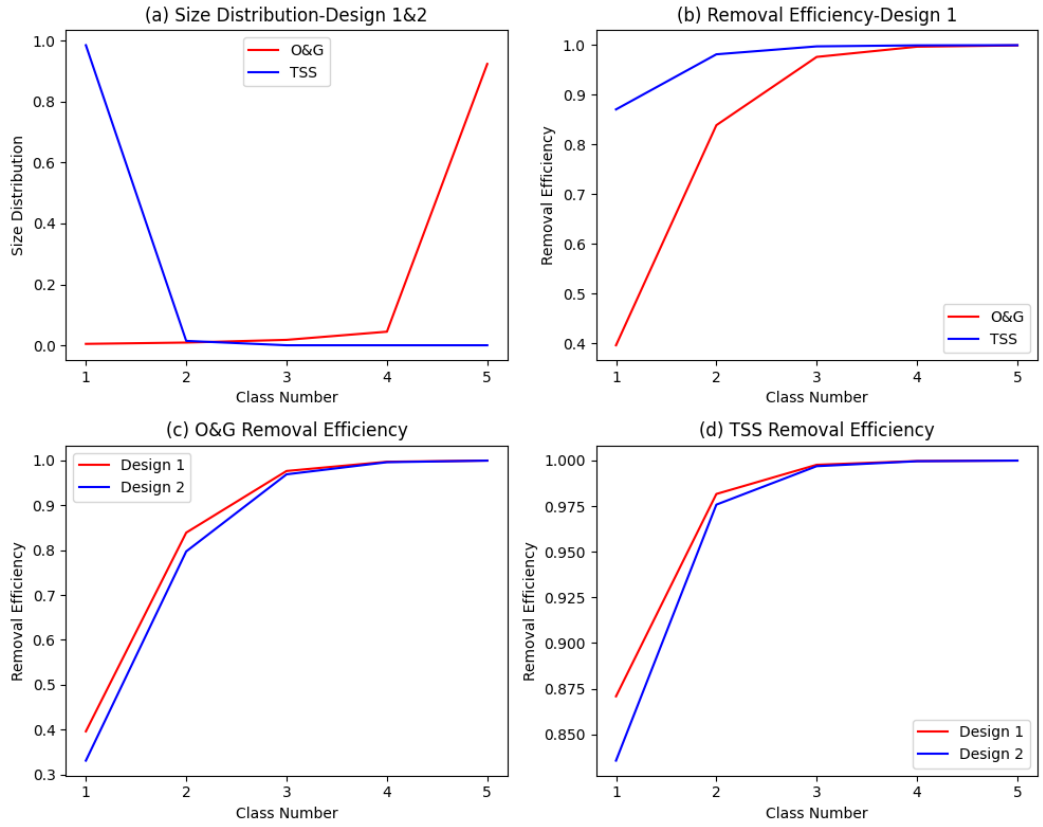

Figure 6.11: *Size Distribution and Removal Efficiency of Oil & Gas (O&G) and Total Suspended Solid (TSS) by Hydrocyclone (HC) using 5 volume classes* n_c

suspended solids for design 1. We can see the removal efficiency of oil & grease is between 0.4 and 0.85 for classes 1 and 2 and above 0.9 for the remaining classes. For total suspended solids, the removal efficiency is around 0.88 for the first class and above 0.9 for the rest. In the case of oil & grease, the removal efficiency is above 0.9 in classes 4 and 5 where most of the volume is and it is less than 90 for total suspended solids in class 1 where most of the volume has been shifted. Higher removal efficiency with higher volume results in lower concentration output as in the case of oil & grease and lower removal efficiency with higher volume results in higher output concentration.

The other observation we can notice from Figure (6.10) is that the output range of oil & grease is clustered around a small range for each number of classes. On the contrary, for total suspended solids, the concentration output varies from 17.6 to 29.9 mg/L for all classes. In the case of oil & grease, although there is a difference

in the removal efficiency between design 1 and 2 for 5 classes as shown in Figure (6.11 (c)), this difference is in classes 1 to 3 where there is a small fraction of volume. In classes 4 and 5, the removal efficiency is almost 1.0 for both designs. Changing the value of design variables will not affect the separated volume of oil & grease significantly.

In the case of total suspended solids, Figure (6.11 (d)) shows the removal efficiency for total suspended solids particles for the two designs. In design 1, the removal efficiency of class 1 is 0.88 compared with 0.84 for design 2. With almost all the volume of total suspended solids shifted to class 1, a small variation in the removal efficiency results in a relatively significant change in the output concentration.

6.2.2.3 Flowsheet

The obtained solutions represent different configurations as shown in Figure (6.12) which displayed the configurations of the process including the sludge option. The problem was solved to meet the requirements of discharge which are 40 mg/L for oil & grease and 30 mg/L for total suspended solids. Two units could meet these requirements for all classes except for 20, which needed three stages.

In the case of 5 and 10 classes, the only units that do not have constraints related to the inlet stream for the first stage are the American Petroleum Institute separator and the Corrugated Plate Interceptors separator. The latter was chosen in all solutions as a primary treatment unit due to its smaller footprint and hence cost and emission although its separation efficiency is lower than that of the American Petroleum Institute separator. The purpose of the first stage was to meet the inlet requirements of the next unit which is Hydrocyclone and Centrifuge separators which is why a relatively lower removal efficiency was needed to remove all the droplets and particles larger than 200 and 100 μm.

For the second stage, Nutshell Filter, and Microfiltration Membrane have higher inlet constraints that can not be met be met by the Corrugated Plate Interceptors separator. This leaves us with Hydrocyclone, Centrifuge, and Induced Gas Flotation. The inlet concentration requirement for Induced Gas Flotation is

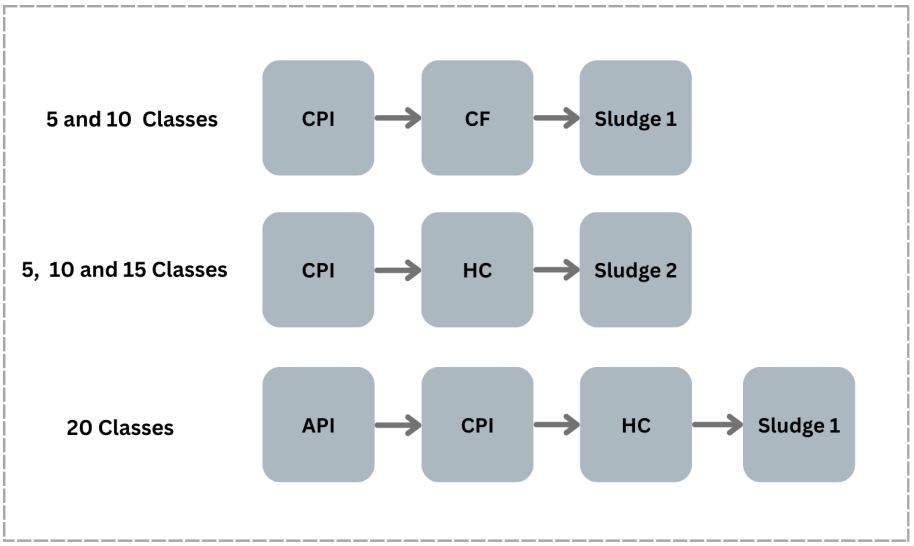

Figure 6.12: *Flowsheets obtained by solving the multi-objective optimization for different number of classes where API is American Petroleum Institute separator, CPI is corrugated Plate Interceptors separator, HC is Hydrocyclone separator, CF is Centrifuge separator, Sludge 1 is machine thickening and Sludge 2 is machine thickening and incineration*

1,000 mg/L which was met in some of the obtained designs by Corrugated Plate Interceptors separator. However, Hydrocyclone and Centrifuge have a higher inlet concentration limit which gives them an advantage over Induced Gas Flotation. Additionally, Hydrocyclone and Centrifuge have lower capital and operating costs compared with Induced Gas Flotation. The only requirements of the Hydrocyclon and Centrifuge that need to be met are not to have droplets and particles of diameter more than 200 and 100 μm respectively which was satisfied by the Corrugated Plate Interceptors separator.

The alternating between Hydrocyclon and Centrifuge represents the trade-off between cost and emission. While the cost of a Centrifuge is higher in all the designs, it is emission is lower than that of a Hydrocyclon. This is because the main factor that affects the emission in the case of Hydrocyclon and Centrifuge is the size of the unit which is larger in the case of Hydrocyclon than Centrifuge.

In case of 15 classes, due to the wider spread of volume between the classes, with Corrugated Plate Interceptors separator, the requirements of Centrifuge could not be satisfied which is removing the droplets and particles larger than 100 μm

which means Hydrocyclon was the only option given that the other options were eliminated as explained above. Therefore, for 15 classes, the only configuration was a Corrugated Plate Interceptor separator followed by a Hydrocyclon. Similarly, for 20 classes, with the American Petroleum Institute separator and Corrugated Plate Interceptors separator, it was not possible to meet the requirement for a Centrifuge, so Hydrocyclon was chosen.

The sludge fraction produced by the configuration from the initial stream accounts for approximately 0.4%, aligning closely with literature findings [Andreoli et al., 2007] which reported a value of 0.265%. Among the sludge options considered, the third option—machine thickening and melting—was consistently outperformed by the second option, machine thickening, and composting, in terms of both cost and emissions. Consequently, the first and second options were chosen as the primary choices, representing a trade-off between cost and emissions. This contradiction is reflected in the two separate clusters observed in the Pareto front illustrated in Figure (6.9). Detailed cost and emission values for the sludge options can be found in Table (A.24) in Appendix (A).

6.2.2.4 Design Variables

All the identified designs have the same configurations; Corrugated Plate Interceptors separator followed by Hydrocyclone. The values of the design variables of these two units are discussed below. The design variables of the Corrugated Plate Interceptors separator unit are displayed using a parallel coordinates plot, Figure (6.13).

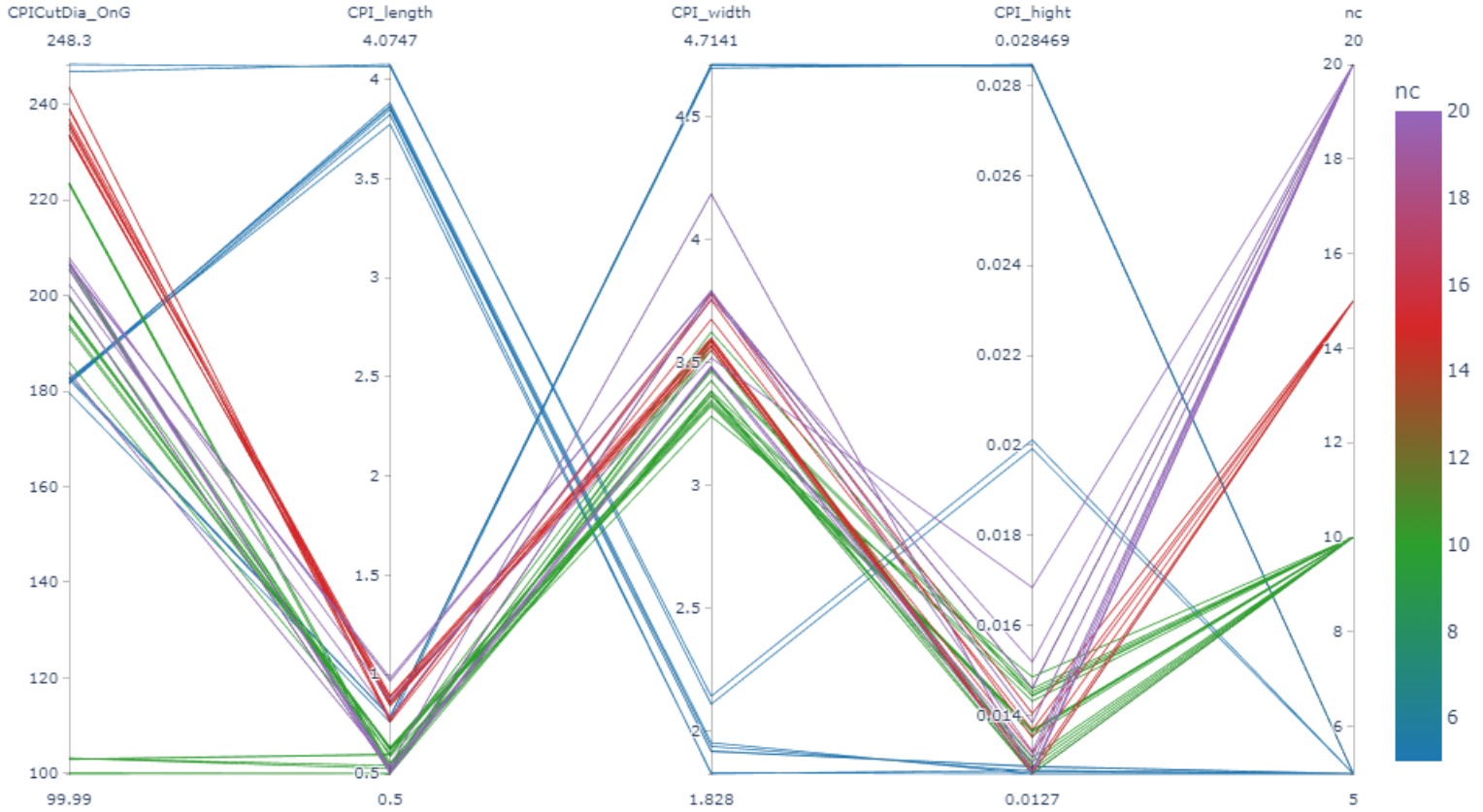

Figure 6.13: *A parallel coordinate visualization diagram showing the range of the Corrugated Plate Interceptors separator design variables for different numbers of classes n_c*

Corrugated Plate Interceptors separator cut diameter: The cut diameter of the oil droplets is closer to the upper bound, 270 μm, than to the lower bond which is 30 μm as shown in Figure (6.13). For 5 classes, it is above 180 μm as it is enough to meet the requirements for both Hydrocyclone and Centrifuge which are 100 and 200 μm respectively. In the case of 10 classes, it is closer to 100 μm when the next unit is Centrifuge and closer to 200 μm when the next is Hydrocyclone. For 15 and 20 classes, the value is higher than 180 μm and below it for 20 classes. Given the logarithmic scale of the size distribution, as shown in Table (6.8), and to meet the inlet requirement of Hydrocyclone, the minimum possible cost can be achieved by removing only the classes with diameter larger than 200 μm. In the case of 20 classes, the cut diameter falls between 174.2 μm and 215 μm while in the case of 5 classes, it is closer to the upper bound, 270 μm.

Table 6.8: The droplets/particles diameter of oil & grease ($O\&G$) and total suspended solids (TSS) in the produced water inflow based on the parameters given in Table (6.2) for different numbers of classes

i	5	10	15	20
1	4.5	4.5	4.5	4.5
2	12.6	7.1	6.1	5.6
3	34.9	11.2	8.1	7.0
4	96.6	17.7	10.9	8.6
5	267.3	27.8	14.6	10.7
6		43.8	19.5	13.3
7		68.8	26.2	16.5
8		108.2	34.9	20.4
9		170.1	46.7	25.3
10		267.3	62.5	31.4
11			83.6	38.9
12			111.7	48.2
13			149.4	59.7
14			199.8	73.9
15			267.3	91.6
16				113.5
17				140.6
18				174.2
19				215.7
20				267.3

Corrugated Plate Interceptors plate length and width: Figure (6.14) explains the relation between the length and width of Corrugated Plate Interceptors plates. While opting for a bigger plate by increasing the length and the width maintains a laminar flow and increases the separation area, it compromises the cost. On the other hand, low values of both dimensions reduce the cost but increase the turbulence of the flow which violates the design requirements of maintaining a low Reynolds number and hence a laminar flow.

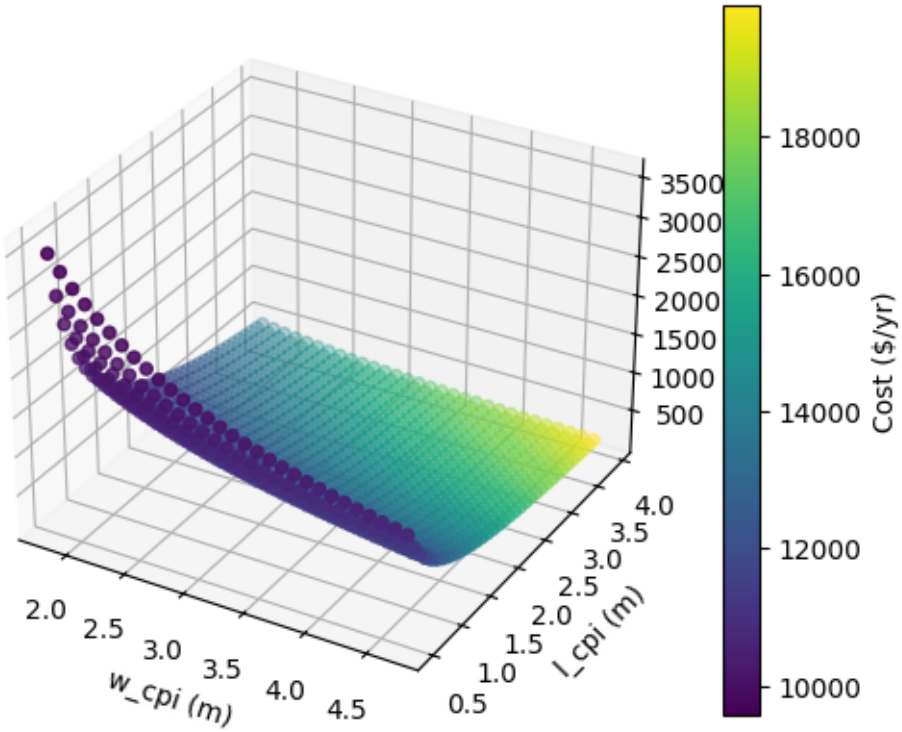

Figure 6.14: *Reynolds Number vs. Width and Length with Cost Variation of Corrugated Plate Interceptors separator unit*

We can also notice that the value of the Corrugated Plate Interceptors width varies from the lower to the upper bound unlike the length that is constrained between the lower bound and 1.89 m, the upper bound is around 4 m. This is because the ratio between the Corrugated Plate Interceptors unit width and the width of the tank that contains it is lower than that between the Corrugated Plate Interceptors length and the tank length, 1 and 2.4 respectively. This makes the cost more sensitive to the changes in the length compared with the

width.

Distance between Corrugated Plate Interceptors plates: The spacing between plates in the Corrugated Plate Interceptors typically is closer to the lower bound, often around 0.0127, with an upper limit of 0.05 m. Reduced spacing requires lower velocities for particles to settle down the channel and subsequently be removed. Given the droplet/particle rise velocity is directly proportional to particle size, smaller droplets can be separated effectively at shorter distances.

Furthermore, the spacing plays a critical role in maintaining laminar flow within the unit, with a Reynolds number lower than 2,000. Increasing the distance between plates can increase flow turbulence, thereby violating design constraints. Moreover, opting for smaller plate distances results in more compact units, resulting in reduced capital costs.

Number of Hydrocyclones: Increasing the number of parallel Hydrocyclone units leads to a decrease in the flow rate per Hydrocyclone, thereby reducing the flow velocity within the unit. The flow velocity is inversely proportional to the cut diameter of the Hydrocyclone. Consequently, maintaining a higher flow rate within the unit enhances its separation efficiency, resulting in fewer units being needed to achieve the desired efficiency compared to a higher number of units. This elucidates why, in all cases, the number of units is either 1 or 2, closer to the lower bound of this variable compared to the upper bound.

Diameter of Hydrocyclone: Similar to the Hydrocyclone number, increasing the diameter affects the separation negatively. A larger diameter corresponds to a larger body diameter, which in turn leads to an increased cut diameter and hence decreases the ability of the Hydrocyclone to separate smaller droplets and particles. This explains why the value of the Hydrocyclone diameter is closer to the lower bound which is 0.45 m. In all cases, the value of this variable was less than 1 m.

6.2.2.5 Volume Conservation

Due to the discretization of the volume space, the volume conservation is affected by the number of classes. To measure the amount of volume lost for each number of classes, the area under the curve for each case study, as shown in Figure (6.15) along with the curve in Figure (6.1), are estimated using the trapezoidal rule. Following that, the area of each case was compared to the original one to estimate the conserved volume of the contaminants. Figure (6.16) summarizes the findings.

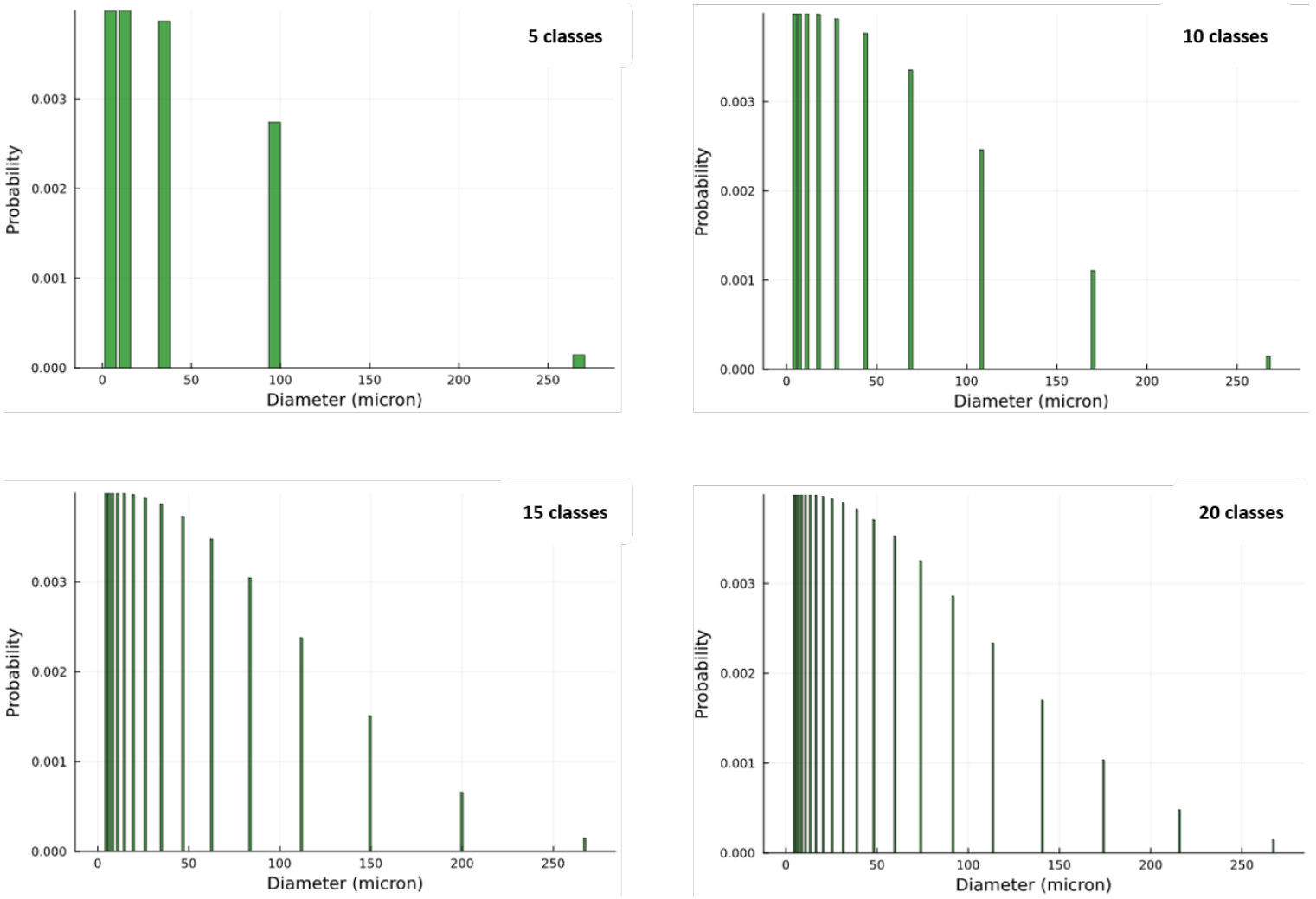

Figure 6.15: *Area under the curve for the contaminant volume distribution for different number of classes*

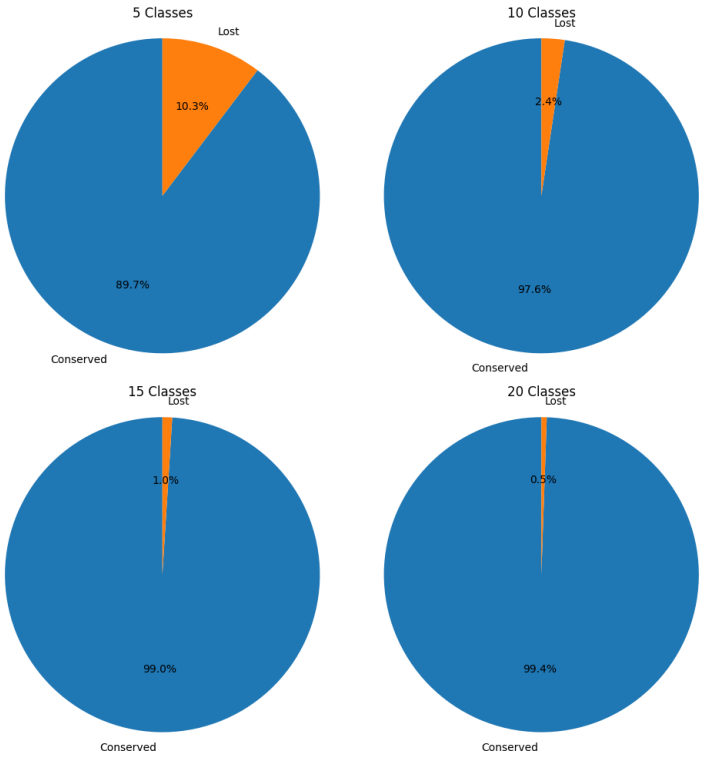

Figure 6.16: *The fraction of the conserved vs lost volume as a result of discretizing the volume space for different number of classes*

6.2.3 Conclusion

Based on the above results, it's evident that changing the number of classes affects the objective function values or the obtained designs. They also influence the final concentration of contaminants. Additionally, a fraction of the volume is lost due to the discretization method applied to the volume space, with the lost volume showing an inverse relationship with the number of classes. Contrarily, as the number of classes increases, so does the computational demand.

The subsequent case studies in the coming section will be addressed using 10, 15, and 20 classes, as these configurations resulted in higher volume conservation compared to the 5-class scenario.

6.3 Impact of Input Parameters on Process Design

In this section, the model parameters shown in Table (6.2) are varied to create different case studies to illustrate the model's capability to handle streams with various

characteristics in terms of the water volume, initial and final contaminant concentration, and droplet/particle distribution.

6.3.1 Illustrative Example

By varying the value of the above-mentioned parameters, the cases displayed in Table (6.9) were obtained. A standard deviation of 100 was used to generate all the distributions.

Table 6.9: Different case studies obtained by varying the model parameters in Table (6.2 for various final produced water destinations where TSS_f is the concentration of the total suspended solids (TSS) for the final destination, $O\&G_f$ is the concentration of the oil & grease ($O\&G$) for the final destination, TSS_i and $O\&G_i$ are the initial concentrations of oil & grease ($O\&G$) and total suspended solids (TSS), $logV^{min}$ and $logV^{max}$ are the logarithmic corresponding values of the smallest and largest diameter in the volume space of contaminant droplets and particles, n_c is the number of discrete volume classes, μ is mean of diameters for the size distribution, Q is the initial mass flowrate of the inlet stream

Case No.	Destination	TSS_f	$O\&G_f$	TSS_i	$O\&G_i$	Q	n_c	μ	$\log v_{min}$	$\log v_{max}$
1	Cooling Towers	150	42	1,000	1,850	500	10	22	12	14
2							10	280	9	17
3							15			
4							20			
5	Irrigation	0.0	0.05	189	560	250	10	400	9	17
6								280		
7								30		
8	Re-injection	42	10	500	560	100	10	10	10.6	16

6.3.2 Results and Analysis

Number of Classes: Similar to the discharge case study in the previous section, the multi-objective optimization problem was solved for cases (2),(3), and (4) in Table (6.9) each with a different number of classes. The obtained designs are similar for all number of classes which is Corrugated Plate Interceptors separator only, however, the final level of contaminants concentration varies with the class sizes. Table (6.10) displays the output concentration of the contaminants for selected designs from 10, 15, and 20 classes. The value of oil & grease concentration varied for all the cases, unlike that of the total suspended solids which resulted in almost the same concentration for 15 and 20 classes.

Table 6.10: Final concentration of oil & grease ($O\&G$) and total suspended solids (TSS) obtained by solving the multi-objective optimization problem for 10, 15, and 20 classes n_c to meet the requirement of cooling towers.

n_c	10	15	20
$O\&G$	0.60	0.33	0.90
TSS	147.67	149.40	148.97

Droplet/Particle Size Distribution: For the cooling tower destination, cases (1) and (2) have been solved with different size ranges and hence different means and different size distributions. Each case resulted in different designs with one unit only. Figure (6.17) shows the configurations obtained for each case. Given the final requirement of the cooling tower is 150 mg/L for total suspended solids concentration, a single unit was sufficient to meet this requirement.

In case (1), the droplet and particle diameters range from 12.4 to 57.6 μm. With a mean diameter of around 22 μm, the size distribution is centered. The narrower range resulted in droplet/particle of diameter lower than 200 μm which meets the inlet requirement of Hydrocyclone as a primary unit. In case (2), the droplets and particle diameters are between 1.2 to 576 μm. The three primary options are the American Petroleum Institute separator, Corrugated

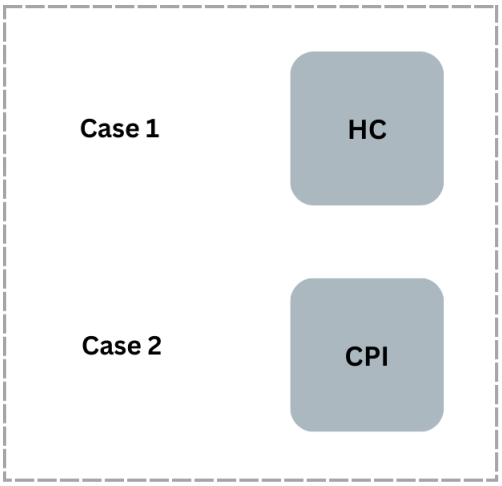

Figure 6.17: *Process design obtained by solving the multi-objective optimization problem for cases (1) and (2) each has a different size distribution range to meet the cooling towers requirements where HC is Hydrocyclone and CPI is Corrugated Plate Interceptors separator.*

Plate Interceptors separator, and Hydrocyclone. Hydrocyclone requirements are not met given the wider range of droplets larger than 200 μm so it was not chosen. The other two candidates are the American Petroleum Institute separator and the Corrugated Plate Interceptors separator. The coalescence rate in the American Petroleum Institute separator is higher than that of the Corrugated Plate Interceptors separator with a higher cost and emission. Given that the mean is around 280 μm, the contaminants volume is shifted towards the larger classes, therefore a lower coalescence rate is sufficient to meet the final requirements which make the Corrugated Plate Interceptors separator a better option than the American Petroleum Institute separator.

Mean Diameter: For irrigation destination, cases (5), (6), and (7) have been solved with different means and consequently a right-skewed, centered, and left-skewed distributions. In the latter, more volume is allocated to the smaller classes which requires a higher removal efficiency and hence higher cost and emission compared with the other two cases. This is demonstrated in Figure (6.18) where the right-skewed distribution is by far higher in cost and emission.

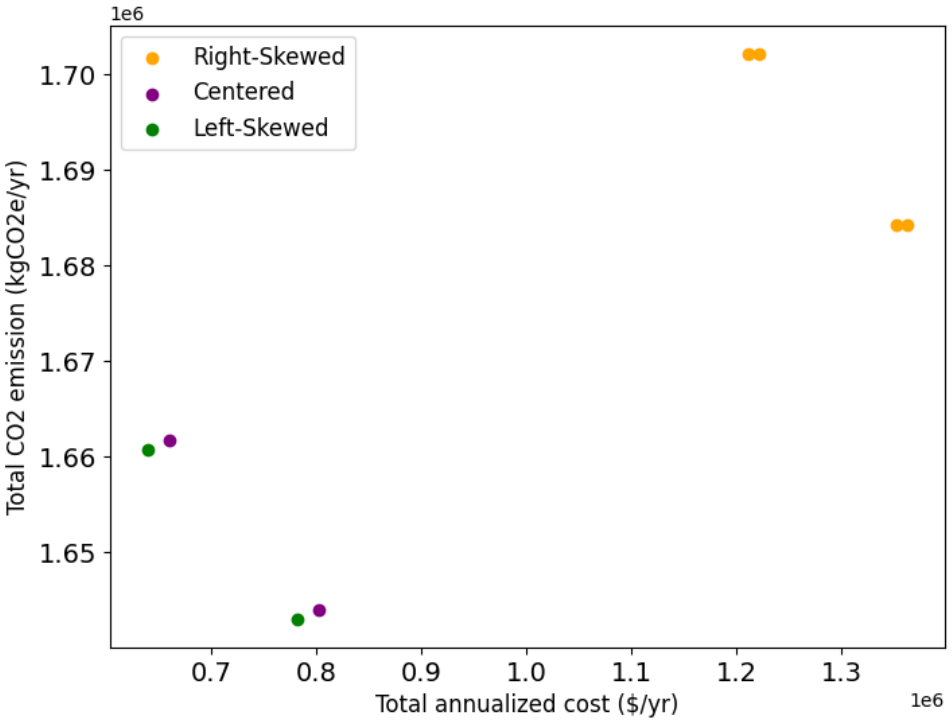

Figure 6.18: *Set of non-dominated solutions obtained by solving the multi-objective optimization problem for cases (5), (6) and (7) using the same diameter range with different means to meet the requirements of irrigation*

Having the mean values at 280 and 400 μm in cases (6) and (7) results in a volume shift towards the larger classes. Notably, the minimum cut diameters of all primary units—150 for μm, 30 for Corrugated Plate Interceptors separator, and 5 for Hydrocyclone—are substantially lower than these means. The configuration needed to fulfill the strict outlet concentration requirement for irrigation consists of only two units: Corrugated Plate Interceptors separator and Microfiltration. In contrast, in case (5), four units were needed to meet the same requirements; American Petroleum Institute separator, Corrugated Plate Interceptors separator, Hydrocyclone, and Microfiltration. Figure (6.19) shows the process diagrams for these cases.

Final Destinations: Figure (6.20) displays the Pareto fronts for cases (2), (5), and (8) in addition to the discharge case from the previous section. With the final concentration requirements stricter in some cases compared with others,

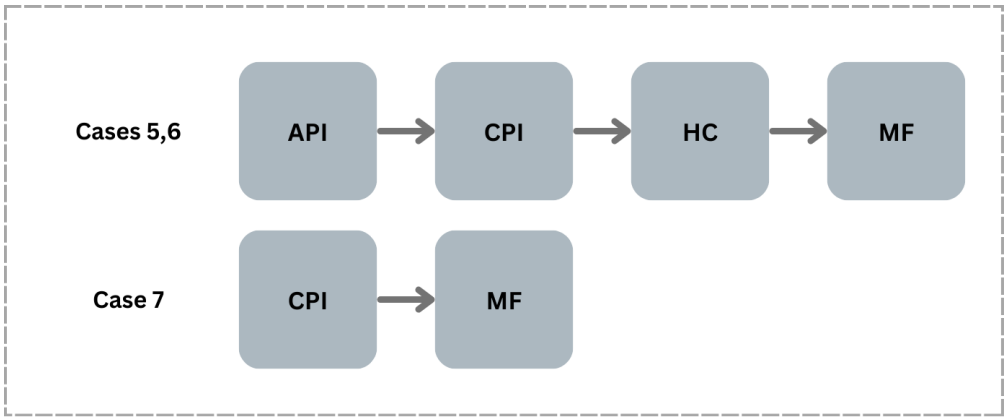

Figure 6.19: *Process design obtained by solving the multi-objective optimization problem for cases (5), (6) and (7) each case has a different mean diameter to meet the irrigation requirements where API is American Petroleum Institute separator, CPI is Corrugated Plate Interceptors separator, HC is Hydrocyclone and MF is Microfiltration Membrane.*

other factors such as water stream volume, size distribution, and initial contaminants concentration contributed to raising the cost and emission of destinations with less strict requirements. For example, in the case of discharge, the final requirements for oil & grease and total suspended solids are 40 and 30 mg/L compared to 150 mg/L for total suspended solids in cooling towers. The cost and emission of the latter are higher than that of the former due to the significantly higher stream volume, 500 compared with 250 ton/hr, and higher total suspended solids initial concentration, 1,000 compared with 500 mg/L. When comparing the irrigation and re-injection cases, the main contributor to increasing the cost and emission of the re-injection is the value of the mean being around 10 compared with 400 μm for irrigation. Figure (6.21) shows the process configurations obtained to meet the requirements of re-injection.

6.3.3 Conclusion

The above case studies demonstrated the ability of the model to handle various stream characteristics in terms of water stream volume, initial concentration, and final requirements which were translated into different specifications, designs, and objective values. The model could also capture the impact of the volume discretiza-

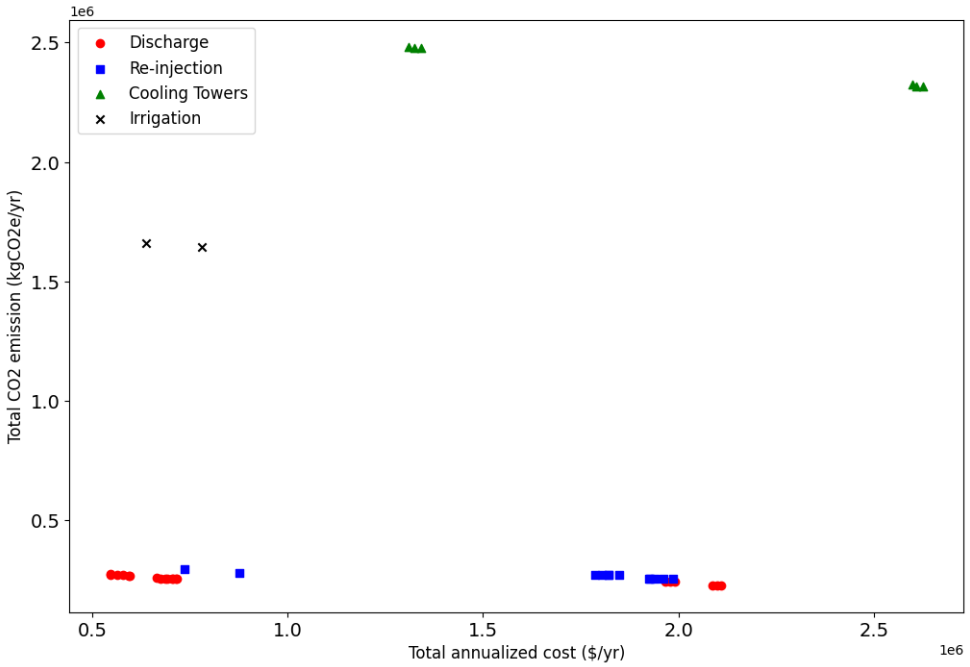

Figure 6.20: *Set of non-dominated solutions obtained by solving the multi-objective optimization problem for different destinations*

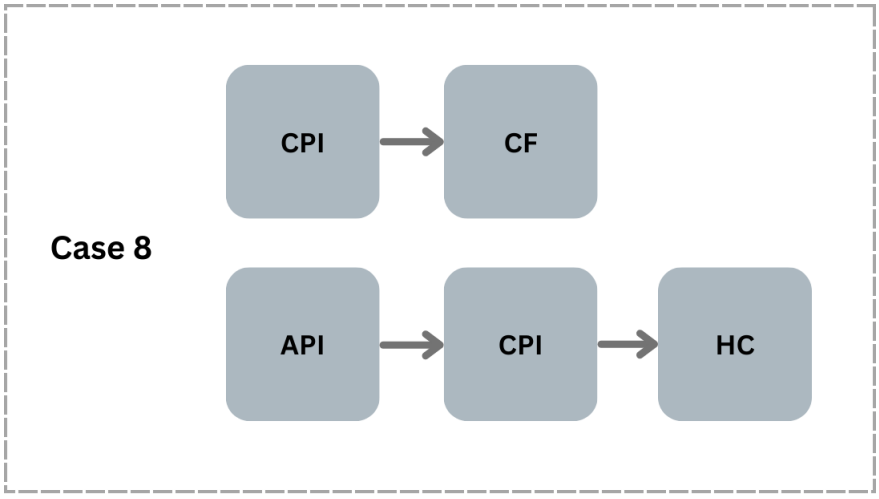

Figure 6.21: *Process designs obtained by solving the multi-objective optimization problem for cases (8) to meet the requirements of re-injection where API is American Petroleum Institute separator, CPI is Corrugated Plate Interceptors separator, HC is Hydrocyclone and CF is Centrifuge separator.*

tion and size distribution as it was shown in the case of different diameter ranges, cases (1) and (2), and different means for irrigation destination in cases (5), (6), and (7).

6.4 Impact of Breakage and Coalescence Models

The purpose of this section is to test the proposed model's ability to capture the impact of different breakages and coalescence mechanisms on the process performance. This will be achieved by replacing selected kernels adapted in the above case studies with different ones and comparing the initial distribution with the one obtained from the Population Balance Equations for each case. The alternative kernels are related to the following phenomena:

- Droplet breakage in turbulent flow (Case 2)
- Particle breakage in laminar and turbulent flow (Case 3)
- Droplet coalescence in laminar flow (Case 4)
- Droplet coalescence in turbulent flow (Case 5)

In addition to the above phenomena, the original model will be solved assuming the breakage and coalescence rates are zero which means the size distribution of droplets and particles will remain the same after implementing the population balance equations. This case study will enable us to identify the impact that the breakage and coalescence/aggregation phenomena have on the process configurations. This case will be referred to as (Case 0) and the original as (Case 1).

Refer to Table (6.12) in Chapter (3) page 63 for the list of original kernels.

6.4.1 Illustrative Example

Produced water from an onshore facility of an oil and gas industry is treated to meet re-injection requirements. The main contaminants to be removed from the feed stream are *Oil and Grease* and *Total Suspended Solids*. The water stream characteristics used to solve this problem along with the initial concentration and the re-injection requirements of the contaminants are listed in Table (6.11). Table (6.12) presents the alternative kernels used to replace the ones in the original case study. The mathematical formulation of these kernels is listed in Chapter (5).

Table 6.11: Parameter values for the re-injection case study where $logV^{min}$ and $logV^{max}$ are the logarithmic corresponding values of the smallest and largest diameter in the volume space of contaminant droplets and particles, n_c is the number of discrete volume classes, μ is mean of diameters for the size distribution, q is the initial mass flowrate of the inlet stream, σ is the standard deviation of the volume distribution, $C_{in,OnG}$ and $C_{in,TSS}$ are the initial concentrations of oil & grease ($O\&G$) and total suspended solids (TSS), $C_{f,OnG}$ and $C_{f,TSS}$ are the concentrations of the oil & grease ($O\&G$) and total suspended solids (TSS) for the final destination

Parameter	Value	Unit
$logV^{min}$	10.6	-
$logV^{max}$	16	-
n_c	10	-
μ	10	μm
σ	100	-
q	100	ton/hr
$C_{in,OnG}$	560	mg/L
$C_{in,TSS}$	500	mg/L
$C_{f,OnG}$	42	mg/L
$C_{f,TSS}$	10	mg/L

6.4.2 Results and Analysis

As shown in Figure (6.22), using different breakage and coalescence models has a significant impact on the values of the objective functions as also is proven by the changes in the obtained configurations in Table (6.13) which show the number of obtained designs and the different configurations. Because each configuration consists of multiple units, a selected unit will be chosen from each configuration to compare the change in distribution obtained by each. The following paragraphs present the basis on which the units are chosen.

- When comparing Case (0) with Case (1), the purpose is to find out how solving the original problem without considering the breakage and coalescence will change the obtained configurations or the system performance. Since both cases resulted in different configurations, the size distribution from the first unit in each configuration is compared (American Petroleum Institute separator vs Corrugated Plate Interceptors separator) as both have the same inlet specifications in addition to Centrifuge unit in both cases for configu-

Table 6.12: Alternative breakage and coalescence kernels used for the modeling of the evolution of droplet size distribution

Phenomena	Classification	Flow Type	Mechanism	Reference
Breakage	Droplets	Turbulent	Turbulent fluctuation and collision - eddy's energy	[MARTÍNEZ-BAZÁN et al., 1999]
Coalescence	Droplets	Laminar	Buoyancy-induced collision and energy model	[Friedlander, 2000, Prince and Blanch, 1990, Sovova, 1981]
		Turbulent	Turbulent collisions and film drainage	[Prince and Blanch, 1990, Kamp et al., 2001, Liao and Lucas, 2010b]
Breakage	Particles	Laminar and Turbulent	Shear rate-Power Law Model	[Pandya and Spielman, 1983]

rations (American Petroleum Institute separator, Corrugated Plate Interceptors separator, Centrifuge) and (Corrugated Plate Interceptors separator, Centrifuge).

- For Case (1) vs Case (2), the breakage kernel of droplets in turbulent flow used in Case (1) was replaced by the alternative one in Case (2). Both cases resulted in a common configuration (Corrugated Plate Interceptors separator, Centrifuge). Centrifuge is the only unit in both configurations with turbulent flow. Therefore, the droplet size distribution of Centrifuge in these two cases will be compared.

- In Case (1) vs Case (3), the breakage kernel of particles in laminar and turbulent flow used in Case (1) was replaced by the alternative one in Case (3). Two

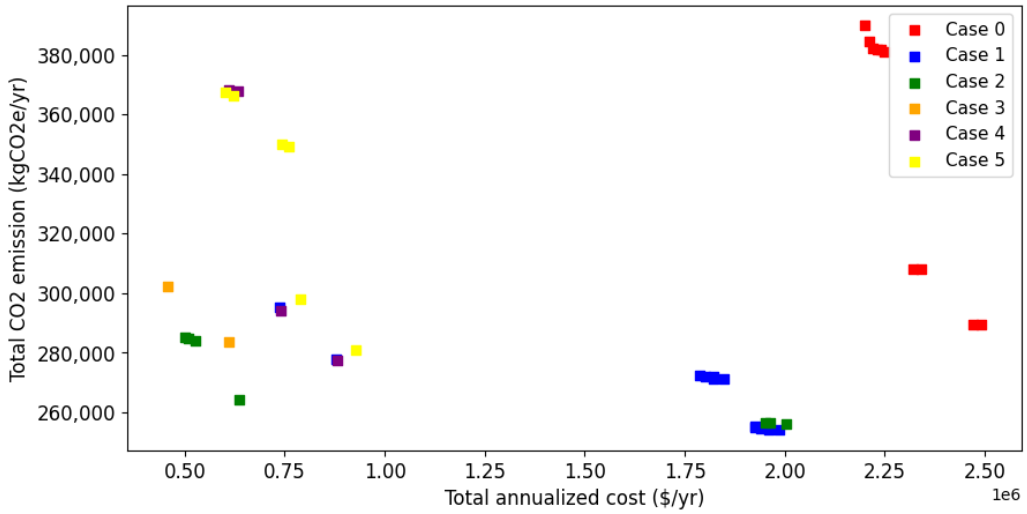

Figure 6.22: *Sets of non-dominated solutions obtained for solving the multi-objective optimization problem using 10 classes for re-injection destination. The different colors represent the solution set obtained without considering the impact of breakage and coalescence (case 0), the original case (case 1), and four cases where the breakage and coalescence models have been changed (cases 2 to 5).*

Table 6.13: The number of non-dominated solutions/designs and the different configurations obtained by solving the re-injection problem with different breakage and coalescence models for oil droplets and solid particles using 10 classes where API is American Petroleum Institute separator, CPI is Corrugated Plate Interceptors separator, HC is Hydrocyclone and CF is Centrifuge separator and IGF is Induced Gas Flotation

Case	No of designs	Configurations
0	10	API, CPI, CF IGF, CPI, CF
1	12	API, CPI, HC CPI, CF
2	7	CPI, HC CPI, CF
3	2	CPI, HC
4	4	API, CPI, HC IGF, CPI, HC
5	6	IGF, CPI, HC API, CPI, HC

configurations have been obtained by solving Case (3) compared with only 1 in Case (1). For comparison, the particle size distribution of Centrifuge and Hydrocyclone units in configurations (American Petroleum Institute separa-

tor, Corrugated Plate Interceptors separator, Hydrocyclone) and (Corrugated Plate Interceptors separator, Centrifuge) are compared.

- In Case (1) vs Case (4), the droplet coalescence kernel in laminar flow is replaced in the Case (4) model. Changing the coalescence kernel resulted in different process configurations in each case with a common one (American Petroleum Institute separator, Corrugated Plate Interceptors separator, Hydrocyclone). Since the kernel is related to the laminar flow, the size distribution of the American Petroleum Institute separator in both cases is compared.

- For Case (1) vs Case (5), the coalescence kernel of droplets in turbulent flow used in Case (1) was replaced by the alternative one in Case (5). Each case resulted in two configurations with a common one (American Petroleum Institute separator, Corrugated Plate Interceptors separator, Hydrocyclone). For comparison, a unit from the common configuration between both is chosen. Hydrocyclone is the only unit in both configurations with turbulent flow. Therefore, the droplet size distribution of Hydrocyclone in these two cases will be compared.

Without breakage and coalescence: Figure (6.23 (a)) illustrates the influence of coalescence on oil & grease droplet distribution for American Petroleum Institute separator in Case (0) and Corrugated Plate Interceptors separator in Case (1). In the American Petroleum Institute separator unit, droplet distribution remained unchanged following the Population Balance Equations as the coalescence rate is zero which means the size distribution will remain the same after implementing the Population Balance Equations. This is demonstrated by the identical distributions in the green and orange lines. However, in the Corrugated Plate Interceptors separator unit where the coalescence rate has a positive value, the impact of coalescence is obvious as most of the droplets in the smaller classes collide with each other and form bigger droplets. This explains the noticeable shift in volume towards the larger droplet classes.

Conversely, in the Centrifuge unit, with a breakage rate equal to zero, the distribution of the total suspended solid particles remained the same after the implementation of the population balance equations. When using a breakage kernel with a positive value, all the droplets in classes 2 to 10 broke into smaller droplets and thus the volume has shifted to class 1. This shift significantly impacted the process design, requiring higher removal efficiency and hence higher cost as smaller droplets require higher efficiency. This is demonstrated in Figure (6.22) where the solution set of Case (0) is closer to the lower left of the graph meaning lower cost and emission compared with Case (1).

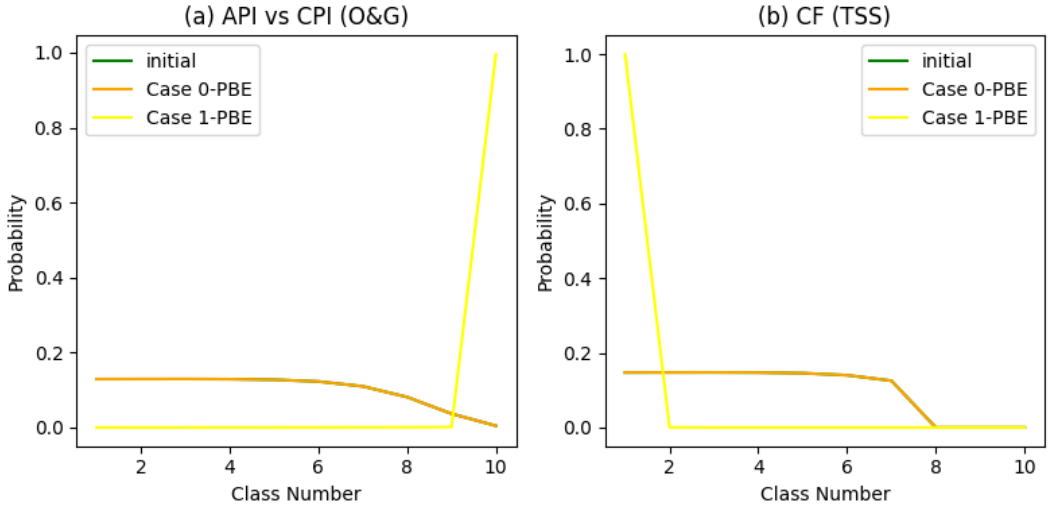

Figure 6.23: *Comparison of droplet size distributions with and without accounting for breakage and coalescence phenomena. Case (0) illustrates the droplet size distribution in the American Petroleum Institute (API) separator and Centrifuge (CF) units, while Case (1) shows the changed distribution in the Corrugated Plate Interceptors separator (CPI) and CF units, incorporating the effects of breakage and coalescence where (O&G) is oil & grease and TSS is total suspended solids.*

Droplet breakage in turbulent flow: Figure (6.24 (a)) presents the oil & grease droplet distribution for Cases (1) and (2) after the population balance equations. Both kernels resulted in the same distribution in the Centrifuge unit. This is because the breakage models did not impact both cases and the change

in the size distribution is due to the coalescence only which shifted the volume to the larger classes. This is evident by the red and blue lines which are lower from classes 1 to 7 and higher after that.

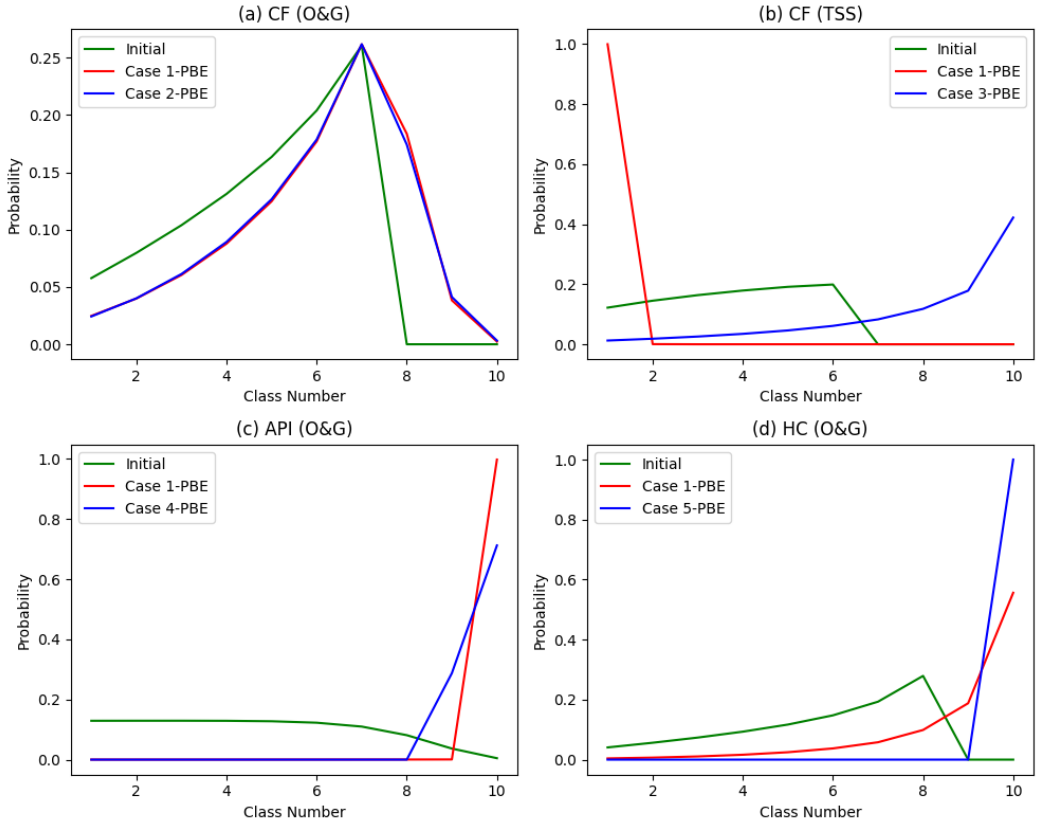

Figure 6.24: *Changes in the droplet and particle size distribution resulted from using different breakage and coalescence kernels. Each graph represents the change in selected units with different colors representing the initial distribution and the ones obtained after the implementation of the Population Balance Equations (PBEs) where (O&G) is oil & grease, TSS is total suspended solids, CF is Centrifuge separator, API is American Petroleum Institute separator and HC is Hydrocyclone*

In case (1), the breakage rate is higher for the larger classes and almost negligible for the smaller ones. As shown by the green line, the volume at the larger classes is zero for the initial distribution, therefore the breakage did not have an impact. Based on the adopted model, larger droplets possess a greater surface area compared with smaller ones, causing them more exposed to fluctuations in fluid velocity. Consequently, larger droplets experience higher kinetic energy from the surrounding flow. According to [Coulaloglou and

Tavlarides, 1977], droplets with turbulent kinetic energy surpassing their surface tension exhibit a higher breakage rate. This phenomenon is particularly pronounced for larger droplets, where the impact of turbulent kinetic energy overcomes the resistance exerted by surface tension, resulting in a high rate of breakage.

In case 2, the breakage rate was zero for all classes. This is because the breakage rate proposed by [MARTÍNEZ-BAZÁN et al., 1999] is based on the difference between turbulent stresses and surface pressure. The breakage rate will vanish when the surface stress that resists the droplet deformation is larger than the turbulent stress that prompts the deformation and breakage, which is the case in our model.

In Figure (6.22), the design shared between Case (1) and (2), represented as (Corrugated Plate Interceptors separator, Centrifuge), is shown near each other towards the lower right of the diagram, highlighted by the green and blue squares. Conversely, the design unique to Case (1) and (2), represented as (American Petroleum Institute separator, Corrugated Plate Interceptors separator, Hydrocyclone) and (Corrugated Plate Interceptors separator, Hydrocyclone) respectively, are positioned towards the lower left side of the plot. This difference arises from the inclusion of the Centrifuge unit in the common configuration, which incurs a higher cost compared with the American Petroleum Institute separator and Hydrocyclone units. Although the latter units are characterized by lower costs, they exhibit higher emissions due to their larger size relative to the Centrifuge unit.

Particle breakage in laminar and turbulent flow: Replacing the exponent model with the power law model for the total suspended solid particle breakage resulted in a negligible breakage rate which is evidenced in the impact of coalescence only that shifted the volume towards the larger classes as shown in the blue line. On the other hand, the exponent model resulted in a high breakage rate. The red line in Figure (6.24 (b)) shows how the whole volume was shifted to class 1. Since both models are empirical, the different results

obtained from both models highlight the variability and limitations inherent in empirical approaches. The effectiveness of such methods relies heavily on experimental data quality, underlying assumptions, and parameter sensitivity.

This difference has impacted the obtained sets of non-dominated solutions in both cases. As breakage affects the separation negatively, the cost and emission of Case (3) are lower than that of Case (1). This is evident in Figure (6.22) where the curve of Case (3) is closer to the lower left side of the graph.

Droplet coalescence in laminar flow: Both cases resulted in a high coalescence rate for oil droplets. The green line in Figure (6.24 (c)) indicates that the majority of the volume was initially distributed equally between classes 1 to 7 and then started to decrease at 8 and 9 to reach 0 at 10. After the Population Balance Equations, the volume distribution has shifted from the smaller classes and concentrated on the larger ones. However, In Case (4), we can notice the volume was distributed between classes 9 and 10 while in Case (1) it was shifted completely to class 10.

In these two cases, different collision frequency and coalescence efficiency kernels were applied. In Case 1, the collision frequency is derived from gradient-induced velocity, coupled with the film drainage model. Conversely, Case 2 utilized droplet buoyancy for collision frequency, employing the energy model for coalescence efficiency. Despite the differing mechanisms employed by these models, the agreement in results across varied approaches indicates that the selected kernels effectively capture the underlying mechanisms under the given conditions.

Given the similar droplet distributions in both scenarios, the resulting designs are closely aligned in Figure (6.22). The design from Case 1, which includes a Centrifuge, is positioned towards the lower right of the graph, indicating a higher cost. Conversely, the design from Case (4) is towards the upper left, indicating higher emissions due to the selection of the Induced Gas Flotation unit. The elevated emissions are associated with the use of methane gas for

bubble generation.

Droplet coalescence in turbulent flow: The alternative model resulted in a relatively higher coalescence rate compared with the original model as shown in Figure (6.22). The blue line in Figure (6.24 (d)) shows the shift of volume from all the classes to class 10 while in Case (1) the volume is shifted and distributed between classes 4 to 10. The relatively small difference in the distribution was expected in this case as the same coalescence mechanism theory is used for both cases which is the film drainage. The only difference between the two cases is the method used to quantify the coalescence efficiency between the droplets while the collision frequency is the same for both.

6.4.3 Conclusion

In this section, we have demonstrated the influence of breakage and coalescence phenomena on process design, as evidenced by the comparing designs obtained for Case (0) and Case (1), and their subsequent effects on cost and emissions. Our proposed model can capture size distribution changes resulting from various mechanisms and methods used to quantify breakage and coalescence phenomena. This ability was evident across different configurations, distributions, and objective function values. Notably, certain kernels exhibited negligible impact on droplet and particle size distribution, attributable to complex dynamics between dispersed and continuous phases, as observed in Case (2). Furthermore, in Case (3), the minimal influence on size distribution could be attributed to the empirical nature of both models, potentially resulting in less accurate outcomes when applied to different problems.

Chapter 7

Conclusion and Future Work

This chapter summarizes the work accomplished in this thesis and the major contributions followed by potential directions for future work to address this work's limitations.

7.1 Summary

Produced Water is a major concern in the oil and gas industry that needs to be addressed to meet the regulatory requirements and secure another source of fresh water. Designing an effective treatment system for produced water is complex due to the diverse contaminants it contains, often leading to high operational costs that make reuse options less economically attractive compared with re-injection or discharge. This thesis provides a multi-objective model that trades off between the Total Annualised Cost of the system and its environmental impact subject to final destination requirements. Serving as a decision-making tool, this model facilitates the optimization of produced water treatment designs, aiming to address current industry challenges and transform produced water from a waste stream into a valuable resource for beneficial reuse.

To achieve this goal, a single objective model proposed by [Bagheri et al., 2018] as a mixed integer non-linear programming model is extended. Units' cost, removal efficiency, and sludge production are modeled as functions of unit sizing. Additionally, the environmental impact of the system operations was quantified by summing up the CO_2 emission resulting from the energy consumption and sludge

generation of each unit. The problem was then formulated and solved as a multi-objective optimization problem using a heuristic approach known as Fresa to generate the Pareto-front for the system's total annualized cost and environmental impact.

Another contribution of this thesis is the integration of the impact of the change in contaminants droplets and particle size distribution on the process design. The evolution of droplets/particle size distribution was captured using Population Balance Equations (PBEs). To incorporate the PBEs into the unit models, a discrete formulation of the droplets/particles volume space has been proposed and integrated within the breakage and coalescence kernels for each unit. These kernels are also functions of the unit design variables and system operation conditions. The changes in the particle and droplet size distribution were obtained by solving as a set of ordinary differential equations within each unit and were passed as an input for the next processing stage.

The multi-objective optimization model was solved using a nature-inspired solver called Fresa whose performance was evaluated using a case study with 10 classes. The case study was solved for different values of Fresa generation number, number of solutions to propagate, similarity index, initial solution, and number of runs. The findings revealed that Fresa was able to generate a good solution with 1,000 generations, 20 solutions to propagate, and a 10^4 similarity index. Also, the different initialization and multiple runs resulted in almost the same solutions with small variations due to the stochastic nature of the solver. These parameters were fixed in the subsequent case studies.

The proposed volume space discretization was tested by varying the number of volume classes from 5 to 20 using the same case study. Changing the number of classes resulted in different sets of non-dominated solutions and process designs. Similarly, the final stream specifications have varied with the number of classes. Additionally, the impact of discretization on contamination volume conservation was explored. The higher number of classes resulted in a smaller fraction of lost volume. The lost volume reached 10% for 5 classes followed by 2.4% for 10, 1% for 15 classes, and 0.5% for 20 classes. Based on these results, the remaining case

studies were solved for 10, 15, and 20 classes.

To test the model's ability to handle various stream volumes and specifications, droplets and particle size distribution, and final destination requirements, several case studies were solved for different levels of these aspects. This variation resulted in different designs and objective function values. Similarly, the breakage and coalescence kernels integrated within the population balance equations were varied to test the model's ability to capture the change in the droplets and particle size distribution due to different mechanisms. The proposed model was found to be able to handle all the evaluated case studies for the given scope of this work. This suggests the potential for extending the model's capabilities to develop a more comprehensive tool for guiding the decision-making process in designing produced water treatment systems. The subsequent section outlines potential enhancements to further improve the proposed model's effectiveness.

7.2 Recommendations for Future Work

This thesis covered the design of the produced water treatment process however, it has some limitations that can be addressed in future works as follows:

Treatment system scope: The current scope of the produced water treatment process handles only two contaminants; Oil & Grace and Total Suspended Solids. To achieve the overall goal of making produced water a potential source of water for different destinations, more contaminants have to be removed to achieve the requirements of these destinations. Consequently, different treatment units are needed to handle the additional contaminants.

Energy sources and consumption: In this study, it was assumed that fossil fuel is the only source of energy to run the system which is also the main contributor to the CO_2 emission. Other sources of energy could be considered to lower emissions and provide more environmental solutions. Another option would be to quantify the amount of energy that can be recovered from the system to supply it with energy to lower the consumption of energy and the system's operating cost. On the units' level, given that the specific energy

consumption of the units is given parameters, modeling them as a function of the units' design variables will improve the accuracy of the cost and emission objectives.

Droplets and particles size distribution: The Population Balance Equations were solved assuming a discrete volume space of droplets and particles. Solving the model with a continuous space can contribute to more precise values of the objective functions. Another assumption that can be examined is the selection of the uniform daughter droplet distribution for the breakage models. The problem could be solved for different daughter distribution functions as presented in the literature to assess their impact on the overall process performance.

Design with uncertainty: The composition and volume of produced water show significant variation across different geographical locations, as evidenced by multiple studies in the literature. This variability has a significant influence on the design and performance of treatment processes, as demonstrated in various case studies. Expanding the scope of our model to explicitly address input parameter uncertainty will enhance its capability to accommodate diverse scenarios effectively.

Other criteria: The proposed model covered two aspects of the treatment process which are cost and environmental impact, which is based on the CO_2 emission. Other green house gases can be included, especially when expanding the scope of the problem to include more processing units, such as Methane and Nitrogen. Also, other objective functions can be addressed such as the social impact of the system and the resources recovery from the treatment operations.

Decision-making methodology: To improve the decision-making power of the model, Multi-Criteria Decision Analysis can be integrated with the existing multi-objective optimization model to assist in selecting the overall best solution from the set of the Pareto-optimal.

Chapter 8

Publications

Falahi, M., Dua, V., & Fraga, E. S. (2023). Discrete Formulation for Multi-objective Optimal Design of Produced Water Treatment. Chemical Engineering Transactions, 99, 553-558.

Appendix A

Input parameters

This appendix includes the values of the parameters used to solve the proposed model.

Table A.1: Common model parameters

Parameter	Description	Value	Unit	Reference
g	Gravitational acceleration	9.81	m/s^2	-
$d_{conv.}$	Conversion factor from μm to m for droplet/particle size	10^{-6}	-	-
$f_{conv.}$	Conversion factor to convert flowrate from ton/hr to m^3/s	0.000274	m^3/s	-
ρ_c	Density of the continuous phase (water)	988	kg/m^3	[National Institute of Standards and Technology, Accessed 2023]
ρ_d	Density of the dispersed phase (oil)	900	kg/m^3	[tra]
ρ_{TSS}	Density of the total suspended solids (TSS)	1,270	kg/m^3	[U.S. Environmental Protection Agency, Accessed on Month Day, Year]
ρ_{CH_4}	Density of the methane gas	162.7	kg/m^3	[Air Liquide, Accessed on Month Day, Year]
ρ_{PW}	Density of produced water	1014	kg/m^3	[Pollyea et al., 2019]
ρ_{sludge}	Density of sludge	1,200	kg/m^3	
σ	Interfacial tension between oil and water	0.04	N/m	[Kim and Burgess, 2001]
μ_d	Viscosity of the dispersed phase (oil)	0.0138	$kg/m.s$	[Alomair et al., 2016]
μ_c	Water viscosity	0.00054	$kg/m.s$	[Journal of Physical and Chemical Reference Data, Accessed on July 5, 2023]
C_{SK}	Cost of belt oil skimmer unit	450	$/unit	[CNC OIL SKIMMERS Ltd]
μ_{PW}	Absolute viscosity of PW at temperature = 50°	0.0005	$kg/m.s$	

Table A.2: API model parameters

Parameter	Definition	Unit	Value	Reference
n_{API}	Number of API channels	-	2	[American Petruelem Institute, 1990]
r^e_{API}	Specific energy consumption of API unit	kWh/ton	0.19	[Bagheri et al., 2018]
TH_{BF}	API baffle thickness	m	0.05	[Poly Processing Company, 2023]
Cts_{Mtr}	Baffle material cost*	\$/ton	877	[AG Metal Miner, 2023]

* Baffles are made out of carbon steel. To convert the cost to m^3, multiply by the density of carbon steel, which is $7,840$ kg/m^3, and divide by 1,000.

Table A.3: CPI model parameters

Parameter	Definition	Unit	Value	Reference
C_{CPI}	CPI unit cost	$\$/m^3$	500	
r^e_{CPI}	Specific energy consumption of CPI unit	kwh/ton	0.19	[Bagheri et al., 2018]

Table A.4: HC model parameters

Parameter	Definition	Unit	Value	Reference
r^e_{HC}	Specific energy consumption of HC unit	3	kwh/ton	[Neesse et al., 2015]

Table A.5: IGF model parameters

Parameter	Definition	Unit	Value	Reference
C_{RS}	Rotor and stator cost	$\$/unit$	746.61	[CEE, 2023]
γ	Surface Tension of Water in contact with Air	N/m	0.0679	[Vargaftik et al., 1983]
k_p	mass transfer coefficient	$1/min$	0.3	[Gorain et al., 1997]
r^e_{IGF}	specific energy consumption of IGF unit	kwh/ton	4.83	[Son et al., 2023]

Table A.6: NF model parameters

Parameter	Definition	Unit	Value	Reference
Cts_{medium}	Cost of the walnut granular	$\$/ton$	500	[Sand Blasters, 2023]
ρ_{medium}	Density of the walnut granular medium	kg/m^3	1,260	[Flowspec Shengda, 2023]
BW^r_{NF}	Backwash rate of NF	$m^3/m^2.min$	0.0416	[Flowspec Shengda, 2023]
BW^{fre}_{NF}	Frequency of backwash of NF membrane	hr^{-1}	0.041	[Sadeghi et al., 2020]
BW^d_{NF}	Duration of backwash of NF membrane	min	20	[Sadeghi et al., 2020]
$porosity$	Filtration bed porosity	-	0.36	[Segismundo et al., 2016]
α	Empirical fitting factor	-	1	[Lawler and Nason, 2006]
A_h	Hamker constant	-	10^{-13}	[Lawler and Nason, 2006]
K_B	Boltzmann constant	j/k	1.38065×10^{-23}	[Tufenkji and Elimelech, 2004]
T	Absolute temperature	K	298	[Lawler and Nason, 2006]
d_{col}	Collector diameter	m	0.0009	[Lawler and Nason, 2006]
r^e_{NF}	Specific energy consumption of NF unit	kwh/ton	0.27	[Arous et al., 2023]

Table A.7: CF model parameters

Parameter	Definition	Unit	Value	Reference
r^e_{CF}	Specific energy consumption of CF unit	kwh/ton	4	[Abu-Shamleh and Najjar, 2020]
$speed$	CF rotational speed	RPM	15,000	[Doran, 2013b]

Table A.8: MF model parameters

Parameter	Definition	Unit	Value	Reference
Cts_{area}	Cost per area of the MF membrane	$\$/m^2$	3,000	[Nandi et al., 2008]
BW^{r}_{MF}	Backwash rate of MF membrane	$m^3/m^2.hr$	1.2	[Le Gouellec et al., 2004]
BW^{fre}_{MF}	Frequency of backwash of MF membrane	$1/hr$	2	[Raffin et al., 2012]
BW^{d}_{MF}	Duration of backwash of MF membrane	min	6	[Nandi et al., 2008]
r^{e}_{MF}	Specific energy consumption of MF unit	kwh/m^3	0.4	[Hakami et al., 2020]
Cln^{fre}_{MF}	Frequency of chemical cleaning $tech$	0.0027	$1/h$	

Table A.9: Droplet breakage model inputs

Parameter	Definition	Value	Unit	Reference
C_3	Constant	0.00481	-	[Liao and Lucas, 2009b]
C_4	Constant	0.08	-	[Liao and Lucas, 2009b]
α_d	Volume fraction of the dispersed phase $O\&G$ [1]	Calculated Variable	-	-
$d_{OnG,k}$	Diameter of $O\&G$ droplet of class k [2]	Calculated Variable	μm	-
ε	Energy dissipation rate of the unit [3]	Calculated Variable	m^2/s^3	-
β	Constant	0.25	-	[MARTÍNEZ-BAZÁN et al., 1999]
K_g	Constant	8.2	-	[MARTÍNEZ-BAZÁN et al., 1999]

[1] refer to $V^{init,total}_{OnG}$ in Eq. (5.3.0.3) Section (5.3).
[2] refer to Eq. (5.3.0.3) Section (5.2.0.3).
[3] refer to Section (4.2) where ε is calculated for each unit.

Table A.10: Droplet coalescence model inputs

Parameter	Definition	Value	Unit	Reference
$d_{TSS,k}$	Diameter of TSS droplet of class k	Calculated Variable [1]	μm	
ε_{unit}	Energy dissipation rate of the unit	Calculated Variable[2]	m^2/s^3	
c	Constant	10^9	-	[Prince and Blanch, 1990]
C_{12}	Constant	10^9		[Sovova, 1981]
C_{13}	Constant	$7.5x10^3$		[Sovova, 1981]
C_{vm}	Constant	0.8		[Liao and Lucas, 2010a]

[1] refer to Eq. (5.3.0.3) Section (5.2.0.3).
[2] refer to Section (4.2) where ε is calculated for each unit.

Table A.11: Particle breakage model inputs

Parameter	Definition	Value	Unit	Reference
B	Fitting parameter that represents the critical force needed for the breakage of aggregates	5	-	[Jeldres et al., 2018]
$d_{TSS,k}$	Diameter of TSS particle of class k	Calculated Variable [1]	μm	
$v_{TSS,k}$	Volume of TSS particle of class k	Calculated Variable [1]	μm	
ε_{unit}	Energy dissipation rate of the unit	Calculated Variable[2]	m^2/s^3	

[1] refer to Eq. (5.3.0.3) Section (5.2.0.3).
[2] refer to Section (4.2) where ε is calculated for each unit.

Table A.12: Particle aggregation model inputs [Song et al., 2018]

Parameter	Definition	Value	Unit
k_B	Boltzmann constant	1.38065×10^{-23}	J/K
T	Fluid temperature	50	$^\circ$
k_f	fluid properties parameter	0.87	-
H	Hamaker constant representing van der Walls force	1.7×10^{-20}	J
$d_{TSS,k}$	Diameter of TSS droplet of class k	Calculated Variable [1]	μm
ε_{unit}	Energy dissipation rate of the unit	Calculated Variable[2]	m^2/s^3

[1] refer to Eq. (5.4).
[2] refer to Section (4.2) where ε is calculated for each unit.

Table A.13: PBE model inputs

Parameter	Definition	Value	Unit
$n_{cont,k,0}$	initial number of droplets of class i at t=0	Calculated Variable[1]	-
Rt_{unit}	residence time of the unit	Calculated Variable	sec
δt	the step size of the residence time	1	sec
$v_{cont,k}$	volume of droplet/particle of contaminant $cont$ and class k	Calculated Variable[2]	m^3
$A_{i,j}$	coalescence rate between droplets of class i and $k-i$	Calculated Variable [3]	μm
G_i	The breakage rate of droplets of class i	Calculated Variable [4]	μm
$\Gamma_{i,k}$	The probability density function (PDF) of droplets breaking from class i to k	Calculated Variable[5]	m^2/s^3

[1] refer to Eq. (5.8).
[2] refer to Eq. (5.3).
[3] refer to Eq. (5.18, 5.28, 5.49).
[4] refer to Eq. (5.9, 5.32).
[5] refer to Eq. (5.11, 5.35).

Table A.14: Separation model inputs

Parameter	Definition	Value	Unit
$d_{cont,i}$	Initial number of droplets of class i	Calculated Variable[1]	μm
$CD_{tech,cont}$	Cut diameter of $cont$ by $tech$	Calculated Variable [2]	μm
$V^{c,in}_{cont,i}$	Initial total volume per class i for each $cont$	Calculated Variable[3]	m^3
$Rv_{tech,cont,i}$	Removal efficiency of technology $tech$ for each class i of contaminant $cont$	Calculated Variable[4]	%

[1] refer to Eq. (5.4) in Section (5.2.0.3).
[2] refer to Section (4.2) where $CutDia_{tech,cont}$ is determined for each unit.
[3] refer to Eq. (5.7) in Section (5.3.0.3).
[4] refer to Section (4.2) where $Rv_{tech,cont,i}$ is determined for each unit.

Table A.15: Capital cost estimation parameters

input	description	value	reference
f_p	cost of piping	0.8	[Towler and Sinnott, 2012]
f_er	cost of equipment erection	0.3	[Towler and Sinnott, 2012]
f_el	electrical cost	0.2	[Towler and Sinnott, 2012]
f_i	instrumentation and control cost	0.3	[Towler and Sinnott, 2012]
f_c	civil cost	0.3	[Towler and Sinnott, 2012]
f_s	structures and buildings cost	0.2	[Towler and Sinnott, 2012]
f_l	lagging and paint cost	0.1	[Towler and Sinnott, 2012]
f_m	material factor for carbon steel	1	[Towler and Sinnott, 2012]
OS	cost of off-sites	0.3	[Towler and Sinnott, 2012]
DE	design and engineering cost	0.3	[Towler and Sinnott, 2012]
X	contingency cost	0.1	[Towler and Sinnott, 2012]
P	working capital	0.15	[Towler and Sinnott, 2012]
OS	the cost of off-sites	0.3	[Towler and Sinnott, 2012]
DE	the design and engineering cost	0.3	[Towler and Sinnott, 2012]
X	the contingency cost	0.1	[Towler and Sinnott, 2012]
2024_{Index}	cost index in year 2023	813.0	[Tom Rodgers, 2023]
2010_{Index}	cost index in year 2010	532.9	[Tom Rodgers, 2023]
$Cts^{cp}_{j,tech}$	capital cost of $tech$	Calculated Variable [1]	[Tom Rodgers, 2023]

[1] refer to Section (4.2) where *CCost* is calculated for each unit.

Table A.16: Treatment model inputs

Parameter	Definition	Value	Unit
Cst^{elc}	Cost of electricity	0.189	$\$/kwh$
Cst_{CH4}	Cost of methane gas	1.19	$\$/L$
rc^{acid}	Acid concentration per area	Table (A.20)	mg/m^2
Cst^{acid}	Cost of acid	Table (A.17)	$\$/mg$
rc^{base}	Base concentration per area	Table (A.20)	mg/m^2
Cst^{base}	Cost of base	Table (A.17)	$\$/mg$
Cst^{w}	Cost of water	Table (A.17)	$\$/m^3$
r^{e}_{tech}	Specific energy consumption for the treatment technologies.	Table (A.21)	kWh/t
$r^{c}_{tech,chem}$	Fraction of chemicals for each $tech$	Table (A.20)	mg/L
ρ_{chem}	Density of chemical $chem$	Table (A.17)	kg/m^3
Cts_{chem}	Cost of $chem$	Table (A.17)	$\$/ton$
BW^{r}_{tech}	Backwash rate of technology $tech$	Tables (A.6 and A.8)	$m^3/m^2.m$
BW^{fre}_{tech}	Frequency of backwash of technology $tech$	Tables (A.6 and A.8)	$1/h$
Cln^{fre}_{tech}	Frequency of chemical cleaning $tech$	Tables (A.8)	$1/h$
BW^{d}_{tech}	Backwash duration of technology $tech$	Tables (A.6 and A.8)	min
Cst_{slg}	Cost of sludge handling system slg	Tables (A.24)	$\$/t_{DM}$
$area_{MF}$	Area of technology $tech$	Calculated Variable[1]	m^2
q_{tech}	Water flow rate at technology $tech$	Calculated Variable	m^2/s^3
no_{tech}	Number of units of technology $tech$	Calculated Variable	-
$V^{total,out}_{cont}$	Total volume for each $cont$ after the separation	Calculated Variable	m^3
C_{cont}	Concentration of contaminate $cont$	Calculated Variable	$kwh/ton.$
qg_{IGF}	Gas flowrate of IGF technology	Calculated Variable	m^3/s
$volume_{tech}$	Volume of the technology $tech$	Calculated Variable	m^3

Table A.17: Chemicals used for PW treatment with their density and cost

No	*chem*	Description	ρ_{chem} (kg/m^3)	Cost $(\$/ton)$	Reference
Ch_1	Polyaluminium Chloride	Reverse demulsifier	1,390	250	[Chemifloc Group] [Yixing Bluwat Chemicals Co., Ltd.]
Ch_2	Chlorine	Biocide	1,467	150	[The Chlorine Institute] [Leon Becker]
Ch_3	Sodium Polyphosphate	Scale inhibitor	1,330	91,380	[Nikandrov and Mikhailov, 2005] [Chemical Book]
Ch_4	Imidazoline	Corrosion inhibitor	1,233	2,500	[MERCK] [Made-in-China]
Ch_5	Hydrochloric Acid	Cleaning acid	1,048	179	[Hydroland] [CHEM-ANA-LYST]
Ch_6	Sodium Hydroxide	Cleaning base	2,130	570	[Gul et al., 2021] [NaO] [ECHEMI Group]

Table A.18: Emission model inputs

Parameter	Definition	Value	Unit
EF_{chem}	Emission factor of chemical *chem*	Table (A.23)	$KgCO_2e/ton$
EF^g	Emission factor of methane gas	Table (A.23)	$KgCO_2e/kg$
EF^{elect}	Emission factor of electricity	Table (A.23)	$KgCO_2e/kwh$
EF_w	Emission factor of treating water	Table (A.23)	$KgCO_2e/kg$
EF_{slg}	Emission factor of sludge option *slg*	Table (A.24	$KgCO_2e/ton_{DM}$
$rc_{tech,chem}$	Fraction of chemicals for each $tech$	Table (A.20)	mg/L
ρ_g	Density of methane gas	Table (A.1)	kg/m^3
ρ_{chem}	Density of chemical *chem*	Table (A.17)	kg/m^3
BW^r_{tech}	Backwash rate of technology $tech$	Tables (A.6 and A.8)	$m^3/m^2.m$
BW^{fre}_{tech}	Frequency of backwash of technology $tech$	Tables (A.6 and A.8)	$1/h$
BW^d_{tech}	Backwash duration of technology $tech$	Tables (A.6 and A.8)	min
Cln^{fre}_{tech}	Frequency of chemical cleaning $tech$	Tables (A.8)	$1/h$
no_{tech}	Number of units of technology $tech$	Calculated Variable	-
E_{tech}	Energy consumption by technology $tech$	Calculated Variable	kwh/hr
q_{tech}	Water flow rate at stage j and technology $tech$	Calculated Variable	m^2/s^3
q^g_{IGF}	Gas flowrate of IGF technology	Calculated Variable	m^3/s
$area_{tech}$	Area of technology $tech$	Calculated Variable	m^2
DM_{tech}	Flowrate of dry matter produced by technology $tech$	Calculated Variable	ton/hr

Table A.19: Superstructure model inputs

Parameter	Definition	Value	Unit
H^{op}	operating hours per year	8,760	hr
C_{cont}^{final}	maximum allowable outlet concentration of *cont*	model parameter	mg/L
q_{tech}	flow rate at technology $tech$	Calculated Variable	ton/hr
$C_{tech,cont}^{out}$	outlet concentration of contaminant *cont* by technology $tech$	Calculated Variable	mg/L
$Cts_{tech}^{cp,2023}$	capital cost as of 2023 of technology $tech$	Calculated Variable	$\$/hr$

Table A.20: Processing units' chemical consumption (mg/L) [Bagheri et al., 2018]

$tech$	Ch_1	Ch_2	Ch_3	Ch_4	Ch_5	Ch_6
API	0.0	0.0	0.0	0.0	0.0	0.0
CPI	0.0	0.0	0.0	0.0	0.0	0.0
HC	45	0.0	0.0	0.0	0.0	0.0
IGF	60	0.0	0.0	0.0	0.0	0.0
NF	0.0	5	0.0	0.0	0.0	0.0
CF	30	0.0	0.0	0.0	0.0	0.0
MF	0	15	0	0	2.2[1]	4[1]

[1] the unit for the acid and base cleaning chemicals is mg/m^2 per backwash.

Table A.21: Processing units' data

Unit	r^e (kwh/ton)[1]	$Solids^{dry}$ %	Reference
API	0.19	1	[Patil et al., 2020] [Milledge and Heaven, 2011]
CPI	0.19	3	[Patil et al., 2020] [Milledge and Heaven, 2011]
HC	1.1	5	[emi, Accessed: 2023]
IGF	0.7	7	[Patil et al., 2020] [Milledge and Heaven, 2011]
NF	0.4	8	[Patil et al., 2020] [Milledge and Heaven, 2011] [Arous et al., 2023]
CF	0.75	10	[Patil et al., 2020] [Milledge and Heaven, 2011]
MF	0.96	4.6	[Nutriman Consortium, 2023]

[1] the values of the specific energy consumption are taken from [Bagheri et al., 2018].

Table A.22: Cut diameter of contaminants by technology $tech$ in μm [Stewart and Arnold, 2011]

tech	OnG	TSS	TDS
API	100	100	
CPI	30	30	
IGF	15	15	
NF	5	5	
CF	10	10	
MF	1	1	

Table A.23: Emission factor for different items in ($kgCO_2e$)

Item	factor	unit	Reference
Electricity	0.2	kwh	[UK Government]
Methane	84	kg	[Climate Change Connection]
Ch_1	0.131		
Ch_2	2.1	kg	[Euro Chlor]
Ch_3	5	kg	[Carbon Cloud]
Ch_4	0		
Ch_5	0.99	kg	[City of Winnipeg]
Ch_6	1.12	kg	[City of Winnipeg]

Table A.24: Cost and Emissions of sludge handling options [Hong et al., 2009]

slg	Description	Cost $\$/t_{DM}$	Emission $KgCO_2e/t_{DM}$
1	machine thickening	600.32	625.4
2	machine thickening and incineration	259.69	668.9
3	machine thickening and melting	326.96	698

Appendix B

Julia code

The Julia code of the proposed model can be accessed using this link:
https://github.com/MariamFalahi/JuliaCode/blob/main/SSVsCode.ipynb

Bibliography

Stephen Nalley and Angelina LaRose. International energy outlook 2021 (ieo2021), 2021. URL https://www.eia.gov/outlooks/ieo/. Accessed 2022-09-15.

Peter McCabe. Oil and natural gas: global resources. *Fossil Energy*, pages 5–16, 01 2020. doi: https://doi.org/10.1007/978-1-4939-9763-3_71.

Produced Water Society. Global hydrocarbon production, 2024. URL https://producedwatersociety.com/. Accessed 6 March 2024.

Kingsley Tamunokuro Amakiri, Naomi Amoni Ogolo, Athanasios Angelis-Dimakis, and Oshienemen Albert. Physicochemical assessment and treatment of produced water: A case study in niger delta nigeria. *Petroleum Research*, 8(1): 87–95, 2023. doi: https://doi.org/10.1016/j.ptlrs.2022.05.003.

Arturo Alarcon-Rodriguez, Graham Ault, and Stuart Galloway. Multi-objective planning of distributed energy resources: A review of the state-of-the-art. *Renewable and Sustainable Energy Reviews*, 14(5):1353–1366, 2010.

Agendra Gangwar, Shweta Rawat, Akhil Rautela, Indrajeet Yadav, Anushka Singh, and Sanjay Kumar. Current advances in produced water treatment technologies: a perspective of techno-economic analysis and life cycle assessment. *Environment, Development and Sustainability*, pages 1–35, 2024. doi: https://doi.org/10.1007/s10668-024-04558-w.

Marzieh Bagheri, Ramin Roshandel, and Jalal Shayegan. Optimal selection of an

integrated produced water treatment system in the upstream of oil industry. *Process Safety and Environmental Protection*, 117:67–81, 2018.

GuangChun Song, YuXing Li, WuChang Wang, Kai Jiang, Zhengzhuo Shi, and Shupeng Yao. Numerical simulation of pipeline hydrate particle agglomeration based on population balance theory. *Journal of Natural Gas Science and Engineering*, 51:251–261, 2018.

Maurice Stewart and Ken Arnold. Front matter. In *Produced Water Treatment Field Manual*, pages i–ii. Gulf Professional Publishing, Boston, 2011. ISBN 978-1-85617-984-3. doi: https://doi.org/10.1016/B978-1-85617-984-3.00008-0. URL https://www.sciencedirect.com/science/article/pii/B9781856179843000080.

Jinglan Hong, Jingmin Hong, Masahiro Otaki, and Olivier Jolliet. Environmental and economic life cycle assessment for sewage sludge treatment processes in japan. *Waste Management*, 29(2):696–703, 2009.

Scott Nyquist. Energy 2050: Insights from the ground up, 2016. URL https://www.mckinsey.com/industries/oil-and-gas/our-insights/energy-2050-insights-from-the-ground-up. Accessed 2022-09-13.

Ebenezer Igunnu and George Chen. Produced water treatment technologies. *International Journal of Low-Carbon Technologies*, 9(3):157–177, 07 2012. doi: 10.1093/ijlct/cts049.

Mohammad Al-Ghouti, Maryam Al-Kaabi, Mohammad Ashfaq, and Dana Da'na. Produced water characteristics, treatment and reuse: A review. *Journal of Water Process Engineering*, 28:222–239, 2019. doi: https://doi.org/10.1016/j.jwpe.2019.02.001.

Samira Ghafoori, Mohamed Omar, Negin Koutahzadeh, Sohrab Zendehboudi, Rana N. Malhas, Mariam Mohamed, Shouq Al-Zubaidi, Khadija Redha, Fatimah

Baraki, and Mehrab Mehrvar. New advancements, challenges, and future needs on treatment of oilfield produced water: A state-of-the-art review. *Separation and Purification Technology*, 289:120652, 2022. doi: https://doi.org/10.1016/j.seppur.2022.120652.

Jisi Zheng, Bing Chen, Worakanok Thanyamanta, Kelly Hawboldt, Baiyu Zhang, and Bo Liu. Offshore produced water management: A review of current practice and challenges in harsh/arctic environments. *Marine pollution bulletin*, 104(1-2): 7–19, 2016. doi: https://doi.org/10.1016/j.marpolbul.2016.01.004.

Slavko Nesic and Vlada V Streletskaya. An integrated approach for produced water treatment and injection. *Teopecypcw*, 20(1 (eng)), 2018. doi: https://doi.org/10.18599/grs.2018.1.25-31.

Ibidapo Obe, TA Fashanu, Peter O Idialu, Tope O Akintola, and Kingsley E Abhulimen. Produced water re-injection in a non-fresh water aquifer with geochemical reaction, hydrodynamic molecular dispersion and adsorption kinetics controlling: model development and numerical simulation. *Applied Water Science*, 7 (3):1169–1189, 2017. doi: 10.1007/s13201-016-0490-4.

John Veil and Corrie Clark. Produced water volume estimates and management practices. *SPE Production & Operations*, 26(03):234–239, 2011. doi: https://doi.org/10.2118/0311-0077-JPT.

Robert S Ayers and Dennis W Westcot. *Water quality for agriculture*, volume 29. Food and Agriculture Organization of the United Nations Rome, 1985. ISBN 92-5-102263-1.

Vinod Atmaram Mendhe, Subhashree Mishra, Atul Kumar Varma, and Awanindra Pratap Singh. Coalbed methane-produced water quality and its management options in raniganj basin, west bengal, india. *Applied Water Science*, 7(3):1359–1367, 2017. doi: https://doi.org/10.1007/s13201-015-0326-7.

MSH Bader. Seawater versus produced water in oil-fields water injection oper-

ations. *Desalination*, 208(1-3):159–168, 2007. doi: https://doi.org/10.1016/j.desal.2006.05.024.

Salem Alzahrani and Abdul Wahab Mohammad. Challenges and trends in membrane technology implementation for produced water treatment: A review. *Journal of Water Process Engineering*, 4:107–133, 2014. doi: https://doi.org/10.1016/j.jwpe.2014.09.007.

A. Fakhru'l-Razi, Alireza Pendashteh, Zurina Zainal Abidin, Luqman Chuah Abdullah, Dayang Radiah Awang Biak, and Sayed Siavash Madaeni. Application of membrane-coupled sequencing batch reactor for oilfield produced water recycle and beneficial re-use. *Bioresource Technology*, 101(18):6942–6949, 2010. ISSN 0960-8524. doi: https://doi.org/10.1016/j.biortech.2010.04.005.

Carolyn M. Cooper, James McCall, Sean C. Stokes, Cameron McKay, Matthew J. Bentley, James S. Rosenblum, Tamzin A. Blewett, Zhe Huang, Ariel Miara, Michael Talmadge, Anna Evans, Kurban A. Sitterley, Parthiv Kurup, Jennifer R. Stokes-Draut, Jordan Macknick, Thomas Borch, Tzahi Y. Cath, and Lynn E. Katz. Oil and gas produced water reuse: Opportunities, treatment needs, and challenges. *ACS ES&T Engineering*, 2(3):347–366, 2021. doi: https://doi.org/10.1021/acsestengg.1c00248.

Alban Echchelh, Tim Hess, and Ruben Sakrabani. Reusing oil and gas produced water for irrigation of food crops in drylands. *Agricultural Water Management*, 206:124–134, 2018. doi: https://doi.org/10.1016/j.agwat.2018.05.006.

Abass Olajire. Recent advances on the treatment technology of oil and gas produced water for sustainable energy industry-mechanistic aspects and process chemistry perspectives. *Chemical Engineering Journal Advances*, 4:100049, 2020. doi: https://doi.org/10.1016/j.ceja.2020.100049.

Xiaoqiang Jia, Dayao Jin, Chen Li, and Wenyu Lu. Characterization and analysis of petrochemical wastewater through particle size distribution, biodegradability, and

chemical composition. *Chinese Journal of Chemical Engineering*, 27(2):444–451, 2019. ISSN 1004-9541. doi: https://doi.org/10.1016/j.cjche.2018.04.030.

Changjun Li and Qian Huang. Analysis of droplet behavior in a de-oiling hydrocyclone. *Journal of Dispersion Science and Technology*, 38(3):317–327, 2017. doi: https://doi.org/10.1080/01932691.2016.1164062.

WAM Ghoneim, AA Helal, and MG Abdel Wahab. Minimizing energy consumption in wastewater treatment plants. In *2016 3rd international conference on renewable energies for developing countries (REDEC)*, pages 1–8. IEEE, 2016. doi: 10.1109/REDEC.2016.7577507.

Mengjie Yang, Man Peng, Dong Wu, Haoyuan Feng, Yixian Wang, Yongpeng Lv, Fengyun Sun, Sanjib Sharma, Yue Che, and Kai Yang. Greenhouse gas emissions from wastewater treatment plants in china: Historical emissions and future mitigation potentials. *Resources, Conservation and Recycling*, 190:106794, 2023. ISSN 0921-3449. doi: https://doi.org/10.1016/j.resconrec.2022.106794.

Guozhu Mao, Haoqiong Hu, Xi Liu, John Crittenden, and Ning Huang. A bibliometric analysis of industrial wastewater treatments from 1998 to 2019. *Environmental Pollution*, 275:115785, 2021. doi: https://doi.org/10.1016/j.envpol.2020.115785.

Azmatullah Noor, Shamsul Rahman Mohamed Kutty, Mohamed Hasnain Isa, Izharul Haq Farooqi, Augustine Chioma Affam, Abdullahi Haruna Birniwa, and Ahmad Hussaini Jagaba. 7 - treatment innovation using biological methods in combination with physical treatment methods. In Afzal Husain Khan, Nadeem A. Khan, Mu. Naushad, and Hamidi Abdul Aziz, editors, *The Treatment of Pharmaceutical Wastewater*, pages 217–245. Elsevier, 2023. ISBN 978-0-323-99160-5. doi: https://doi.org/10.1016/B978-0-323-99160-5.00010-2.

Shirra Freeman, Andy M Booth, Isam Sabbah, Rachel Tiller, Jan Dierking, Katja Klun, Ana Rotter, Eric Ben-David, Jamileh Javidpour, and Dror L Angel. Be-

tween source and sea: The role of wastewater treatment in reducing marine microplastics. *Journal of environmental Management*, 266:110642, 2020.

Latifah Abdul Ghani, Nora'aini Ali, Ilyanni Syazira Nazaran, and Marlia M Hanafiah. Environmental performance of small-scale seawater reverse osmosis plant for rural area water supply. *Membranes*, 11(1):40, 2021.

Reem Shaheen and Edit Cséfalvay. The role of coagulation and microfiltration in seawater pre-treatment. *Periodica Polytechnica Chemical Engineering*, 66(4): 557–564, 2022. doi: https://doi.org/10.3311/PPch.20025.

Mohammad Badruzzaman, Nikolay Voutchkov, Lauren Weinrich, and Joseph G Jacangelo. Selection of pretreatment technologies for seawater reverse osmosis plants: A review. *Desalination*, 449:78–91, 2019.

Thomas Altmann, Ana Rousseva, Johannes Vrouwenvelder, Michael Shaw, and Ratul Das. Effectiveness of ceramic ultrafiltration as pretreatment for seawater reverse osmosis. *Desalination*, 564:116781, 2023.

Semion Brover, Yaal Lester, Asher Brenner, and Eyal Sahar-Hadar. Optimization of ultrafiltration as pre-treatment for seawater ro desalination. *Desalination*, 524: 115478, 2022.

Saisai Lin, Haiyang Zhao, Liping Zhu, Tao He, Shengfu Chen, Congjie Gao, and Lin Zhang. Seawater desalination technology and engineering in china: A review. *Desalination*, 498:114728, 2021.

Osman Shamet and Mohamed Antar. Mechanical vapor compression desalination technology–a review. *Renewable and Sustainable Energy Reviews*, 187:113757, 2023.

Emad Ali, Jamel Orfi, Hany AlAnsary, Saleh Baakeem, Ahmad S Alsaadi, and Noreddine Ghaffour. Advanced structures of reversal multi-stage flash desalination. *Desalination*, 571:117095, 2024.

Nada Abounahia, Ibrar Ibrar, Tayma Kazwini, Ali Altaee, Akshaya K Samal, Syed Javaid Zaidi, and Alaa H Hawari. Desalination by the forward osmosis: Advancement and challenges. *Science of The Total Environment*, page 163901, 2023.

Yunhwan Kim, Yong-Gyun Park, and Kiho Park. Optimal design strategy, heuristics, and theoretical analysis of multi-stage reverse osmosis for seawater desalination. *Desalination*, page 117534, 2024.

Dipti Christian, Aakanksharaje Gaekwad, Hetvi Dani, MA Shabiimam, and Anurag Kandya. Recent techniques of textile industrial wastewater treatment: a review. *Materials Today: Proceedings*, 77:277–285, 2023.

Sharjeel Waqas, Noorfidza Yub Harun, Nonni Soraya Sambudi, Kunmi Joshua Abioye, Muhammad Hamad Zeeshan, Abulhassan Ali, Aymn Abdulrahman, Loai Alkhattabi, and Ahmad S Alsaadi. Effect of operating parameters on the performance of integrated fixed-film activated sludge for wastewater treatment. *Membranes*, 13(8):704, 2023.

Zubair Hashmi, Muhammad Roil Bilad, Fahrurrozi, Juliana Zaini, Jun Wei Lim, and Yusuf Wibisono. Recent progress in microalgae-based technologies for industrial wastewater treatment. *Fermentation*, 9(3):311, 2023.

Rukiye Oztekin and Delia Teresa Sponza. Treatment of wastewaters from the olive mill industry by sonication. *Journal of Chemical Technology & Biotechnology*, 88(2):212–225, 2013.

SF Ahmed, M Mofijur, Samiha Nuzhat, Anika Tasnim Chowdhury, Nazifa Rafa, Md Alhaz Uddin, Abrar Inayat, TMI Mahlia, Hwai Chyuan Ong, and Show Pau Loke Chia, Wen Yi. Recent developments in physical, biological, chemical, and hybrid treatment techniques for removing emerging contaminants from wastewater. *Journal of hazardous materials*, 416:125912, 2021.

Kingsley Tamunokuro Amakiri, Anyela Ramirez Canon, Marco Molinari, and

Athanasios Angelis-Dimakis. Review of oilfield produced water treatment technologies. *Chemosphere*, 298:134064, 2022.

Mohammed A Boraey. A hydro-kinematic approach for the design of compact corrugated plate interceptors for the de-oiling of produced water. *Chemical Engineering and Processing-Process Intensification*, 130:127–133, 2018.

Ramsey White, Simone Mulas, and Ahmed Al-Jughayman. Enhanced produced water deoiling using a centrifugal separator. In *Abu Dhabi International Petroleum Exhibition and Conference*, page D011S003R004. SPE, 2020.

AV Lekomtsev, VA Mordvinov, P Yu Ilyushin, VS Bakaneev, and KV Kornilov. Centrifugal separation in the treatment of produced water for its subsequent injection into a reservoir. *Chemical and Petroleum Engineering*, 56:979–987, 2021.

Masoud Nasiri and Iman Jafari. Produced water from oil-gas plants: A short review on challenges and opportunities. *Periodica Polytechnica Chemical Engineering*, 61(2):73–81, 2017.

Mary Kay Camarillo and William T Stringfellow. Biological treatment of oil and gas produced water: a review and meta-analysis. *Clean Technologies and Environmental Policy*, 20:1127–1146, 2018.

Amarjit Rajbongshi and Subrata Borgohain Gogoi. Microfiltration, ultrafiltration and nanofiltration as a post-treatment of biological treatment process with references to oil field produced water of moran oilfield of assam. *Petroleum Research*, 2023.

Asad Asad, Dan Sameoto, and Mohtada Sadrzadeh. Overview of membrane technology. In *Nanocomposite membranes for water and gas separation*, pages 1–28. Elsevier, 2020.

Viviani Onishi, Alba Carrero-Parreño, Juan A Reyes-Labarta, Rubén Ruiz-Femenia, Raquel Salcedo-Díaz, Eric S Fraga, and José A Caballero. Shale gas

flowback water desalination: Single vs multiple-effect evaporation with vapor recompression cycle and thermal integration. *Desalination*, 404:230–248, 2017a.

Devin L Shaffer, Laura H Arias Chavez, Moshe Ben-Sasson, Santiago Romero-Vargas Castrillón, Ngai Yin Yip, and Menachem Elimelech. Desalination and reuse of high-salinity shale gas produced water: drivers, technologies, and future directions. *Environmental science & technology*, 47(17):9569–9583, 2013.

Angela Szep and Robert Kohlheb. Water treatment technology for produced water. *Water Science and Technology*, 62(10):2372–2380, 2010.

Christoph Josef Backi and Sigurd Skogestad. A simple dynamic gravity separator model for separation efficiency evaluation incorporating level and pressure control. In *2017 American Control Conference (ACC)*, pages 2823–2828. IEEE, 2017.

Thomas E Schultz. Get the most out of api separators: the keys to maximizing performance include a realistic, educated awareness of the separator's capabilities, an understanding of how the device functions, and an appreciation of what it should have in the way of support equipment. *Chemical Engineering*, 112(7): 38–43, 2005.

American Petruelem Institute. Monographs on refinery environmental control-management of water discharges, 1990. URL `https://standards.globalspec.com/std/95137/api-publ-421`. accessed 22 July 2021.

William E Odiete and Jonah C Agunwamba. Novel design methods for conventional oil-water separators. *Heliyon*, 5(5), 2019.

Jayaprakash Saththasivam, Kavithaa Loganathan, and Sarper Sarp. An overview of oil–water separation using gas flotation systems. *Chemosphere*, 144:671–680, 2016.

Patrik Sobolciak, Anton Popelka, Aisha Tanvir, Mariam A Al-Maadeed, Samer Adham, and Igor Krupa. Materials and technologies for the tertiary treatment of

produced water contaminated by oil impurities through nonfibrous deep-bed media: A review. *Water*, 12(12):3419, 2020.

Selvaraj Munirasu, Mohammad Abu Haija, and Fawzi Banat. Use of membrane technology for oil field and refinery produced water treatment—a review. *Process safety and environmental protection*, 100:183–202, 2016.

Pauline Doran. Chapter 8 - mixing. In Pauline Doran, editor, *Bioprocess Engineering Principles (Second Edition)*, pages 255–332. Academic Press, London, second edition edition, 2013a. ISBN 978-0-12-220851-5. doi: https://doi.org/10.1016/B978-0-12-220851-5.00008-3.

Yixiang Liao and Dirk Lucas. A literature review of theoretical models for drop and bubble breakup in turbulent dispersions. *Chemical Engineering Science*, 64(15): 3389–3406, 2009a.

Dirk GAL Aarts, Henk NW Lekkerkerker, Hua Guo, Gerard H Wegdam, and Daniel Bonn. Hydrodynamics of droplet coalescence. *Physical review letters*, 95(16): 164503, 2005.

Giovanni Soligo, Alessio Roccon, and Alfredo Soldati. Breakage, coalescence and size distribution of surfactant-laden droplets in turbulent flow. *Journal of Fluid Mechanics*, 881:244–282, 2019.

Shouci Lu, Yuqing Ding, and Jinyong Guo. Kinetics of fine particle aggregation in turbulence. *Advances in Colloid and Interface Science*, 78(3):197–235, 1998. ISSN 0001-8686. doi: https://doi.org/10.1016/S0001-8686(98)00062-1.

Ricardo I Jeldres, Phillip D Fawell, and Brendan J Florio. Population balance modelling to describe the particle aggregation process: A review. *Powder technology*, 326:190–207, 2018.

Yixiang Liao and Dirk Lucas. A literature review on mechanisms and models for the coalescence process of fluid particles. *Chemical Engineering Science*, 65(10): 2851–2864, 2010a.

Michael Prince and Harvey Blanch. Bubble coalescence and break-up in air-sparged bubble columns. *AIChE journal*, 36(10):1485–1499, 1990.

Sheldon Friedlander. *Smoke, dust, and haze*, volume 198. Oxford university press New York, 2000.

Tiefeng Wang, Jinfu Wang, and Yong Jin. Population balance model for gas- liquid flows: Influence of bubble coalescence and breakup models. *Industrial & engineering chemistry research*, 44(19):7540–7549, 2005.

S Kalkach-Navarro, RT Lahey Jr, and DA Drew. Analysis of the bubbly/slug flow regime transition. *Nuclear engineering and design*, 151(1):15–39, 1994.

WJ Howarth. Coalescence of drops in a turbulent flow field. *Chemical Engineering Science*, 19(1):33–38, 1964.

H Sovova. Breakage and coalescence of drops in a batch stirred vessel—ii comparison of model and experiments. *Chemical Engineering Science*, 36(9):1567–1573, 1981.

L Doubliez. The drainage and rupture of a non-foaming liquid film formed upon bubble impact with a free surface. *International journal of multiphase flow*, 17 (6):783–803, 1991.

Seymour L Ross. *Measurements and models of the dispersed phase mixing process*. University of Michigan, 1971.

AM Kamp, AK Chesters, C Colin, and Jean Fabre. Bubble coalescence in turbulent flows: A mechanistic model for turbulence-induced coalescence applied to microgravity bubbly pipe flow. *International Journal of Multiphase Flow*, 27(8): 1363–1396, 2001.

TGM Van de Ven and SG Mason. The microrheology of colloidal dispersions vii. orthokinetic doublet formation of spheres. *Colloid and Polymer Science*, 255: 468–479, 1977.

Igor Ekhiel'evich Dzyaloshinskii, Efrat M Lifshitz, and Lev P Pitaevskii. The general theory of van der waals forces. *Advances in Physics*, 10(38):165–209, 1961.

Xu Xiao, Yang Qiang, and Wang Hualin Chaoyang, W. Impact of bubble coalescence on separation performance of a degassing hydrocyclone [j]. *Separation and Purification Technology*, 152, 2015.

M Smoluchowski. Versuch einer mathematischen theorie der koagulationskinetik kolloider lösungen. *Zeitschrift für physikalische Chemie*, 92(1):129–168, 1918.

Stelios Rigopoulos. Population balance modelling of polydispersed particles in reactive flows. *Progress in Energy and Combustion Science*, 36(4):412–443, 2010.

Z Melzak. A scalar transport equation. *Transactions of the American Mathematical Society*, 85(2):547–560, 1957.

Costas Kiparissides, Alexandros Alexopoulos, Abraham Roussos, Georgios Dompazis, and Costas Kotoulas. Population balance modeling of particulate polymerization processes. *Industrial & engineering chemistry research*, 43(23):7290–7302, 2004.

Amlan Datta and Raj K Rajamani. A direct approach of modeling batch grinding in ball mills using population balance principles and impact energy distribution. *International Journal of Mineral Processing*, 64(4):181–200, 2002.

Jannike Solsvik and Hugo A Jakobsen. The foundation of the population balance equation: a review. *Journal of Dispersion Science and Technology*, 36(4):510–520, 2015.

Hecham Omar and Sohrab Rohani. Crystal population balance formulation and solution methods: a review. *Crystal Growth & Design*, 17(7):4028–4041, 2017.

Ramin Raesi and Reza Maddahian. Numerical investigation of air-injected deoiling hydrocyclones using population balance model. *Chemical Engineering Science*, 248:117103, 2022.

Lei Xing, Minghu Jiang, Lixin Zhao, Jinming Gao, and Lin Liu. Design and analysis of de-oiling coalescence hydrocyclone. *Separation Science and Technology*, 57(5):749–767, 2022.

Qian Huang and Xueyuan Long. Analysis of the influencing factors on oil removal efficiency in large-scale flotation tanks: Experimental observation and numerical simulation. *Energies*, 13(4):927, 2020.

Xiaolei Cai, Jiaqing Chen, Meili Liu, Yipeng Ji, and Shan An. Numerical studies on dynamic characteristics of oil-water separation in loop flotation column using a population balance model. *Separation and Purification Technology*, 176:134–144, 2017a.

Xiaolei Cai, Jiaqing Chen, Meili Liu, Yipeng Ji, Guodong Ding, and Long Zhang. Cfd simulation of oil–water separation characteristics in a compact flotation unit by population balance modeling. *Journal of Dispersion Science and Technology*, 38(10):1435–1447, 2017b.

C Tsouris and LL Tavlarides. Breakage and coalescence models for drops in turbulent dispersions. *AIChE Journal*, 40(3):395–406, 1994.

Hean Luo and Hallvard F Svendsen. Theoretical model for drop and bubble breakup in turbulent dispersions. *AIChE journal*, 42(5):1225–1233, 1996.

Naonori Nishida, George Stephanopoulos, and Arthur W Westerberg. A review of process synthesis. *AIChE Journal*, 27(3):321–351, 1981.

George Stephanopoulos and Arthur W. Westerberg. Studies in process synthesis—ii: Evolutionary synthesis of optimal process flowsheets. *Chemical Engineering Science*, 31(3):195–204, 1976. ISSN 0009-2509. doi: https://doi.org/10.1016/0009-2509(76)85057-9. URL `https://www.sciencedirect.com/science/article/pii/0009250976850579`.

James M Douglas. A hierarchical decision procedure for process synthesis. *AIChE journal*, 31(3):353–362, 1985.

Ignacio E Grossmann. Mixed-integer programming approach for the synthesis of integrated process flowsheets. *Computers & chemical engineering*, 9(5):463–482, 1985.

Qi Chen and IE Grossmann. Recent developments and challenges in optimization-based process synthesis. *Annual review of chemical and biomolecular engineering*, 8:249–283, 2017.

Jun Fu and Fangyin Tian. Dynamic optimization of nonlinear systems with guaranteed feasibility of inequality-path-constraints. *Automatica*, 127:109516, 2021. ISSN 0005-1098. doi: https://doi.org/10.1016/j.automatica.2021.109516.

Mariya Koleva, Eleftheria Polykarpou, Songsong Liu, Craig Styan, and Lazaros Papageorgiou. Synthesis of water treatment processes using mixed integer programming. In *Computer Aided Chemical Engineering*, volume 37, pages 1379–1384. Elsevier, 2015.

Qiping Zhu, Bingjian Zhang, Qinglin Chen, Ming Pan, Jingzheng Ren, and Chang He. Optimal synthesis of water networks for addressing high-concentration wastewater in coal-based chemical plants. *ACS Sustainable Chemistry & Engineering*, 5(11):10792–10805, 2017.

Kashif Iqbal, Wei Jiang, Rui Ma, and Chun Deng. Synthesis of large-scale total water network with multiple water resources under seasonal flow rate constraints. *Journal of Cleaner Production*, 337:130462, 2022. ISSN 0959-6526. doi: https://doi.org/10.1016/j.jclepro.2022.130462.

Resul Al, Chitta Ranjan Behera, Krist V. Gernaey, and Gürkan Sin. Stochastic simulation-based superstructure optimization framework for process synthesis and design under uncertainty. *Computers Chemical Engineering*, 143: 107118, 2020. ISSN 0098-1354. doi: https://doi.org/10.1016/j.compchemeng.2020.107118. URL `https://www.sciencedirect.com/science/article/pii/S0098135419310737`.

Chun Deng, Wei Jiang, Wenjin Zhou, and Xiao Feng. New superstructure-based optimization of property-based industrial water system. *Journal of Cleaner Production*, 189:878–886, 2018. ISSN 0959-6526. doi: https://doi.org/10.1016/j.jclepro.2018.03.314. URL `https://www.sciencedirect.com/science/article/pii/S0959652618310011`.

Hande Bozkurt, Alberto Quaglia, Krist V Gernaey, and Gürkan Sin. A mathematical programming framework for early stage design of wastewater treatment plants. *Environmental Modelling & Software*, 64:164–176, 2015.

Viviani Onishi, Rubén Ruiz-Femenia, Raquel Salcedo-Díaz, Alba Carrero-Parreño, Juan A Reyes-Labarta, Eric S Fraga, and José A Caballero. Process optimization for zero-liquid discharge desalination of shale gas flowback water under uncertainty. *Journal of cleaner production*, 164:1219–1238, 2017b.

Alba Carrero-Parreño, Viviani. Onishi, Rubén Ruiz-Femenia, Raquel Salcedo-Díaz, José A. Caballero, and Juan A. Reyes-Labarta. Optimization of multistage membrane distillation system for treating shale gas produced water. *Desalination*, 460: 15–27, 2019. ISSN 0011-9164. doi: https://doi.org/10.1016/j.desal.2019.03.002.

Alba Carrero-Parreno, Viviani Onishi, Raquel Salcedo-Díaz, Ruben Ruiz-Femenia, Eric S Fraga, Jose A Caballero, and Juan A Reyes-Labarta. Optimal pretreatment system of flowback water from shale gas production. *Industrial & Engineering Chemistry Research*, 56(15):4386–4398, 2017.

CA Coello Coello. Evolutionary multi-objective optimization: a historical view of the field. *IEEE computational intelligence magazine*, 1(1):28–36, 2006.

P. Ngatchou, A. Zarei, and A. El-Sharkawi. Pareto multi objective optimization. In *Proceedings of the 13th International Conference on, Intelligent Systems Application to Power Systems*, pages 84–91, 2005. doi: 10.1109/ISAP.2005.1599245.

Eckart Zitzler. *Evolutionary algorithms for multiobjective optimization: Methods and applications*, volume 63. Citeseer, 1999.

Carlos A Coello. An updated survey of ga-based multiobjective optimization techniques. *ACM Computing Surveys (CSUR)*, 32(2):109–143, 2000.

Kalyanmoy Deb. *Multi-objective optimization using evolutionary algorithms*, volume 16. John Wiley & Sons, 2001.

A Ghane-Kanafi and E Khorram. A new scalarization method for finding the efficient frontier in non-convex multi-objective problems. *Applied Mathematical Modelling*, 39(23-24):7483–7498, 2015.

Lei Xiujuan and Shi Zhongke. Overview of multi-objective optimization methods. *Journal of Systems Engineering and Electronics*, 15(2):142–146, 2004.

Tadahiko Murata and booktitle=IEEE international conference on evolutionary computation volume=1 pages=289–294 year=1995 organization=IEEE Piscataway Ishibuchi, Hisao. Moga: multi-objective genetic algorithms.

Jeffrey Horn, Nicholas Nafpliotis, and David E Goldberg. A niched pareto genetic algorithm for multiobjective optimization. In *Proceedings of the first IEEE conference on evolutionary computation. IEEE world congress on computational intelligence*, pages 82–87. Ieee, 1994.

Eckart Zitzler and Lothar Thiele. An evolutionary algorithm for multiobjective optimization: The strength pareto approach. *TIK report*, 43, 1998.

James Kennedy and Russell Eberhart. Particle swarm optimization. In *Proceedings of ICNN'95-international conference on neural networks*, volume 4, pages 1942–1948. IEEE, 1995.

Krzysztof Pytel. Hybrid multi-evolutionary algorithm to solve optimization problems. *Applied Artificial Intelligence*, 34(7):550–563, 2020.

Holger R Maier, Saman Razavi, Zoran Kapelan, L Shawn Matott, J Kasprzyk, and Bryan A Tolson. Introductory overview: Optimization using evolutionary algorithms and other metaheuristics. *Environmental modelling & software*, 114: 195–213, 2019.

Christian von Lücken, Carlos Brizuela, and Benjamin Barán. An overview on evolutionary algorithms for many-objective optimization problems. *Wiley interdisciplinary reviews: data mining and knowledge discovery*, 9(1):e1267, 2019.

Borhan Kazimipour, Xiaodong Li, and A Kai Qin. A review of population initialization techniques for evolutionary algorithms. In *2014 IEEE Congress on Evolutionary Computation (CEC)*, pages 2585–2592. IEEE, 2014.

Lorenz T. Biegler and Ignacio E. Grossmann. Retrospective on optimization. *Computers Chemical Engineering*, 28(8):1169–1192, 2004. ISSN 0098-1354. doi: https://doi.org/10.1016/j.compchemeng.2003.11.003. URL https://www.sciencedirect.com/science/article/pii/S0098135403003089.

Viviani Onishi, Mohammad H Khoshgoftar Manesh, Raquel Salcedo-Díaz, Rubén Ruiz-Femenia, Juan A Labarta, and José A Caballero. Thermo-economic and environmental optimization of a solar-driven zero-liquid discharge system for shale gas wastewater desalination. *Desalination*, 511:115098, 2021.

GAMS. Gams: General algebraic modeling system, 2024. URL https://www.gams.com/.

Alba Carrero-Parreño, Viviani Onishi, Rubén Ruiz-Femenia, Raquel Salcedo-Díaz, José A. Caballero, and Juan A. Reyes-Labarta. Multistage membrane distillation for the treatment of shale gas flowback water: Multi-objective optimization under uncertainty. In Antonio Espuña, Moisès Graells, and Luis Puigjaner, editors, *27th European Symposium on Computer Aided Process Engineering*, volume 40 of *Computer Aided Chemical Engineering*, pages 571–576. Elsevier, 2017. doi: https://doi.org/10.1016/B978-0-444-63965-3.50097-0. URL https://www.sciencedirect.com/science/article/pii/B9780444639653500970.

Raquel Salcedo-Díaz, Rubén Ruiz-Femenia, Alba Carrero-Parreño, Viviani Onishi, Juan A. Reyes-Labarta, and José A. Caballero. Combining forward

and reverse osmosis for shale gas wastewater treatment to minimize cost and freshwater consumption. In Antonio Espuña, Moisès Graells, and Luis Puigjaner, editors, *27th European Symposium on Computer Aided Process Engineering*, volume 40 of *Computer Aided Chemical Engineering*, pages 2725–2730. Elsevier, 2017. doi: https://doi.org/10.1016/B978-0-444-63965-3.50456-6. URL https://www.sciencedirect.com/science/article/pii/B9780444639653504566.

Mariya N. Koleva, Songsong Liu, Craig A. Styan, and Lazaros G. Papageorgiou. Multi-objective optimisation approach for the synthesis of water treatment plants. In Zdravko Kravanja and Miloš Bogataj, editors, *26th European Symposium on Computer Aided Process Engineering*, volume 38 of *Computer Aided Chemical Engineering*, pages 2379–2384. Elsevier, 2016. doi: https://doi.org/10.1016/B978-0-444-63428-3.50401-X. URL https://www.sciencedirect.com/science/article/pii/B978044463428350401X.

CA Coulaloglou and Lawrence L Tavlarides. Description of interaction processes in agitated liquid-liquid dispersions. *Chemical Engineering Science*, 32(11):1289–1297, 1977.

Yixiang Liao and Dirk Lucas. A literature review of theoretical models for drop and bubble breakup in turbulent dispersions. *Chemical Engineering Science*, 64(15): 3389–3406, 2009b.

Yixiang Liao and Dirk Lucas. A literature review on mechanisms and models for the coalescence process of fluid particles. *Chemical Engineering Science*, 65(10): 2851–2864, 2010b.

Thomas R Camp. Velocity gradients and internal work in fluid motion. *J. Boston Soc. Civ. Eng.*, 30:219–230, 1943.

PGF Saffman and JS Turner. On the collision of drops in turbulent clouds. *Journal of Fluid Mechanics*, 1(1):16–30, 1956.

J Abrahamson. Collision rates of small particles in a vigorously turbulent fluid. *Chemical Engineering Science*, 30(11):1371–1379, 1975.

Eric S Fraga. Multiple simultaneous solution representations in a population based evolutionary algorithm. *arXiv preprint arXiv:2106.05096*, 2021.

Abdellah Salhi and Eric S Fraga. Nature-inspired optimisation approaches and the new plant propagation algorithm. 2011.

Alistair D Rodman, Eric S Fraga, and Dimitrios Gerogiorgis. On the application of a nature-inspired stochastic evolutionary algorithm to constrained multi-objective beer fermentation optimisation. *Computers & Chemical Engineering*, 108:448–459, 2018.

Eric S Fraga and Oluwamayowa Amusat. Understanding the impact of constraints: a rank based fitness function for evolutionary methods. *Advances in Stochastic and Deterministic Global Optimization*, pages 243–254, 2016.

Jeff Bezanson, Alan Edelman, Stefan Karpinski, and Viral B Shah. Julia: A fresh approach to numerical computing. *SIAM review*, 59(1):65–98, 2017.

Julia Language. *Parallel Computing*, 2024. URL `https://docs.julialang.org/en/v1/manual/parallel-computing/`. Accessed: 2024-07-22.

Christopher Rackauckas and Qing Nie. DifferentialEquations.jl–a performant and feature-rich ecosystem for solving differential equations in Julia. *Journal of Open Research Software*, 5(1), 2017.

DifferentialEquations.jl Development Team. Differentialequations.jl documentation. `https://docs.sciml.ai/DiffEqDocs/stable/solvers/ode_solve/#Explicit-Runge-Kutta-Methods`, 2022. Accessed: April 10, 2024.

Ch Tsitouras. Runge–kutta pairs of order 5 (4) satisfying only the first column simplifying assumption. *Computers & Mathematics with Applications*, 62(2): 770–775, 2011.

Peter Benner and Hermann Mena. Rosenbrock methods for solving riccati differential equations. *IEEE Transactions on Automatic Control*, 58(11):2950–2956, 2013.

LR Klooster. Approximating differential equations using neural odes. B.S. thesis, University of Twente, 2021. URL `http://essay.utwente.nl/87568/`.

Enviro Tech Systems. API 421 Gravity Separator, 2024. URL `https://envirotechsystems.com/produced-water-equipment/api-421-gravity-separator/`. Accessed: January 31, 2024.

Heinrich Schubert. On the turbulence-controlled microprocesses in flotation machines. *International Journal of Mineral Processing*, 56(1):257–276, 1999. ISSN 0301-7516. doi: https://doi.org/10.1016/S0301-7516(98)00048-9. URL `https://www.sciencedirect.com/science/article/pii/S0301751698000489`.

Gavin Towler and Ray Sinnott. *Chemical engineering design: principles, practice and economics of plant and process design*. Elsevier, 2012.

Ifeyinwa Charlotte Okam. *Investigation of oily wastewater treatment processes*. Swansea University (United Kingdom), 2008.

Novena Lany Pangestu, Nurulbaiti Listyendah Zahra, Ariyanti Sarwono, and I Wayan Koko Suryawan. Produced water treatment planning using corrugated plate interceptor and ultra filtration for water recycling. *Jurnal Serambi Engineering*, 6(4), 2021.

Bill Rehm, Jerome Schubert, Arash Haghshenas, Amir Saman Paknejad, and Jim Hughes. Chapter two - situational problems in mpd. In *Managed Pressure Drilling*, pages 39–80. Gulf Publishing Company, 2008. ISBN 978-

1-933762-24-1. doi: https://doi.org/10.1016/B978-1-933762-24-1.50008-5. URL https://www.sciencedirect.com/science/article/pii/B9781933762241500085.

K Rietema. Performance and design of hydrocyclones—iv: Design of hydrocyclones. *Chemical Engineering Science*, 15(3-4):320–325, 1961.

Jolius Gimbun, TG Chuah, Thomas SY Choong, and A Fakhru'l-Razi. A cfd study on the prediction of cyclone collection efficiency. *International Journal for Computational Methods in Engineering Science and Mechanics*, 6(3):161–168, 2005.

Muhammad I Taiwo, Mohammed A Namadi, and B Mokwa. Design and analysis of cyclone dust separator. *Am J Eng Res*, 5(4):130–134, 2016.

M Silva, CA Claumann, RAF Machado, and MB Quadri. Cfd modeling of lapple cyclone for gas-solid separation. *CFD Oil*, 2008.

Thomas J Overcamp and Steven E Scarlett. Effect of reynolds number on the stokes number of cyclones. *Aerosol science and technology*, 19(3):362–370, 1993.

E.S. Tarleton and R.J. Wakeman. 1 - solid/liquid separation equipment. In E.S. Tarleton and R.J. Wakeman, editors, *Solid/Liquid Separation*, pages 1–77. Butterworth-Heinemann, Oxford, 2007. ISBN 978-1-85617-421-3. doi: https://doi.org/10.1016/B978-185617421-3/50001-8. URL https://www.sciencedirect.com/science/article/pii/B9781856174213500018.

JJ Cilliers. Hydrocyclones for particle size separation. *particle size separation*, pages 1819–1825, 2000.

Martina Piccioli, Svein Viggo Aanesen, He Zhao, Marcin Dudek, and Gisle Øye. Gas flotation of petroleum produced water: a review on status, fundamental aspects, and perspectives. *Energy & Fuels*, 34(12):15579–15592, 2020.

Roe-Hoan Yoon, Gaurav Soni, Kaiwu Huang, Seungwoo Park, and Lei Pan. Development of a turbulent flotation model from first principles and its validation. *International Journal of Mineral Processing*, 156:43–51, 2016.

Maurice Stewart and Ken Arnold. Chapter 3 - produced water treating systems. In Maurice Stewart and Ken Arnold, editors, *Emulsions and Oil Treating Equipment*, pages 107–211. Gulf Professional Publishing, Burlington, 2009. ISBN 978-0-7506-8970-0. doi: https://doi.org/10.1016/B978-0-7506-8970-0.00003-7. URL https://www.sciencedirect.com/science/article/pii/B9780750689700000037.

Wanhua Shen, Debjani Mukherjee, Narayan Koirala, Guangji Hu, Kenneth Lee, Min Zhao, and Jianbing Li. Microbubble and nanobubble-based gas flotation for oily wastewater treatment: a review. *Environmental Reviews*, 30(3):359–379, 2022.

Md Shahjahan Kaisar Alam Sarkar, SW Donne, and GM Evans. Hydrogen bubble flotation of silica. *Advanced Powder Technology*, 21(4):412–418, 2010.

DF Lawler and JA Nason. Granular media filtration: old process, new thoughts. *Water Science and Technology*, 53(7):1–7, 2006.

CECO Environmental. Walnut Shell Filters. https://www.cecoenviro.com/products/walnut-shell-filters/, 2023. Accessed on July 17, 2023.

Murray Moo-Young. 2.22 - biofilters. In *Comprehensive Biotechnology (Second Edition)*, pages 303–318. Academic Press, Burlington, second edition edition, 2011. ISBN 978-0-08-088504-9. doi: https://doi.org/10.1016/B978-0-08-088504-9.00408-6. URL https://www.sciencedirect.com/science/article/pii/B9780080885049004086.

Amit Kumar, V Subramanian, Satish K. Velaga, J Kodandaraman, PN Sujatha, R Baskaran, Shekhar Kumar, and BM Ananda Rao. Performance evaluation of a

tubular bowl centrifuge by using laser obscuration method as an online measurement tool. *Separation Science and Technology*, 55(10):1839–1851, 2020.

Zeki Berk. Chapter 9 - centrifugation. In *Food Process Engineering and Technology*, Food Science and Technology, pages 217–232. Academic Press, San Diego, 2009. ISBN 978-0-12-373660-4. doi: https://doi.org/10.1016/B978-0-12-373660-4.00009-0. URL https://www.sciencedirect.com/science/article/pii/B9780123736604000090.

Magdi Abadir. Chapter 7: CENTRIFUGAL SEPARATION OPERATIONS, 2018. URL https://scholar.cu.edu.eg/?q=magdi/files/chen_304_chapter_7_updated_2018.pdf. Accessed: January 31, 2024.

JP Maybury, K Mannweiler, NJ Titchener-Hooker, M Hoare, and P Dunnill. The performance of a scaled down industrial disc stack centrifuge with a reduced feed material requirement. *Bioprocess Engineering*, 18:191–199, 1998.

Reza Sabbagh, Michael G Lipsett, Charles R Koch, and David S Nobes. Hydrocyclone performance and energy consumption prediction: a comparison with other centrifugal separators. *Separation Science and Technology*, 50(6):788–801, 2015.

M Abbasgholipourghadim, M Bin Mailah, I Zaurah, AF Ismail, M Rezaei Dashtarzhandi, and M Abbasgholipourghadim. Membrane surface porosity and pore area distribution incorporating digital image processing. *Recent Advances in Mechanics and Mechanical Engineering; Springer: Berlin, Germany*, 10:118–123, 2016.

Aqua Free. Microfiltration membrane 1.0 mm, 2024. URL :https://www.aqua-free.com/en/product/microfiltration-membrane-10-mm/. Accessed: 2024-06-28.

M van Amsterdam. Factorial techniques applied in chemical plant cost estimation: A comparative study based on literature and cases. *TU Delft*, 1918.

Sasan Mehrabian, Markus Bussmann, and Edgar Acosta. Breakup of high solid volume fraction oil–particle cluster in simple shear flow. *Colloids and Surfaces A: Physicochemical and Engineering Aspects*, 483:25–35, 2015.

Carlos MARTÍNEZ-BAZÁN, JL Montanes, and Juan C Lasheras. On the breakup of an air bubble injected into a fully developed turbulent flow. part 1. breakup frequency. *Journal of Fluid Mechanics*, 401:157–182, 1999.

Jürgen C Flesch, Patrick T Spicer, and Sotiris E Pratsinis. Laminar and turbulent shear-induced flocculation of fractal aggregates. *AIChE journal*, 45(5):1114–1124, 1999.

JD Pandya and LA Spielman. Floc breakage in agitated suspensions: effect of agitation rate. *Chemical Engineering Science*, 38(12), 1983.

Sanjeev Kumar and Doraiswami Ramkrishna. On the solution of population balance equations by discretization—i. a fixed pivot technique. *Chemical Engineering Science*, 51(8):1311–1332, 1996.

Marleen de Jonge and Daan van den Berg. Plant propagation parameterization: Offspring & population size. In *Evostar 2020, The Leading European Event on Bio-Inspired Computation*, 2020.

Sachin Desale, Akhtar Rasool, Sushil Andhale, and Priti Rane. Heuristic and meta-heuristic algorithms and their relevance to the real world: a survey. *Int. J. Comput. Eng. Res. Trends*, 351(5):2349–7084, 2015.

Eric Fraga. *Nature-Inspired Methods for Optimization*. 2022. doi: 10.5281/zenodo.7016482.

Cleverson Vitorio Andreoli, Marcos Von Sperling, and Fernando Fernandes. *Sludge treatment and disposal*. IWA publishing, 2007.

National Institute of Standards and Technology. Nist chemistry webbook. `https://webbook.nist.gov/chemistry/`, Accessed 2023.

About petroleum liquids. https://www.transmountain.com/about-petroleum-liquids. Accessed on July 5, 2023.

U.S. Environmental Protection Agency. Solids module. https://www.epa.gov/sites/default/files/2018-05/documents/solids-module.pdf, Accessed on Month Day, Year.

Air Liquide. Methane encyclopedia. https://web.archive.org/web/20181226083050/https://encyclopedia.airliquide.com/methane?GasID=41, Accessed on Month Day, Year.

Ryan M Pollyea, Martin C Chapman, Richard S Jayne, and Hao Wu. High density oilfield wastewater disposal causes deeper, stronger, and more persistent earthquakes. *Nature communications*, 10(1):3077, 2019.

Hyungchul Kim and Diane J Burgess. Prediction of interfacial tension between oil mixtures and water. *Journal of colloid and interface science*, 241(2):509–513, 2001.

Osamah Alomair, Mohammad Jumaa, Abullhaq Alkoriem, and Mohamed Hamed. Heavy oil viscosity and density prediction at normal and elevated temperatures. *Journal of Petroleum Exploration and Production Technology*, 6:253–263, 2016.

Journal of Physical and Chemical Reference Data. Viscosity of liquid water in the range 8 °c to 150 °c. https://srd.nist.gov/jpcrdreprint/1.555581.pdf, Accessed on July 5, 2023.

CNC OIL SKIMMERS Ltd. Complete oil skimmer with integrated timer ms2t 45mm belt width. URL https://www.cncoilskimmers.co.uk/product-page/complete-oil-skimmer-with-integrated-timer-ms2t-45mm-belt-width. Accessed: July 16, 2023.

Poly Processing Company. Tank Geometry and Wall Thickness. https://blog.polyprocessing.com/blog/

tank-geometry-and-wall-thickness, 2023. Accessed: July 23, 2023.

AG Metal Miner. Carbon steel prices, 2023. URL https://agmetalminer.com/metal-prices/carbon-steel/. Accessed: 23 July 2023.

Th Neesse, J Dueck, H Schwemmer, and M Farghaly. Using a high pressure hydrocyclone for solids classification in the submicron range. *Minerals Engineering*, 71:85–88, 2015.

CEE. 2L75 Rotor and Stator Set (Putzmeister SP11 THF), 2023. URL https://ces-hire.com/product/2l75-rotor-and-stator-set//. Accessed: July 23, 2023.

NB Vargaftik, BN Volkov, and LD Voljak. International tables of the surface tension of water. *Journal of Physical and Chemical Reference Data*, 12(3):817–820, 1983.

BK Gorain, JP Franzidis, and EV Manlapig. Studies on impeller type, impeller speed and air flow rate in an industrial scale flotation cell. part 4: Effect of bubble surface area flux on flotation performance. *Minerals Engineering*, 10(4):367–379, 1997.

Taehun Son, Ha Bich Trinh, Seunghyun Kim, Bayasgalan Dugarjav, and Jaeryeong Lee. Estimation of energy consumption for concentrate process of tungsten ore towards the integration of renewable energy sources in mongolia. *Minerals*, 13 (8):1059, 2023.

Sand Blasters. Walnut Shell, 2023. URL https://www.sandblasters.co.uk/walnut-shell-165-walnut-shell-polishing-media--medium-075-14mm-asp. Accessed: July 23, 2023.

Flowspec Shengda. Nutshell granules, 2023. URL http://www.walnutshellpowder.com/walnut_shell/news_Walnut_shell_filter_specifications.html. Accessed: July 23, 2023.

F Sadeghi, Hamed Bashiri, and AJWH Vissers. Experimental and numerical investigation of backwash flow in nutshell filter. *SPE Production & Operations*, 35 (02):373–383, 2020.

Ezequiel Q Segismundo, Byung-Sik Lee, Lee-Hyung Kim, and Bon-Hong Koo. Evaluation of the impact of filter media depth on filtration performance and clogging formation of a stormwater sand filter. *Journal of Korean Society on Water Environment*, 32(1):36–45, 2016.

Nathalie Tufenkji and Menachem Elimelech. Correlation equation for predicting single-collector efficiency in physicochemical filtration in saturated porous media. *Environmental science & technology*, 38(2):529–536, 2004.

Fatma Arous, Stathis Kyriacou, Hajer Ennouri, Salma Bessadok, and Atef Jaouani. An energy-efficient two-stage passively aerated trickling filter for high-strength wastewater treatment and reuse. *Water and Environment Journal*, 37(2):218–231, 2023.

Amer Abu-Shamleh and Yousef SH Najjar. Optimization of mechanical harvesting of microalgae by centrifugation for biofuels production. *Biomass and Bioenergy*, 143:105877, 2020.

Pauline Doran. Chapter 11 - unit operations. In Pauline M. Doran, editor, *Bioprocess Engineering Principles (Second Edition)*, pages 445–595. Academic Press, London, second edition edition, 2013b. ISBN 978-0-12-220851-5. doi: https://doi.org/10.1016/B978-0-12-220851-5.00011-3. URL https://www.sciencedirect.com/science/article/pii/B9780122208515000113.

BK Nandi, R Uppaluri, and MK Purkait. Preparation and characterization of low cost ceramic membranes for micro-filtration applications. *Applied Clay Science*, 42(1-2):102–110, 2008.

Yann A Le Gouellec, David A Cornwell, and Michael J Macphee. Treating micro-

filtration backwash. *Journal-American Water Works Association*, 96(1):72–83, 2004.

M. Raffin, E. Germain, and S.J. Judd. Influence of backwashing, flux and temperature on microfiltration for wastewater reuse. *Separation and Purification Technology*, 96:147–153, 2012. ISSN 1383-5866. doi: https://doi.org/10.1016/j.seppur.2012.05.030. URL https://www.sciencedirect.com/science/article/pii/S1383586612003164.

Mohammed Wali Hakami, Abdullah Alkhudhiri, Sirhan Al-Batty, Myrto-Panagiota Zacharof, Jon Maddy, and Nidal Hilal. Ceramic microfiltration membranes in wastewater treatment: Filtration behavior, fouling and prevention. *Membranes*, 10(9):248, 2020.

Tom Rodgers. Interactive Graphs for CEPCI, 2023. URL https://personalpages.manchester.ac.uk/staff/tom.rodgers/Interactive_graphs/CEPCI.html?reactors/CEPCI/index.html. Accessed: 18-07-2023.

Chemifloc Group. Safety data sheet poly aluminumchloride. URL https://chemifloc.com/media/1169/polyaluminium-chloride-18.pdf. Accessed: July 16, 2023.

Yixing Bluwat Chemicals Co., Ltd. Bluwat Website. URL https://bluwat01.en.made-in-china.com/?acc=5954797572&cpn=12361708000-114715848861&tgt=kwd-364647786626&net=g&dev=c-&gid=Cj0KCQjwzdOlBhCNARIsAPMwjby3VogI35alrxo0sT6dbOD2LwqEGFY01lcQxSBBumwcB&kwd=polyaluminium%20chloride&mtp=b&gclid=Cj0KCQjwzdOlBhCNARIsAPMwjby3VogI35alrxo0sT6dbOD2LwqEGFY01lcQxSBBumwcB. Accessed: July 17, 2023.

The Chlorine Institute. Chemical Properties of Chlorine. URL https:

//www.chlorineinstitute.org/stewardship/chlorine/chemical-properties/. Accessed: July 16, 2023.

Leon Becker. Chemical Elements by Market Price. URL http://www.leonland.de/elements_by_price/en/list. Accessed: July 17, 2023.

M. I. Nikandrov and Yu. I. Mikhailov. Density and viscosity of sodium phosphate solutions. *Russian Journal of Applied Chemistry*, 78(9):1538–1539, 2005.

Chemical Book. Sodium Polyphosphate - ChemicalBook. URL https://www.chemicalbook.com/Price/Sodium-polyphosphate.htm. Accessed: July 17, 2023.

MERCK. Imidazole. URL https://www.merckmillipore.com/INTL/en/product/Imidazole,MDA_CHEM-814223. Accessed: July 16, 2023.

Made-in-China. Hot China Products - Imidazoline. URL https://www.made-in-china.com/products-search/hot-china-products/Imidazoline.html. Accessed: July 16, 2023.

Hydroland. Hydrochloric Acid. URL http://hydro-land.com/e/ligne-en/doc/HCl.html#:~:text=30%2D34%25%20(density%3A,1149%20%C3%A0%201169%20kg%2Fm3). Accessed: July 16, 2023.

CHEMANALYST. Hydrochloric Acid Price Trend and Forecast. URL https://www.chemanalyst.com/Pricing-data/hydrochloric-acid-61. Accessed: July 16, 2023.

Aysegul Gul, Jakub Hruza, and Fatma Yalcinkaya. Fouling and chemical cleaning of microfiltration membranes: A mini-review. *Polymers*, 13(6):846, 2021.

Density of Sodium Hydroxide [NaOH]. URL https://www.aqua-calc.com/page/density-table/substance/sodium-blank-hydroxide). Accessed: July 16, 2023.

ECHEMI Group. Sodium hydroxide International Price. URL https://www.echemi.com/pip/caustic-soda-pearls-pd20150901041.html. Accessed: July 16, 2023.

Rajshree Amrut Patil, Shankar Balajirao Kausley, Saurabh Milind Joshi, and Aniruddha Bhalchandra Pandit. Chapter 27 - process intensification applied to microalgae-based processes and products. In Eduardo Jacob-Lopes, Mariana Manzoni Maroneze, Maria Isabel Queiroz, and Leila Queiroz Zepka, editors, *Handbook of Microalgae-Based Processes and Products*, pages 737–769. Academic Press, 2020. ISBN 978-0-12-818536-0. doi: https://doi.org/10.1016/B978-0-12-818536-0.00027-0. URL https://www.sciencedirect.com/science/article/pii/B9780128185360000270.

John J Milledge and Sonia Heaven. Disc stack centrifugation separation and cell disruption of microalgae: a technical note. *Environment and Natural Resources Research*, 1(1):17–24, 2011.

Hydrocyclone. https://emis.vito.be/en/bat/tools-overview/sheets/hydrocyclone, Accessed: 2023. Accessed on July 17, 2023.

Nutriman Consortium. Training Material: Nutriman Project, 2023. URL https://nutriman.net/sites/default/files/2020-05/ID_275_Training_material.pdf. Accessed on July 17, 2023.

UK Government. Greenhouse Gas Reporting Conversion Factors 2023. https://www.gov.uk/government/publications/greenhouse-gas-reporting-conversion-factors-2023. Accessed: 18-07-2023.

Climate Change Connection. CO2 Equivalents. https://climatechangeconnection.org/emissions/co2-equivalents/. Accessed: 18-07-2023.

Euro Chlor. The European Chlor-Alkali Industry - An Electricity Intensive Sector Exposed to Carbon Leakage. https://www.eurochlor.

org/wp-content/uploads/2019/04/3-2-the_european_chlor-alkali_industry_-_an_electricity_intensive_sector_exposed_to_carbon_leakage.pdf. Accessed: 18-07-2023.

Carbon Cloud. Title of the Web Page. https://apps.carboncloud.com/climatehub/product-reports/id/1274059693465. Accessed: 18-07-2023.

City of Winnipeg. Appendix 7. https://legacy.winnipeg.ca/finance/findata/matmgt/documents/2012/682-2012/682-2012_appendix_h-wstp_south_end_plant_process_selection_report/appendix%207.pdf. Accessed: 18-07-2023.